Heat balance investigations in tidal areas

van Boxel, J.H.

Publication date
1986
Document Version
Final published version

heat balance investigations in tidal areas

john van boxel

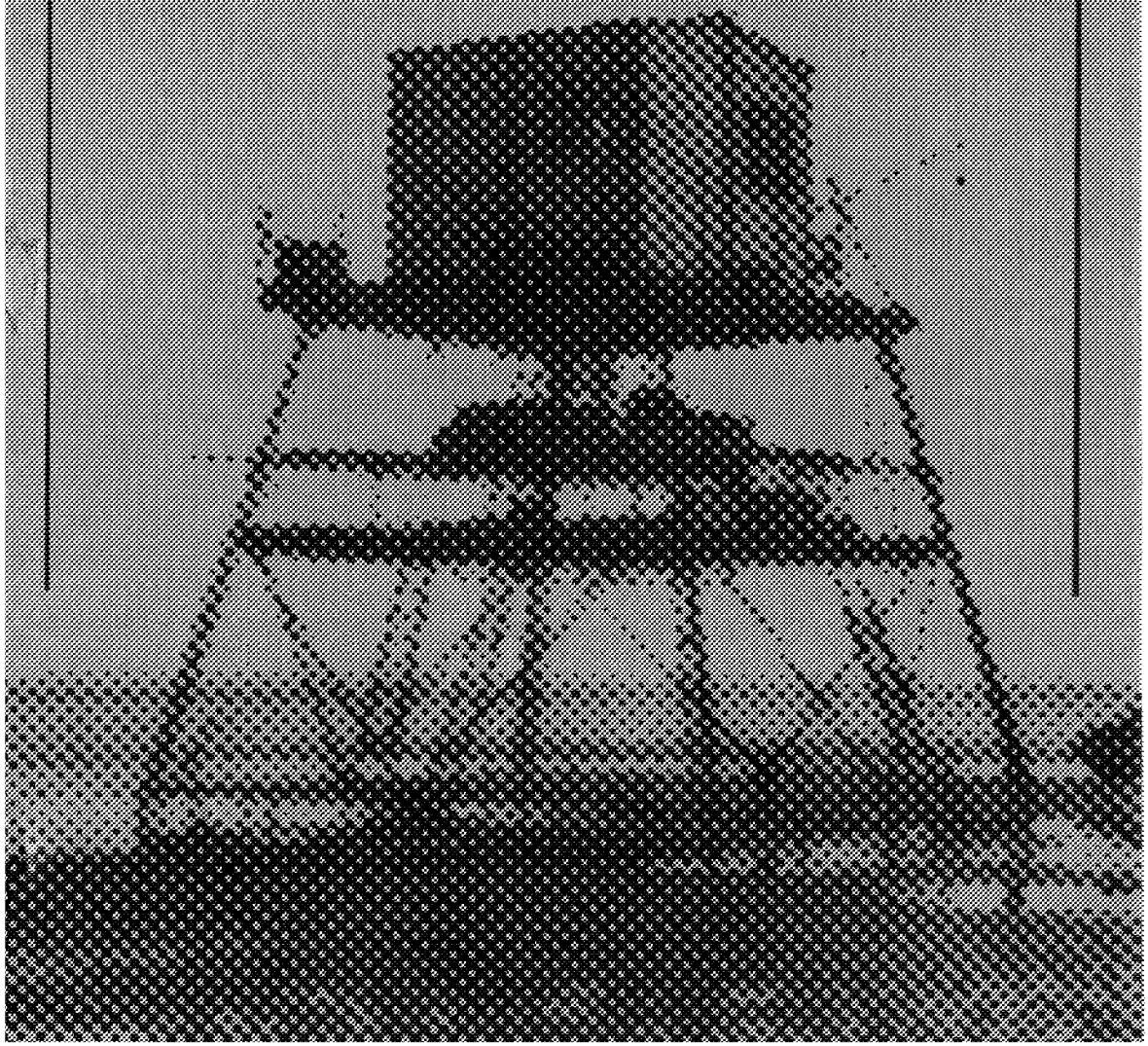

VRIJE UNIVERSITEIT TE AMSTERDAM

HEAT BALANCE INVESTIGATIONS

IN TIDAL AREAS

ACADEMISCH PROEFSCHRIFT

ter verkrijging van de graad van
doctor in de wiskunde en natuurwetenschappen
aan de Vrije Universiteit te Amsterdam,
op gezag van rector magnificus dr. P.J.D. Drenth,
hoogleraar in de faculteit der sociale wetenschappen,
in het openbaar te verdedigen
op donderdag 17 april 1986 te 15.30 uur
in het hoofdgebouw der universiteit,
De Boelelaan 1105

door

JOHANNES HENDRICUS VAN BOXEL

geboren te Raamsdonk

CWI Centre for Mathematics and Computer Science
1986

Promotor : prof. dr. H.F. Vugts
Copromotor : prof. dr. ir. L. Wartena
Referent : prof. dr. J.T.F. Zimmerman

STELLINGEN

I

Hoewel in publicaties over windprofielen in gewassen vaak geen melding wordt gemaakt van de stabiliteit van de grenslaag boven het gewas, en die stabiliteit ook niet is verwerkt in een aantal modellen die de stroming binnen het gewas beschrijven, is de stabiliteit van de grenslaag boven het gewas terdege van invloed op de stroming en de uitwisselingsprocessen binnen het gewas.

II

De door Businger gesuggereerde conclusie, dat de verticale voelbare warmteflux nul is indien de verticale gradiënt in de voelbare warmteflux nul is ($\overline{\partial w' \theta'}/\partial z = \rho^{-1} \partial(\rho \overline{w}\ \overline{\theta})/\partial z = 0$), is zowel fysisch als mathematisch onjuist.
(Businger, J.A., 1982, Equations and concepts, Chapter 1 in Atmospheric turbulence and air pollution modelling, Ed. F.T.M. Nieuwstadt and H. van Dop, D. Reidel publishing Company, Dordrecht, Holland.)

III

Voor de berekening van de bodemwarmteflux in een homogene bodem, waarvan zowel het warmtegeleidingsvermogen als de warmtecapaciteit per volume-eenheid bekend zijn, is het voldoende het verloop van de bodemtemperatuur op één diepte dicht bij het oppervlak te meten.

IV

In een stationaire grenslaag boven een homogeen oppervlak (geen gradiënten in oppervlakteruwheid en -temperatuur) onder niet neutrale omstandigheden is de gemiddelde horizontale warmteflux niet gelijk aan nul.

V

Het gebruik van de bulkmethode voor het berekenen van de fluxen van impuls, voelbare warmte en waterdamp is boven ruwe oppervlakken niet goed mogelijk, omdat dan de bulkoverdrachtscoëffiënten te sterk afhankelijk zijn van de oppervlakteruwheid en de stabiliteit van de grenslaag (zie figuur 2.2 in dit proefschrift).

VI

Bij het gebruik van de flux-profiel relaties voor het berekenen van de fluxen van voelbare en latente warmte boven sterk verdampende oppervlakken kan de invloed van de vochtflux op de Monin-Obukhovlengte niet worden verwaarloosd.

VII

De term 2-dimensionale turbulentie is principiëel onjuist, omdat een aantal voor turbulentie karakteristieke processen niet in twee dimensies kunnen worden gerealiseerd.

VIII

De "Lyman-alfa", een instrument dat vaak hygrometer wordt genoemd, is niet in staat het vochtgehalte van de lucht te meten, doch meet slechts vochtfluctuaties.

IX

Door de grotere stabiliteit van de nachtelijke atmosferische grenslaag is de topsnelheid van motoren 's nachts gemiddeld hoger dan overdag.

X

Het gebruik van een tekstverwerker voor het opstellen van een proefschrift levert geen tijdsbesparing op voor de promovendus, maar neemt alleen de typistes werk uit handen.

XI

Wanneer men de tijd fysisch interpreteert zou het gezegde "grote gebeurtenissen werpen hun schaduw vooruit" moeten luiden "grote gebeurtenissen werpen hun schaduw achteruit".

XII

Inpoldering van de Waddenzee zou haar warmtebalans aanzienlijk vereenvoudigen.

ERRATA AT: HEAT BALANCE INVESTIGATIONS IN TIDAL AREAS

J.H. VAN BOXEL, 1986

PAGE	LINE	EQ.	PRINTED IS	THIS SHOULD BE
14	21		Q_l W m^{-2} heat production ….	Q_l W m^{-1} heat production ….
17	5-6		ratio of the molecular masses of dry air and water ($\varepsilon = M_d / M_w$)	ratio of the molecular masses of water and dry air ($\varepsilon = M_w / M_d$)
17	30		ω_n s^{-1} phase angle of the n^{th} harmonic	ω_n s^{-1} angular velocity of the n^{th} harmonic
25	33	2.5	$\rho_w c_w \frac{\partial T_w}{\partial t}$ = ...	$V_w \rho_w c_w \frac{\partial T_w}{\partial t}$ = ...
27	17		(2.5) through (2.11)	(2.6) through (2.11)
27	21	2.14	$Q_w = \rho_a L_w u_* q_*$	$Q_w = \rho_a L_e u_* q_*$
55	1		where $\varepsilon = M_d / M_w$	where $\varepsilon = M_w / M_d$
56	7		Monin-Obukhov length changes less than 0.1%	reciprocal Monin-Obukhov length changes less than 0.001 m^{-1}
65	16	3.23	U = 0.01 + 20 * | ∂H / ∂t |	U = 0.01 + 20 * 1800 * | ∂H / ∂t |
81	5	4.4	$\frac{Q_b}{Q_{bp}} = \frac{1}{1 - \alpha \frac{d_p}{A_p^{0.5}} \left(1 - \frac{\lambda_b}{\lambda_p}\right)}$.	$\frac{Q_{bp}}{Q_b} = \frac{1}{1 - \alpha \frac{d_p}{A_p^{0.5}} \left(1 - \frac{\lambda_b}{\lambda_p}\right)}$.
121	4		J.Am.Meteor.Soc. 19, 90-97	J.Appl.Meteor. 19, 90-97
127	10		…. masses of dry air and water vapor	…. masses of water vapor and dry air
127	11		($\varepsilon = M_d / M_w$)	($\varepsilon = M_w / M_d$)
127	27	A3.4	$\overline{w' T_s'} = \overline{w' T'} + \frac{0.3192}{\varepsilon} \overline{w' q'} - 2 \frac{\overline{T}\,\overline{U}}{C_s^2} \overline{u' w'}$	$\overline{w' T_s'} = \overline{w' T'} + \frac{0.3192}{\varepsilon} \overline{T}\,\overline{w' q'} - 2 \frac{\overline{T}\,\overline{U}}{C_s^2} \overline{u' w'}$

11/03/90, John van Boxel

VRIJE UNIVERSITEIT TE AMSTERDAM

HEAT BALANCE INVESTIGATIONS

IN TIDAL AREAS

VRIJE UNIVERSITEIT TE AMSTERDAM

HEAT BALANCE INVESTIGATIONS

IN TIDAL AREAS

ACADEMISCH PROEFSCHRIFT

ter verkrijging van de graad van
doctor in de wiskunde en natuurwetenschappen
aan de Vrije Universiteit te Amsterdam,
op gezag van rector magnificus dr. P.J.D. Drenth,
hoogleraar in de faculteit der sociale wetenschappen,
in het openbaar te verdedigen
op donderdag 17 april 1986 te 15.30 uur
in het hoofdgebouw der universiteit,
De Boelelaan 1105

door

JOHANNES HENDRICUS VAN BOXEL

geboren te Raamsdonk

Centre for Mathematics
and Computer Science
1986

Promotor	: prof. dr. H.F. Vugts
Copromotor	: prof. dr. ir. L. Wartena
Referent	: prof. dr. J.T.F. Zimmerman

VOORWOORD

Dat alleen mijn naam op de omslag van dit proefschrift prijkt, zou kunnen suggereren dat ik dit onderzoek in mijn eentje heb uitgevoerd. Dat is beslist niet het geval. Zeer velen hebben, ieder op hun eigen wijze, een bijdrage geleverd aan dit onderzoek. Een ieder die heeft meegewerkt aan de totstandkoming van dit proefschrift ben ik daarvoor zeer erkentelijk. Een aantal personen en instellingen wil ik nog met name noemen.

Promotor Hans Vugts, jij hebt een zeer grote bijdrage geleverd. In het eindstadium, bij het op papier zetten van de resultaten, waren je op- en aanmerkingen van onschatbare waarde. Ook in eerdere stadia werkte je enthousiasme inspirerend en in het veld liep je het hardst van allemaal.

Bert Wartena, jij hebt mij in Wageningen de eerste beginselen van de meteorologie bijgebracht. Dit promotieonderzoek heb je als co-promotor vanaf het begin gevolgd. Je kritieken heb ik steeds als bijzonder stimulerend ervaren.

Fred Cannemeyer, je was niet alleen een collega en een "klankbord" voor sommige van mijn problemen, maar zonder jou zouden de veldwerken zeer moeilijk uitvoerbaar geworden zijn. Je loopt wel iets minder hard dan Hans, maar je inzet is er niet minder om.

Sjef Zimmerman, als referent heb je via kritieken een bijdrage geleverd aan de uiteindelijke versie van dit proefschrift. Bovendien was het NIOZ, mede dank zij jouw hulp, bereid vele faciliteiten ter beschikking te stellen.

Henk Tennekes, jouw opmerkingen omtrent de tekst en inhoud van dit werk hebben de waarde ervan zeer zeker verhoogd.

De studenten Steve van Amerongen, Stephen Tjemkes, Ronald van der Bunt en Erik Lambooy hebben, in het kader van hun veldwerk meteorologie, zich ieder een maand beziggehouden met de dagelijkse beslommeringen van het veldwerk. Een deel van de door hun verzamelde en verwerkte gegevens is in dit proefschrift opgenomen.

De elektronische werkplaats, te weten Johan de Lange en Hans van Rheenen, waren steeds snel bereid te helpen wanneer er problemen waren met elektronische apparatuur. Daarvoor waren zij zelfs bereid de veilige beschutting van de VU te verlaten en de reis naar het Waddengebied te aanvaarden.

De mechanische werkplaats, bestaande uit Theo Hamer, Nico van Harlingen, Peter Ploeger, Hans Bakker en Jan Vink, bouwde een deel van de apparatuur. Ook waren zij steeds beschikbaar bij het opbouwen en afbreken van het veldwerk. Daarbij werden vaak lange dagen gemaakt en soms zeer lange dagen. Weer of geen

weer, het werk ging door. Soms stonden zij tot hun middel in het water, terwijl de laarzen slechts tot hun liezen reikten. Jongens bedankt voor jullie grandioze inzet.

Henri Sion tekende de meeste tekeningen en Cees van der Bliek, onze fotograaf, zorgde dat alle figuren haarscherp en op het juiste formaat werden afgedrukt. Saskia Kars typte een deel van de gegevens in en was tevens behulpzaam bij het samenvoegen van diverse computertekeningen tot een geheel.

Het NIOZ (Nederlands Instituut voor het Onderzoek der Zee) op Texel stelde zeer vele faciliteiten ter beschikking, zoals slaapverblijven op Texel, boten voor vervoer van apparatuur en mensen naar en van het Balgzand en diverse meetinstrumenten. Daarvoor ben ik de directie van het NIOZ zeer erkentelijk. Ook het technisch en het varend personeel van het NIOZ wil ik bedanken voor de prettige samenwerking.

De Vakgroep Natuur- en Weerkunde van de Landbouw Hogeschool te Wageningen stelde de naalden ter beschikking die gebruikt zijn voor de meting van het warmtegeleidingsvermogen van de wadbodem. In het bijzonder Ies van Haneghem en Hennie Boshoven wil ik hiervoor bedanken.

Tenslotte mag niet onvermeld blijven dat een deel van de in dit onderzoek gebruikte apparatuur kon worden aangeschaft dankzij een belangrijke financiele bijdrage van ZWO (Nederlandse Organisatie voor Zuiver-Wetenschappelijk Onderzoek).

CONTENTS

LIST OF SYMBOLS

SYMBOLS OF QUANTITIES	DIMENSION IN SI-UNITS	DESCRIPTION
A	K	amplitude of the temperature wave in the soil.
$\underline{a}$	$m^2 s^{-1}$	thermal diffusity of the soil.
a_h	$W\ m^{-2}$	constant for estimating net radiation.
a_i		constant for estimating net radiation (a_i = 0.660, Idso 1983).
A_j	K	variable in the modified Jaeger model.
A_n	K	amplitude of n^{th} harmonic in Fourier analysis.
a_n	K	Fourier cosine coefficient.
A_p	m^2	surface of the soil heat flux plate.
a_s	$W\ m^{-2}K^{-6}$	constant for estimating net radiation.
A_w	$W\ m^{-2}$	advection through the water.
A_1,A_2	m^2	surfaces.
a_2,a_3		constants in the profile theory (we used 1.0 for both).
B	K	variable in the modified Jaeger model.
b_h	$W\ m^{-2}$	constant for estimating net radiation.
b_i	mb^{-1}	constant for estimating net radiation (b_i = 5.95 * $10^{-5} mb^{-1}$, Idso 1983).
b_n	K	Fourier sine coefficient.
b_p	$W\ m^{-2}$	constant for estimating net radiation.
c_b	$J\ kg^{-1}K^{-1}$	specific heat of the soil
c_c	$J\ kg^{-1}K^{-1}$	specific heat of chalk.
C_d		aerodynamic drag coefficient.
C_E^*		e-power of the constant of Euler (1.78107...)
C_h		bulk aerodynamic coefficient for the exchange of sensible heat.

SYMBOLS OF QUANTITIES	DIMENSION IN SI-UNITS	DESCRIPTION
c_h		constant for estimating net radiation.
c_i	K^{-1}	constant for estimating net radiation (c_i = 1500 K^{-1}, Idso 1983).
c_l	$J\ K^{-1}m^{-1}$	specific heat per unit length of needle for thermal conductivity measurements.
c_p	$J\ kg^{-1}K^{-1}$	specific heat of air at constant pressure.
c_q	$J\ kg^{-1}K^{-1}$	specific heat of quartz.
C_s	$m\ s^{-1}$	sound velocity.
C_w		bulk aerodynamic coefficient for the exchange of water vapor.
c_w	$J\ kg^{-1}K^{-1}$	specific heat of water.
D	m	damping depth of the temperature wave in the soil.
d_h		constant for estimating net radiation.
d_p	m	thickness of the soil heat flux plates.
d_s	m	span between the sonic probe heads.
E	Ks	variable in the modified Jaeger model.
e		natural base of logarithms (2.71828...).
E_a	$J\ m^{-2}$	amount of energy accumulated per unit area in the water.
e_a	mb	water vapor pressure in the air.
E_m	J	amount of energy accumulated in the entire Mok Bay.
E_n	J	amount of heat stored in the Mok Bay.
e_n	mb	saturated water vapor pressure at wet bulb temperature.
E_v	J	energy content of a water volume
F	m^3s^{-1}	water flow through the tidal channel.

SYMBOLS OF QUANTITIES	DIMENSION IN SI-UNITS	DESCRIPTION
f_c	s^{-1}	cut off frequency.
F_d	$W\ m^{-2}$	heat flux divergence in the water.
F_t	W	advection of heat through the tidal inlet.
F_t'	W	heat flux through the tidal inlet.
F_w	m^3s^{-1}	water flow through the tidal inlet.
F_1-F_4	$W\ m^{-2}$	heat fluxes in the water.
g	m^2s^{-1}	gravitational acceleration.
H	$m\ NAP$	water level relative to NAP (Dutch standard level of reference).
h	m	water depth.
h_1,h_2	m	water level relative to the soil surface.
I	A	electric current.
k		the Von Karman constant (we used 0.41).
KNMI		Koninklijk Nederlands Meteorologisch Instituut (Royal Dutch Meteorological Institute).
L	m	Monin-Obukhov length.
l	m	length.
L_e	$J\ kg^{-1}$	latent heat of evaporation of water ($2.46*10^6\ J\ kg^{-1}$).
LST		local standard time (UTC + 2 hour).
L_v	m	Monin-Obukhov length with the moisture influence incorporated.
L_θ	m	Monin-Obukhov length when the moisture influence is neglected.
M_d	$kg\ kmol^{-1}$	molecular mass of dry air.
M_w	$kg\ kmol^{-1}$	molecular mass of water.
N		fractional cloud cover.
NAP		Dutch standard reference level.

SYMBOLS OF QUANTITIES	DIMENSION IN SI-UNITS	DESCRIPTION
NIOZ		Nederlands Instituut voor het Onderzoek der Zee (The Netherlands Institute for Sea Research).
NTC		thermistor temperature sensor with a negative temperature coefficient.
O_i	m^2	areas of the soil surface between contour lines.
O_w	m^2	wet surface of the Mok Bay.
P	mb	atmospheric pressure.
p		relative duration of bright sunshine.
P_c	s	period of a cyclic variation.
q		specific humidity.
q_a		average specific humidity.
Q_b	$W\ m^{-2}$	soil heat flux.
Q_{bi}	$W\ m^{-2}$	heat flux through a part of the tidal flat soil.
Q_{bp}	$W\ m^{-2}$	soil heat flux measured with the flux plates.
Q_h	$W\ m^{-2}$	sensible heat flux.
Q_{hs}	$W\ m^{-2}$	sensible heat flux measured by the sonic anemometer (uncorrected).
Q_l	$W\ m^{-2}$	heat production per unit length in the needle for thermal conductivity measurements.
Q_w	$W\ m^{-2}$	latent heat flux.
q_*		characteristic specific humidity.
-	m	radius of the needle used for thermal conductivity measurements.
R_l	$\Omega\ m^{-1}$	electric resistance per unit length.
R_n	$W\ m^{-2}$	net radiation.
R_{s0}	$W\ m^{-2}$	incoming short wave radiation across a horizontal plane at the outer limit of the atmosphere.

SYMBOLS OF QUANTITIES	DIMENSION IN SI-UNITS	DESCRIPTION
R_{s1}	$W\ m^{-2}$	incoming short wave radiation across a horizontal plane at the surface.
R_{s2}	$W\ m^{-2}$	short wave radiation reflected by the surface.
S	?	real signal (units depend on kind of signal).
s	?	measured or filtered signal.
S_e		solar elevation.
T	K or ^oC	temperature.
T_a	K	air temperature.
T_b	K or ^oC	soil temperature.
$\overline{T}_b$	K or ^oC	mean soil temperature.
T_d	K or ^oC	dry bulb temperature.
T_g	K	water temperature in the tidal inlet.
T_j	K	temperature of needle for thermal conductivity measurements.
T_j^*	^oC	corrected needle temperature.
T_n	^oC	wet bulb temperature.
t_r	s	response time.
T_{ref}	K	reference temperature.
T_s	K	temperature measured by the sonic anemometer.
T_v	K	virtual temperature.
T_w	K or ^oC	water temperature.
T_0	K	surface temperature.
t_0	s	time delay in the modified Jaeger model.
T_1, T_2	K	temperatures.
t_1, t_2	s	times.
U	$m\ s^{-1}$	water flow velocity.
u	$m\ s^{-1}$	horizontal wind speed.

SYMBOLS OF QUANTITIES	DIMENSION IN SI-UNITS	DESCRIPTION
U_1, U_2	$m\ s^{-1}$	water flow velocities at points 1 and 2.
u_*	$m\ s^{-1}$	friction velocity.
UTC	h	Universal time coordinated.
V_w	m^3	water volume of the Mok Bay.
V_x	$m\ s^{-1}$	component of the wind speed in the x-direction.
V_1, V_2	m^3	water volumes.
w	$m\ s^{-1}$	vertical wind speed.
X		function in the profile theory.
x	m	distance in the x-direction.
Y		function in the profile theory.
y		distance in the y-direction.
$y_1 - y_6$		constants in the profile theory.
z	m	height above the surface (negative in the soil).
z_0	m	roughness length.
z_1, z_2	m	reference height or depth.

GREEK SYMBOLS

SYMBOLS OF QUANTITIES	DIMENSION IN SI-UNITS	DESCRIPTION
α		albedo.
α_f		filter constant.
α_j		variable in the modified Jaeger model..
α_p		meter constant of the soil heat flux plates.
β		Bowen ratio.

SYMBOLS OF QUANTITIES	DIMENSION IN SI-UNITS	DESCRIPTION
γ	K^{-1}	psychrometer constant.
γ_j		constant in the modified Jaeger model..
ϵ		ratio of the molecular masses of dry air and water ($\epsilon = M_d/M_w$).
θ	K	potential temperature.
θ_v	K	virtual potential temperature.
θ_*	K	characteristic potential temperature.
λ	$W\ m^{-1}K^{-1}$	thermal conductivity of the soil.
λ_b	$W\ m^{-1}K^{-1}$	thermal conductivity of the soil.
λ_p	$W\ m^{-1}K^{-1}$	thermal conductivity of the soil heat flux plates.
ρ_a	$kg\ m^{-3}$	density of air.
ρ_b	$kg\ m^{-3}$	density of the soil.
ρ_c	$kg\ m^{-3}$	density of chalk.
ρ_q	$kg\ m^{-3}$	density of quartz.
ρ_w	$kg\ m^{-3}$	density of water.
σ	$W\ m^{-2}K^{-4}$	Stefan Bolzman constant ($5.67 * 10^{-8}\ W\ m^{-2}K^{-4}$).
	$N\ m^{-2}$	surface stress.
ϕ_h		function in the profile theory.
ϕ_m		function in the profile theory.
ϕ_n		phase angle of the n^{th} harmonic.
ϕ_w		function in the profile theory.
ψ_h		function in the profile theory.
ψ_m		function in the profile theory.
ψ_w		function in the profile theory.
ω	s^{-1}	angular velocity.
ω_n	s^{-1}	phase angle of the n^{th} harmonic.

CHAPTER 1

INTRODUCTION

In meteorology the interaction of the atmosphere with the underlying earth surface is of utmost importance. Solar radiation and the inputs of heat and water vapor at the surface are the main driving forces for most meteorological processes. The exchange of heat and water vapor between the surface and the atmosphere is strongly related to the radiation balance of the surface and, to a lesser extend, to the soil heat flux. One way of studying all these phenomena together is to investigate the heat balance, or energy balance, of the surface.

The heat balance of the earth surface has been the subject of many meteorological studies. Most of these studies deal with land or sea surfaces. The heat balance of tidal flats however has been scarcely investigated. Ayers (1965) published on the heat budget of Barnstable Harbour, Massachusetts, but he did not mention important terms such as evaporation and the loss of long wave radiation during the night. In 1975 Vugts and Zimmerman revealed the principle of the 15-day temperature cycle occurring on tidal flats. Andrews (1976) established that the albedo of water is less than that of the different tidal flat surfaces (especially under sunny weather conditions). For the temperature course in the tidal flat soil he found diurnal variations of 10 K just below the surface and about 3 and 0.5 K at depths of 15 and 40 cm (in summer). A comparison of the surface heat fluxes above water and above dry tidal flats showed that there is a considerable difference between the two surfaces in all seasons. Becht (1976) studied the heat balance of tidal flats with the aid of a laboratory model and concluded that the mathematical models he developed for the calculation of soil and water temperatures were useful for further research. Heath (1977) concluded that in Pauatahanui inlet, New Zealand, the heat exchange between the water and the mud flats (covering about 25 % of the bay) has a neglectable influence on the heat balance of the inlet. De Wilde and Berghuis (1979) described the course of water and sediment temperatures on a tidal flat in the Dutch Wadden Sea for a period of 17 months. Andrews (1980) measured the thermal properties of tidal flat soils and discussed the heat exchange between the soil

and the tidal waters. One of his conclusions is that under favourable conditions in summer enough heat is stored in the uppermost 25 *cm* of the sediment to heat a water layer of about 1.5 *m* in depth 0.5 *K* during the next tide. Harrison (1981) suggested that the heat transfer in muddy sediments is not entirely by conduction, but that percolating sea water is in itself a vehicle for heat transport. Vugts and Zimmerman (1982) carried out heat balance calculations for the Mok Bay in the Dutch Wadden area for three days in 1973. They concluded that, although their model could not predict the fine structure of the temperature curve, its behaviour is quite reasonable. Harrison (1985) found that temperature gradients in muddy inter-tidal sediments can be large, although these sediments remain saturated with water. He observed a 15-day period in the temperatures of the upper sediment layers, but not for the deeper (26.5 *cm*) levels. Vugts and Zimmerman (1985) described the heat balance for the Mok Bay for a 15-day period in 1974. They conclude that the water in the Mok Bay is not completely mixed and that it is possible to predict the change of the water temperature with a simple model and some "bulk"-parameters.

The tidal flat surface is very different from any land or sea surface. When the tidal flats are not inundated, they show little resemblance with a land surface, because the surface is extremely smooth, it remains very wet and there is hardly any vegetation. These features have direct consequences for the heat balance. When the tidal flats are flooded they differ from a sea or ocean, because they are much shallower, which causes temperature variations to be an order of magnitude larger than in open sea. The tidal cycle, which causes a periodic alternation between the flooded and the "dry" tidal flats, also has a periodicity in itself of about 15 days (Vugts and Zimmerman 1975). Also the tide moves enormous amounts of water, which can carry huge amounts of heat with them. All together this makes the heat balance of tidal flats quite different from that above a land or sea surface and it complicates the research.

A good insight of the heat balance of tidal areas is necessary to understand the ecology of the area, as well as many meteorological processes. The ecology of a tidal inlet is dependent on the thermal regime in the water and the soil, which is ruled by the heat balance. The importance of the thermal regime to the ecology of tidal areas was, for instance, recognized by and Heath (1977) and De Wilde and Berghuis (1979). The latter authors found from data, obtained in the field as well as in the laboratory, that for the bivalve Macoma Baltica the successive temperature maxima in spring play a role in the process of the liberation of the gametes. For most local meteorological processes the surface heat balance is an important factor, e.g. the formation of fog or boundary layer clouds and the development of land or sea breezes above the Dutch Wadden isles. These local processes may have a regional impact; e.g. boundary layer clouds can drift land inwards. Also a good

insight in the heat balance above tidal flats might contribute to the understanding of heat balances under other conditions.

The *aim* of this research is to provide a better understanding of the thermal conditions and the heat balance of tidal areas and to describe the heat fluxes above tidal flats and tidal waters. We tried to do this by developing models, which describe the course of the water temperature in a tidal area in relation with meteorological parameters. To verify the models, measurements have been carried out in the Dutch Wadden area during the summer seasons of 1982 and 1983. Also different methods of measuring the various terms of the heat balance are compared.

In the following, chapter two gives a theoretical background, which is needed to cope with the problem. Chapter three describes the measurements and their use in the provided theory. In chapter four some measurement methods are compared in order to be able to make a choice about which method should be used in the actual heat balance calculations. In chapter five the heat balance of tidal areas is treated for some different cases, using the measurement results and the last chapter contains the conclusions and some recommendations for further research. At the end of the thesis the references to literature and some appendices are given.

In this manuscript there are some departures from standard notations. Where times are used, they are in LST (local standard time), which is UTC plus 2 hours (in summer). A decimal point is used in stead of a decimal comma in order to keep the notations compatible with computer outputs. To avoid confusion a '*' was used as multiplication sign in stead of an 'x'.

CHAPTER 2

THEORETICAL BACKGROUND

In this chapter a review is given of the theory, which we need to investigate the heat balance of tidal flats. The application of this theory is treated in more detail in chapter 3. The issues dealt with in this section are heat balances and the ways to calculate the terms of these balances.

2.1. Heat balances.

According to the basic law of conservation of energy the change in energy of a system is equal to the algebraic sum of the energy fluxes into and out of the system. This is the most general form of a heat balance. Application of this definition to specific systems leads to different heat balances. In sections 2.1.1 and 2.1.2 two examples are given of a heat balance for a specific system. Other examples can be found in the literature. The heat balance of tidal flats has been investigated earlier by Vugts and Zimmerman (1975, 1982 and 1985) and by Becht (1976). Heath (1977) has written a paper on the heat balance of a coastal inlet with some tidal flats. The literature contains many publications about heat balances for non-tidal waters, for example Vugts (1974), Keijman (1974), Gunneberg (1976) and De Bruin (1982).

In this chapter the following **sign convention** is used: All heat fluxes into the evaluated system have a positive sign. So when evaluating the heat balance of a volume of water on the tidal flat, the sensible heat flux is called positive when it is directed downwards and the soil heat flux is called positive when it is directed upwards. The vertical axis (z-axis) is positive in the upward direction.

2.1.1. Heat balance at a fixed point.

There are two cases for the heat balance at a fixed point on the tidal flat, one describing the situation with water on the tidal flat and the other one describing the situation when the tidal flat is not inundated. First a heat balance will be derived for a column $(\Delta x, \Delta y, h)$ of water on the tidal flat. Later it will be evaluated what

the consequences are for the heat balance if there is no water on the tidal flat.

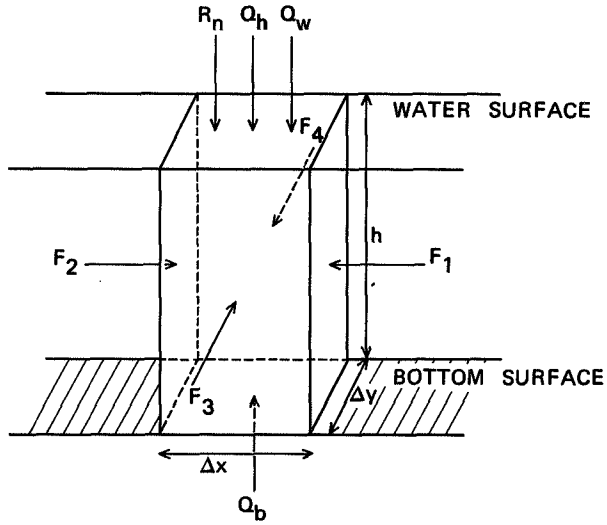

Figure 2.1: *Energy fluxes towards a volume of water.*

The thermal energy of the water column is defined by:

$$E_v = \rho_w c_w \, h \, (T_w - T_{ref}) \, \Delta x \, \Delta y \, , \qquad [W] \; (2.1)$$

where E_v is the thermal energy content of the water column, ρ_w is the density of water, c_w its the specific heat, T_w is the average water temperature in the evaluated column and T_{ref} is an arbitrary reference temperature. The heat balance for this volume of water can now be written as:

$$\frac{\partial}{\partial t}(\rho_w c_w \Delta x \, \Delta y \, h \, T_w) = \Delta x \, \Delta y \, (R_n + Q_h + Q_w + Q_b) + \\ + \Delta x \, h \, (F_3 + F_4) + \Delta y \, h \, (F_1 + F_2) \, , \qquad [W] \; (2.2)$$

where t is time, R_n is the net radiation and Q_h, Q_w and Q_b are the sensible, the latent and the soil heat flux respectively. F_1 through F_4 are the advective fluxes through the sides of the column (see figure 2.1).

When this equation is evaluated per unit area, all terms have to be divided by $\Delta x \, \Delta y$. When writing the advection $(F_1+F_2+F_3+F_4)$ as derived in section 2.4.1 that the heat balance per unit area can be written as:

$$\rho_w c_w \, h \frac{\partial T_w}{\partial t} = R_n + Q_h + Q_w + Q_b + A_w \, , \qquad [W \; m^{-2}] \; (2.3)$$

where A_w is the net advection of heat by the water. Heat balance formulas in literature often appear in a form similar to (2.3) (e.g. Keijman 1974, Gunneberg

1976, Vugts 1982).

When there is *no water on the tidal flat* the depth of the water layer reduces to zero. Therefore the energy amount of the evaluated system reduces to zero and also the advection through the layer of water becomes zero. In this case the application of the heat balance results in:

$$R_n + Q_h + Q_w + Q_b = 0 . \qquad [W\ m^{-2}]\ (2.4)$$

This equation describes the heat balance for the soil-air interface of a tidal flat which is not inundated.

2.1.2. Heat balance for an area.

The first series of experiments in this project was carried out in the Mok Bay. The bay consists mainly of tidal flats and has only one tidal inlet (for further information see section 3.1). This configuration makes the area very suitable for heat balance calculations. Therefore (2.3) will be adapted in such a way that it can reflect the heat balance of the entire Mok Bay. Because several parameters (for example the depth of the water layer) change with location, it is not possible to write the heat balance for an area as a "surface heat balance" per unit area. The heat balance will be written as a total heat balance for the area, applied to the total volume of water in the bay. Therefore all the terms in (2.3) have to be integrated over the entire area. In the term on the left hand side of equation 2.3 (describing the temperature change of the water) the depth of the water layer has to be replaced by the volume of the water in the bay and the water temperature has to be replaced by the mean temperature of the water in the bay. On the right hand side the net radiation, the sensible heat flux and latent heat flux have to be multiplied by the area in the bay that is covered with water, since the heat exchanges at the dry area do not contribute directly to the change of the water temperature. The advection through the layer of water has to be replaced by a term which describes the advection for the entire area. This term is the advection of heat through the tidal inlet. The soil heat flux depends on how long ago the soil has been flooded and on how much heat has been stored in the soil when it was not covered with water. Therefore the bottom surface is split up into areas between contour lines of equal depth (using the contour lines shown in figure 3.2) and the soil heat flux in each flooded area is calculated separately. These changes result in the following heat balance:

$$\rho_w c_w \overline{\frac{\partial T_w}{\partial t}} = O_w{}^*(R_n + Q_h + Q_w) + F_t + \sum_{flooded} O_i Q_{bi} , \qquad [W]\ (2.5)$$

where O_w is the area covered with water, F_t is the advection of heat through the tidal inlet, O_i's are the separate areas of the bottom surface between the contour

lines and Q_{bi} is the soil heat flux through that surface.

When it is assumed that the whole volume of water in the bay is competely mixed, the temperature of the water leaving the bay (during the ebb-tide) will be equal to the water temperature of the Mok bay water volume. The mean water temperature can be calculated from the heat balance, provided all the other terms are known. Comparison of the calculated water temperature with the temperature of the water leaving the bay (which is measured), gives information on whether important terms have been neglected in the heat balance in (2.5), on the assumptions which have been made and the precision of the measurement of the terms in the heat balance.

2.2. Sensible and latent heat flux.

The equations which describe the sensible and latent heat fluxes are treated in one section because they are very similar and because they are not independent.

The sensible and latent heat fluxes can be calculated from measurements in several ways. Three of them are described in this section, namely the eddy correlation method, the profile method and the bulk method. The eddy correlation method has the best physical foundation, but it also requires the most extensive measurements and calculations and the most expensive equipment. The profile method requires less extensive measurements, but the equations which describe the heat fluxes are semi-empirical. The bulk method requires only simple measurements, but it is based on a crude approximation of the physics and important features (like stability of the atmosphere) are often neglected.

2.2.1. The eddy correlation method.

In a turbulent air flow, parcels of air are transported upwards and downwards continuously due to eddy motion. When the average temperature of the air going up is higher than the average temperature of the air going down, the eddy motion results in a sensible heat flux directed upwards (negative, see section 2.1). In a similar way eddy motion causes a transport of latent heat (moisture) and momentum. When the fluctuations of horizontal wind speed, vertical wind speed, temperature and humidity are measured simultaneously, it is possible to calculate the vertical flux of horizontal momentum, τ, the sensible heat flux, Q_h and the latent heat flux, Q_w from (Monin & Yaglom 1971):

$$\tau = -\rho_a \overline{u'w'} , \qquad [N\ m^{-2}]\ (2.6)$$

$$Q_h = -\rho_a c_p \overline{w'\theta'} , \qquad [W\ m^{-2}]\ (2.7)$$

$$Q_w = -\rho_a L_e \overline{w'q'} , \qquad [W\ m^{-2}]\ (2.8)$$

where ρ_a is the density of air, c_p is the specific heat of air at constant pressure, L_e is the latent heat of vaporization of water and u', w', θ' and q' are the deviations of the horizontal wind velocity, vertical wind velocity, potential temperature and specific humidity from the respective averages. The bars denote time averaging. The minus signs in (2.6) to (2.8) indicate that τ, Q_h and Q_w are defined positive if they are directed downward (see section 2.1). The correlation products in (2.6) to (2.8) can be used to define the friction velocity, u_*, the characteristic potential temperature, θ_* and the characteristic specific humidity, q_* as:

$$u_* = (-\overline{u'w'})^{0.5} = -\overline{u'w'}/u_* , \qquad [m\ s^{-1}]\ (2.9)$$

$$\theta_* = -\overline{w'\theta'}/u_* , \qquad [K]\ (2.10)$$

$$q_* = -\overline{w'q'}/u_* . \qquad [-]\ (2.11)$$

These characteristic quantities are essential in profile theory, as will be shown in the next section.

From the combination of the (2.5) through (2.11) it follows that the fluxes can be written as:

$$\tau = \rho_a u_* u_* , \qquad [N\ m^{-2}]\ (2.12)$$

$$Q_h = \rho_a c_p u_* \theta_* , \qquad [W\ m^{-2}]\ (2.13)$$

$$Q_w = \rho_a L_w u_* q_* . \qquad [W\ m^{-2}]\ (2.14)$$

This notation shows the similarity between the description of the fluxes of momentum, sensible heat and latent heat. It is preferred to use the (2.9) through (2.14) (instead of (2.6) through (2.8)) to describe the turbulent fluxes, because this notation is more consistent with the profile theory.

2.2.2. The flux-profile relationships.

We now turn to the flux-profile relationships and the integration of the profile formulas. In the last part of this section the effect of latent heat flux (moisture transport) on the Monin-Obukhov length is treated. This effect is discussed separately because moisture transport can have a considerable effect on the Monin-Obukhov length when measurements are carried out above water or a very wet surface (such as a "dry" tidal flat).

Many authors (e.g. Busch 1973, Businger 1973, Wieringa 1980 and Dyer 1982) describe the profiles of wind velocity, potential temperature and specific humidity with the following equations:

$$\frac{\partial u}{\partial z} = \frac{u_*}{k\,z}\,\phi_m(z/L)\,, \qquad [s^{-1}]\ (2.15)$$

$$\frac{\partial \theta}{\partial z} = \frac{\theta_*}{k\,z}\,\phi_h(z/L)\,, \qquad [K\ m^{-1}]\ (2.16)$$

$$\frac{\partial q}{\partial z} = \frac{q_*}{k\,z}\,\phi_w(z/L)\,, \qquad [m^{-1}]\ (2.17)$$

where k is the Von Karman constant, z the height above the surface. L, the Monin-Obukhov length, is a parameter which indicates the stability of the atmospheric surface layer. It is negative when the stability is unstable and positive during stable stabilities. In neutral situations it is near infinity. This parameter will be defined more precisely later on in this section. ϕ_m, ϕ_h and ϕ_w are the following functions of z/L:
for $z/L \leq 0$ (unstable)

$$\phi_m = (1-y_1\,z/L)^{-0.25}\,, \qquad (2.18)$$

$$\phi_h = a_2(1-y_2\,z/L)^{-0.50}\,, \qquad (2.19)$$

$$\phi_w = a_3(1-y_3\,z/L)^{-0.50} \qquad (2.20)$$

and for $z/L > 0$ (stable)

$$\phi_m = 1 + y_4\,z/L\,, \qquad (2.21)$$

$$\phi_h = a_2 + y_5\,z/L\,, \qquad (2.22)$$

$$\phi_w = a_3 + y_6\,z/L\,. \qquad (2.23)$$

The Von Karman constant and the constants a_2, a_3 and y_1 through y_6 have been established by many authors (Webb 1970, Dyer 1970, Businger 1971, Wieringa 1980, Dyer 1982 and others). Where in our investigations the flux-profile relationships have been applied, the constants published by Wieringa (1980) have been used, i.e. $k=0.41$, $a_2=a_3=1.0$, $y_1=22$, $y_2=y_3=13$, $y_4=6.9$ and $y_5=y_6=9.2$.

Paulson (1970) integrated (2.15) through (2.23) for unstable cases ($z/L<0$) and Webb (1970) published the results of the integration for stable cases. Their results can be written in the form:

$$u(z) = \frac{u_*}{k}(ln(z/z_0) - \psi_m(z/L))\,, \qquad [m\ s^{-1}]\ (2.24)$$

$$\theta(z) = \frac{\theta_*}{k}(ln(z/z_0) - \psi_h(z/L)) + \theta(z_0) \ , \qquad [K] \ (2.25)$$

$$q(z) = \frac{q_*}{k}(ln(z/z_0) - \psi_w(z/L)) + q(z_0) \ , \qquad [kg\ kg^{-1}] \ (2.26)$$

where z_0 is the roughness length of the underlying surface. For *unstable cases* the following nondimensional functions ψ_m, ψ_h and ψ_w are used (according to Paulson 1970):

$$\psi_m = 2\ \ln(\frac{1+X}{2}) + \ln(\frac{1+X^2}{2}) - 2\ arctg(X) + \pi/2 \ , \qquad (2.27)$$

$$\psi_h = \psi_w = 2\ln(\frac{1+Y^2}{2}) \ , \qquad (2.28)$$

with:

$$X = (1 - y_1\ z/L)^{0.25} \ , \qquad (2.29)$$

$$Y = (1 - y_2\ z/L)^{0.25} \ . \qquad (2.30)$$

For *stable cases* The following functions are used (Webb 1970):

$$\psi_m = -y_4\ z/L \ , \qquad (2.31)$$

$$\psi_h = \psi_w = -y_5\ z/L \ . \qquad (2.32)$$

Using equation (2.24) through (2.32), fitting the measured profile data, results in values for u_*, θ_* and q_*, which can be used to calculate the sensible and latent heat flux with (2.13) and (2.14).

The last part of this section discusses the calculation of the *Monin-Obukhov length*. A formula for the Monin-Obukhov length often found in the literature (for example Businger 1973) is:

$$L_\theta = -\frac{T}{k\ g}\frac{u_*^3}{\overline{w'\ \theta'}} \ , \qquad [m] \ (2.33)$$

where T is the absolute temperature and g the acceleration of gravity. Eq. (2.33) is equivalent with:

$$L_\theta = +\frac{T}{k\ g}\frac{u_*^3}{u_*\ \theta_*} \ . \qquad [m] \ (2.34)$$

Over water surfaces the effect of moisture fluctuations on the density fluctuations cannot be neglected any more. Therefore the Monin-Obukhov length is written correctly as (Busch 1973):

$$L_v = -\frac{T_v}{k\ g}\frac{u_*^3}{\overline{w'\ \theta_v'}} \ , \qquad [m] \ (2.35)$$

where T_v is the virtual temperature (in K) and θ_v is the virtual potential temperature. It can be derived that this formulation is equivalent with:

$$L_v = \frac{T}{k\ g}\ \frac{u_*^3}{u_*\theta_* + T(1/\epsilon - 1)u_* q_*}\ , \qquad [m]\ (2.36)$$

(see for example Bush 1973 eq. 7.12 and 7.13) where ϵ is the ratio of the molecular masses of water vapor and dry air ($\epsilon = M_w/M_d$). Substitution of $u_*\theta_*$ by $Q_h/\rho_a c_p$ (eq. 2.13) and $u_* q_*$ by $Q_w/\rho_a L_e$, introduction of the Bowen ratio ($\beta = Q_h/Q_w$) and assuming $T = 290K$, $c_p = 1010\ J\ K^{-1}kg^{-1}$ and $L_e = 2.46*10^6\ J\ kg^{-1}$ leads to:

$$L_v = L_\theta\ \frac{1}{1 + 0.073/\beta}\ . \qquad [m]\ (2.37)$$

From this equation the effect of neglecting the influence of the moisture fluctuations on the Monin-Obukhov length can be evaluated. Over land the Bowen ratio is typically of the order 1 and the error in the Monin-Obukhov length due to the neglect of moisture fluctuations will be in the order of 7%. Over water surfaces the Bowen ratio usually is much smaller and the error will be considerable. In section 4.1.1 the magnitude of the error in the calculated heat fluxes will be discussed, when the influence of moisture fluctuations on the Monin-Obukhov length is neglected.

2.2.3. The bulk formulas.

The fluxes of momentum, sensible heat and latent heat can be described in terms of bulk coefficients by:

$$\tau = \rho_a\ C_d\ u(z_1)^2\ , \qquad [N\ m^{-2}]\ (2.38)$$

$$Q_h = \rho_a\ c_p\ C_h\ u(z_1)\ (\theta(z_1) - \theta(0))\ , \qquad [W\ m^{-2}]\ (2.39)$$

$$Q_w = \rho_a\ L_w\ C_w\ u(z_1)\ (q(z_1) - q(0))\ . \qquad [W\ m^{-2}]\ (2.40)$$

Many authors have published values for the bulk transfer coefficients C_d, C_h and C_w, e.g. Hicks (1975), Dunkel et al. (1974), Emmanuel (1975), Friehe (1976) and Rao et al. (1980). Reviews on this subject have been written by Robinson (1966), Pond et al. (1974) and Hicks (1975). Most authors found bulk transfer coefficients in the range from $1.2*10^{-3}$ to $1.5*10^{-3}$ (when the height z_1 is taken equal to 10 m). Some investigators found bulk transfer coefficients depending on the wind velocity, e.g. Kondo and Naito (1972), Wieringa (1973), Hicks (1975) and Vugts and Cannemeijer (1981).

The values of the bulk transfer coefficients can be estimated more or less theoretically from comparison of the bulk formulas with the flux-profile

relationships. Combination of (2.39) and (2.40) with (2.24) to (2.26) and substitution of the heat fluxes by (2.13) and (2.14) gives:

$$C_h = C_w = k^2 \, [ln(z_1/z_0) - \psi_m(z_1/L)]^{-1} \, [ln(z_1/z_0) - \psi_h(z_1/L)]^{-1} \, , \quad (2.41)$$

where ψ_m and ψ_h are defined by (2.27) through (2.32). A similar equation can be deduced for the bulk transfer coefficient for momentum. Equation (2.41) shows that the bulk transfer coefficients for heat and water vapor are functions of z_1/L. In figure 2.2 isopleths of C_h ($=C_w$) have been drawn as a function of z_1/z_0 and z_1/L. It can be seen from this figure that the changes in the bulk transfer coefficients due to stability are smaller when z_1/z_0 becomes larger. The arrows indicate the situation above grassland ($z_1=10$ *m* and z_0 is in the order of 10 *mm*) and above tidal flats ($z_1=10$ *m* and z_0 in the order of 0.1 *mm*). Above grassland the ratio of the bulk transfer coefficients at $z_1/L=-0.25$ to that at $z_1/L=+0.25$ is 2.1. Above a tidal flat this ratio is 1.6.

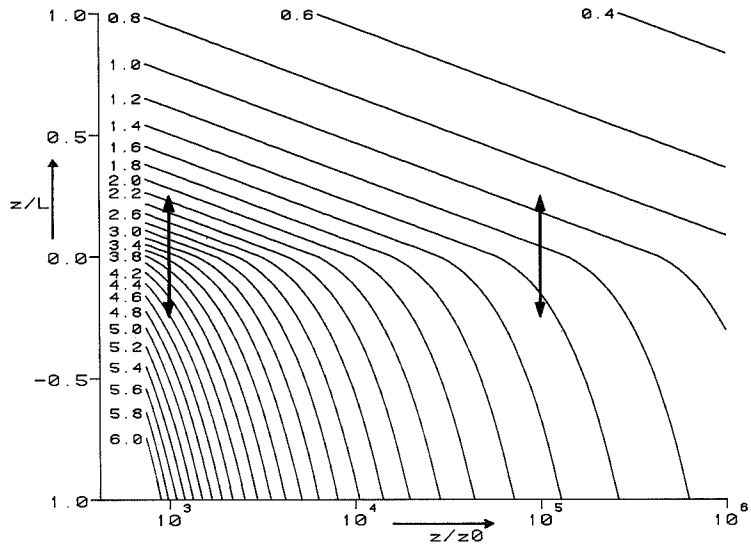

Figure 2.2: *Isopleths of C_h ($*10^3$) as a function of z_1/z_0 and z_1/L.*

The scatter in the bulk transfer coefficients which is found in the literature is not surprising, since the authors calculated the coefficients from measurements under different circumstances. In most applications the bulk transfer coefficients are considered as constants. This can lead to a reasonable accuracy only if they do not change too much due to changes in surface roughness and/or stability. So the bulk formulas with constant transfer coefficients can only be applied in areas with low roughness at near neutral conditions.

In chapter 4 the results from the bulk formulas will be compared with heat fluxes calculated from the profile method, to see whether the bulk formulas are accurate enough for heat balance calculations on tidal flats.

2.3. The soil heat flux.

Usually the soil heat flux is small compared to other terms of the heat balance. However just after the tidal flats have been flooded the soil heat flux can be considerable, because the heat accumulated during the dry tide is returned rather quickly.

In this section it is discussed how the soil heat flux can be obtained directly from the temperature gradient, or from the change of the temperature profile in the soil. We also review the theory about the propagation of temperature waves in the soil.

2.3.1. The gradient method.

The thermal conductivity is defined as the ratio of the heat flux and the temperature gradient (Carlslaw and Jaeger 1959). Therefore the soil heat flux can be expressed as:

$$Q_b = -(\lambda \frac{\partial T_b}{\partial z})_{z=0}, \qquad [W\ m^{-2}] \quad (2.42)$$

where λ is the thermal conductivity of the soil, T_b is the soil temperature and z is the depth.

For the magnitude of the thermal conductivity of the tidal flat soil see section 3.8.5. When the tidal flats are not covered with water the surface temperature has to be estimated from measurements at lower levels. This extrapolation can lead to considerable errors, especially since the gradient has to be calculated from the difference between two temperatures. The magnitude of these errors will be shown in section 4.2.1.

2.3.2. The profile integration method.

All the heat going into the soil through the surface is used to heat the soil, assuming that no evaporation takes place in the soil, that the soil is horizontally homogeneous (no lateral heat fluxes) and that the heat production in the soil due to chemical and biological processes is negligible. Therefore the soil heat flux can be written as:

$$Q_b = -\int_{-\infty}^{0} \rho_b c_b \frac{\partial T_b(z)}{\partial t} \partial z, \qquad [W\ m^{-2}] \quad (2.43)$$

where ρ_b is the density of the soil, c_b is the specific heat of the soil and t is the

time. In practice measurements are carried out on a finite number of depths and at finite time intervals. Then the integration can be written as a sum:

$$Q_b = - \frac{\rho_b c_b}{\Delta t} \sum_i \Delta z_i \, \Delta T_{bi} \, , \qquad [W \, m^{-2}] \; (2.44)$$

where Δt is the time interval used, ΔT_{bi} is the change in temperature of sensor i during the time interval and Δz_i is the thickness of the layer for which the temperature change ΔT_{bi} is representative.

This method is preferred to the gradient method for the following reasons:

It makes better use of all the temperatures measured at different levels. The gradient method only uses the temperature measurements at the highest levels. Therefore when using the profile integration method there is a greater chance that measurement errors are averaged out.

Both methods are based on the measurements of temperature differences. With the profile integration method the temperatures measured with the same sensor are subtracted, while the gradient method subtracts the temperatures measured with different sensors. Therefore the profile integration method is far less sensitive to calibration errors than the gradient method.

2.3.3. Propagation of temperature waves in the soil.

In order to use the gradient method, we have to determine experimentally the thermal diffusity of the soil. This can be done with the aid of the theory that describes the propagation of sinusoidal temperature waves in the soil.

Van Wijk (1966) and Monteith (1973) give rather complete descriptions of the behavior of sine shaped waves in the soil. The main features are summarized below. When the physical properties of the soil are constant with depth, the heat conduction equation can be written as:

$$\frac{\partial T_b}{\partial t} = \underline{a} \, \frac{\partial^2 T_b}{(\partial z)^2} \, , \qquad [K \, s^{-1}] \; (2.45)$$

where $\underline{a}$ is the thermal diffusity of the soil. The thermal diffusity of the soil is equal to:

$$\underline{a} = \frac{\lambda}{\rho_b c_b} \, , \qquad [m^2 s^{-1}] \; (2.46)$$

where λ, ρ_b and c_b are the thermal conductivity, the density and the specific heat of the soil, respectively.

One set of boundary conditions for which the differential equation (2.45) can be solved analytically is a surface temperature that varies sinusoidally and a constant

temperature at infinite depth, equal to the average surface temperature:

$$T_b(0,t) = \overline{T_b} + A(0)\ sin(\omega\ t) \qquad [K]\ (2.47)$$

$$T_b(-\infty,t) = \overline{T_b}\ . \qquad [K]\ (2.48)$$

where $\overline{T_b}$ is the average surface temperature, $A(0)$ is the amplitude of the temperature wave at the surface (zero depth) and ω is the angular velocity of the wave, So ω is described by:

$$\omega = \frac{2\ \pi}{P_c}\ , \qquad [rad\ s^{-1}]\ (2.49)$$

with P_c equal to the period. Under these conditions the differential equation (2.45) can be solved, leading to:

$$T_b(z,t) = \overline{T_b} + A(z)\ sin(\omega\ t + z/D)\ , \qquad [K]\ (2.50)$$

with

$$A(z) = A(0)e^{+z/D}\ , \qquad [K]\ (2.51)$$

where $A(z)$ is the amplitude at depth z (note that the depth is taken negative in the downward direction). The damping depth, D, is the depth where the amplitude of a sinusoidal temperature variation is reduced to e^{-1} (=0.3678...) times the amplitude at the surface. the damping depth is related to the thermal properties of the soil and the angular velocity of the wave by:

$$D = (\ 2\ \underline{a}/\omega\ )^{0.5}\ . \qquad [m]\ (2.52)$$

From the equations 2.51 and 2.52 it can be derived that in the case of a sinusoidally varying surface temperature the thermal diffusity of the soil can be calculated from:

$$\underline{a} = \frac{\omega}{2}\ \frac{(z_1 - z_2)^2}{[ln(A(z_1)) - ln(A(z_2))]^2}\ , \qquad [m^2 s^{-1}]\ (2.53)$$

where z_1 and z_2 are two different depths. Eq. (2.53) is often used to calculate the thermal diffusity of the soil. Andrews (1980, Harrison (1981) and Vugts and Zimmerman (1985) used it to calculate the thermal diffusity of a tidal flat soil. Harrison (1981) found a large scatter in the calculated values, which can be explained by the fact that the surface temperature on tidal flats does not vary sinusoidally.

Because the surface and soil temperatures on tidal flats do not behave sinusoidally, the above theory is expanded, according to Van Wijk (1966), to give a description of non-sinusoidal periodic temperature variations. With the aid of Fourier analysis the temperature variation at the surface can be written as a sum of sine and cosine functions:

$$T_b(0,t) = \overline{T_b} + \sum_{n=1}^{\infty} [a_n cos(n\ \omega_1\ t) + b_n sin(n\ \omega_1\ t)] , \qquad [K]\ (2.54)$$

where n is an integer number varying from 1 to infinity and ω_1 is the angular velocity of the first harmonic, given by (2.49). The coefficients a_n and b_n can be found with Fourier analysis. Equation 2.54 can be written as:

$$T_b(0,t) = \overline{T_b} + \sum_{n=1}^{\infty} [A_n(0)\ sin(n\ \omega_1\ t + \phi_n)] , \qquad [K]\ (2.55)$$

where $A_n(0)$ is the amplitude (at zero depth) of the n-th harmonic and ϕ_n is the phase angle of the n-th harmonic. In this way each periodic surface temperature variation can be written as a superposition of sinusoidal temperature variations, which leads to the following solution of the equation of heat conduction:

$$T_b(z,t) = \overline{T_b} + \sum_{n=1}^{\infty} [A_n(z)\ sin(n\ \omega_1\ t + \phi_n - z/D_n)] , \qquad [K]\ (2.56)$$

with

$$A_n(z) = A_n(0)e^{-z/D_n} , \qquad [K]\ (2.57)$$

$$D_n = \left(2\frac{\underline{a}}{n\ \omega_1} \right)^{0.5} , \qquad [m]\ (2.58)$$

From these equations the decrease of the amplitude with depth can be evaluated separately for each harmonic, to give the thermal diffusity $\underline{a}$ with the aid of (2.53) (use $\omega_n = n * \omega_1$ in stead of ω). All harmonics should give the same thermal diffusity, provided that the properties of the soil are constant with depth (Wartena 1959).

2.4. Advection of heat through the water.

Due to the tidal movement huge amounts of water are moved to and fro continuously. For example in a small bay like the Mok bay the tidal discharge is about $10^6\ m^3$ and through a big tidal inlet like the Marsdiep the discharge is about $10^9\ m^3$ per tide (Zimmerman 1976).

The advection term in the heat balance is rather important because the specific heat of water is large. In the foregoing, two types of advection terms have been mentioned, one describing the advection at one point and the other one describing the flux from an entire area. These two items will be discussed below.

2.4.1. The advection term at one point.

The advection of heat at one point on the tidal flat will be evaluated with the aid of figure 2.3. In figure 2.3 h_1, U_1 and T_1 are the water depth, velocity of the water flow and the water temperature at a given instant at point 1. $Arctan(\Delta h/\Delta x)$ is the slope of the bottom surface. The x-axis is chosen parallel to the water flow direction, so the water flow in the y-direction is zero.

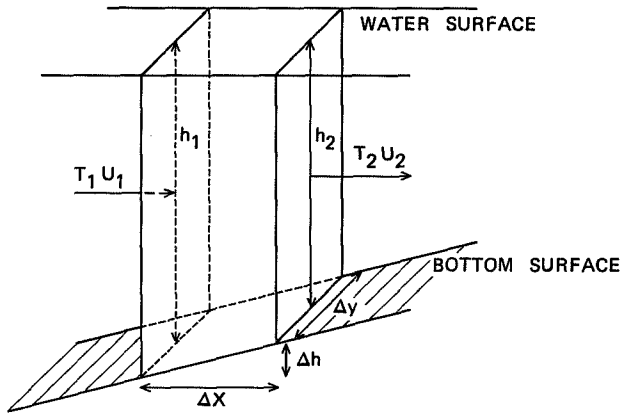

Figure 2.3: *Net flux of heat through the water.*

The heat flux divergence is the difference between the amount of heat entering the volume $\bar{h}\,\Delta y\,\Delta x$ ($\bar{h}$ is the average depth in the volume) through the surface $h_1\Delta y$ and the amount of heat leaving the volume through the surface $h_2\Delta y$. So the flux divergence of heat per unit area is:

$$F_d = \rho_w c_w \frac{h_1 U_1 T_1 \Delta y}{\Delta x\ \Delta y} - \rho_w c_w \frac{H_2 U_2 T_2 \Delta y}{\Delta x\ \Delta y} =$$

$$= \frac{\rho_w c_w}{\Delta x} (h_1 U_1 T_1 - h_2 U_2 T_2)\ , \qquad [W\ m^{-2}]\ (2.59)$$

where F_d is the flux divergence. It can be seen easily that:

$$h_1U_1T_1 - h_2U_2T_2 = (U_1-U_2)\frac{h_1+h_2}{2}\,\frac{T_1+T_2}{2} + (h_1-h_2)\frac{U_1+U_2}{2}\,\frac{T_1+T_2}{2} +$$

$$+(T_1-T_2)\frac{h_1+h_2}{2}\,\frac{U_1+U_2}{2} + \frac{1}{4}(U_1-U_2)(h_1-h_2)(T_1-T_2) \qquad [m^2Ks^{-1}]\ (2.60)$$

When Δx is taken small then $|U_1-U_2| \ll |U_1+U_2|$, $|h_1-h_2| \ll |h_1+h_2|$ and $|T_1-T_2| \ll |T_1+T_2|$, so the last term in (2.60) can be neglected. Substitution of (2.60) into (2.59) and writing the equation as a differential equation gives the following result for a given instant in time:

$$F_d = \frac{\rho_w c_w}{\partial x}(-h\,T_w\,\frac{\partial U}{\partial x}\partial x - U\,T_w\,\frac{\partial h}{\partial x}\partial x - U\,h\,\frac{\partial T_w}{\partial x}\partial x) \quad [W\,m^{-2}]\ (2.61)$$

Since $\rho_w\,\partial h/\partial t$ is the change of mass per unit area (due to a change in the water level), it can be derived in a similar way that:

$$\rho_w\frac{\partial h}{\partial t} = -\rho_w h\,\frac{\partial U}{\partial x} - \rho_w U\,\frac{\partial h}{\partial x}\,. \qquad [kg\,m^{-2}s^{-1}]\ (2.62)$$

The quantity $\partial U/\partial x$, which is difficult to measure, can be eliminated from 2.61 by substitution of 2.62, resulting in:

$$F_d = -\rho_w c_w U\,h\,\frac{\partial T_w}{\partial x} + \rho_w c_w T_w\,\frac{\partial h}{\partial t}\,. \qquad [W\,m^{-2}]\ (2.63)$$

This equation shows that the flux divergence term consists of a term which describes the heat advection and one that describes the change of the mass per unit area (due to a change of the water level). The advection of heat is given by:

$$A_w = -\rho_w c_w U\,h\,\frac{\partial T_w}{\partial x}\,. \qquad [W\,m^{-2}]\ (2.64)$$

This advection term is used in the heat balance. The last term of 2.63 is not neglected, it is eliminated because it also appears on the left side of the heat balance (eq. 2.3) in the term that describes the accumulation of heat in the water, as will be shown in section 2.5.1.

2.4.2. The advection term for the entire Mok Bay.

The flux of heat through the tidal channel into the bay is given by:

$$F_t' = \rho_w\,c_w\,F_w\,T_g\,, \qquad [W]\ (2.65)$$

where T_g is the water temperature in the tidal inlet (in K) and F_w is the flux of water through the tidal inlet (positive if directed towards the bay). The flux of

water can be related to the change of the water volume in the bay by:

$$F_w = \frac{\partial V_w}{\partial t} . \qquad [m^3 s^{-1}] \ (2.66)$$

In equation 2.71 (derived in section 2.5.2) the second term also contains $\partial V_w / \partial t$. This term is a direct consequence of the advection of mass (water) to or from the bay. Therefore this term is incorporated in the advection term resulting in:

$$F_t = \rho_w c_w (T_g - \overline{T_w}) \frac{\partial V_w}{\partial t} , \qquad [W] \ (2.67)$$

where F_t is the advection of heat through the tidal inlet and $\overline{T_w}$ is the average temperature of the bay water. Defined in this way, the advection term describes the contribution of the tidal flows to the change of the average temperature of the bay water. Of course the contribution of advection to the change of the bay water temperature is zero when the temperature of the water entering the bay is equal to the bay water temperature. This is described correctly by equation 2.67.

2.5. Energy accumulation.

The accumulation of energy in the water will be discussed for two cases, the first one being the accumulation of energy per unit area at a fixed point and the second one the accumulation of energy integrated over the entire Mok bay.

2.5.1. Accumulation of heat at a fixed point.

The change in time of the amount of energy accumulated per unit area in a volume of water (with depth h and of unit area) is given by:

$$\frac{\partial E_a}{\partial t} = \frac{\partial}{\partial t} (\rho_w c_w h \ T_w) . \qquad [W \ m^{-2}] \ (2.68)$$

The density of the water ρ_w and its specific heat, c_w, are considered as constants. Since both the depth and the water temperature vary with time, equation 2.68 can be written as:

$$\frac{\partial E_a}{\partial t} = \rho_w c_w h \frac{\partial T_w}{\partial t} + \rho_w c_w T_w \frac{\partial h}{\partial t} . \qquad [W \ m^{-2}] \ (2.69)$$

In equation 2.69 the first term describes the change of the amount of energy accumulated due to the change of the water temperature and the second one the change due to the change of the water depth. The second term is eliminated from the heat balance, because it also appears on the right side of the equality sign in (2.3) in the advection term (see section 2.4.1). It is logical that this term also appears in the advection term, because the volume of water needed to change the water depth, has

to be provided by advection.

2.5.2. Accumulation of heat in the entire Mok Bay.

Analogous to equation 2.68 the change of the amount of heat stored in the Mok bay, E_m, is given by:

$$\frac{\partial E_m}{\partial t} = \frac{\partial}{\partial t} (\rho_w \, c_w \, \overline{T_w} \, V_w) \, , \qquad [W] \ (2.70)$$

where $\overline{T_w}$ is the average water temperature in the Mok bay and V_w is the water volume of the bay. ρ_w and c_w are considered to be constants, but $\overline{T_w}$ and V_w vary with time, so

$$\frac{\partial E_m}{\partial t} = \rho_w c_w V_w \frac{\partial \overline{T_w}}{\partial t} + \rho_w c_w \overline{T_w} \frac{\partial V_w}{\partial t} \, . \qquad [W] \ (2.71)$$

The first term of 2.71 is on the left side of the heat balance for the entire Mok bay (eq. 2.5). The second term is due to the advection of water and therefore incorporated in the advection term (see section 2.4.2).

CHAPTER 3

MEASUREMENT AND CALCULATION OF THE FLUXES

Measurements were carried out during two summer seasons on tidal flats in the Dutch Wadden area. In 1982 measurements were performed in the Mok Bay and in 1983 on the Balgzand. Figure 3.1 indicates the location of these sites.

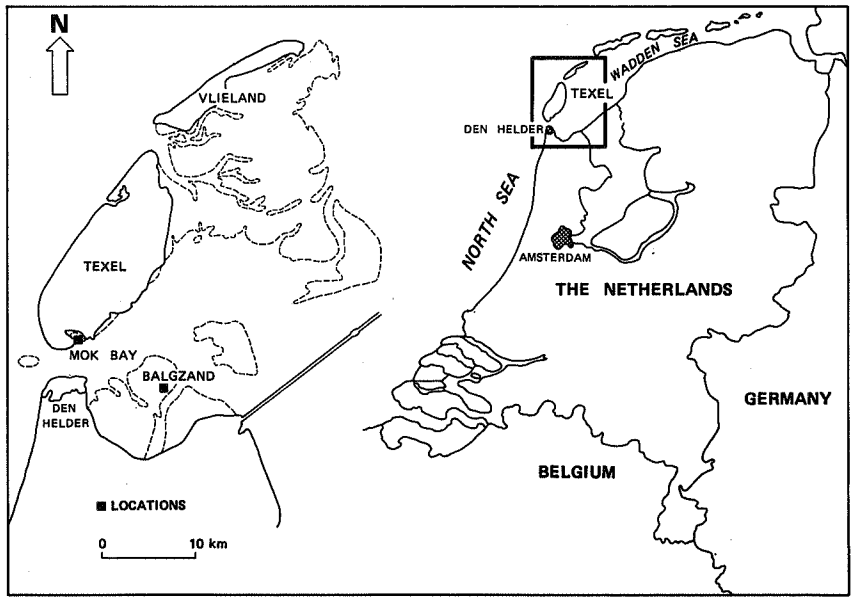

Figure 3.1: *Location of the measurement sites.*

The main difference between the two sites is that it is easier to make a model for heat balance calculations in the Mok Bay than for those on the Balgzand. The Balgzand area on the other hand has the advantage of undisturbed atmospheric flow fields. These issues will be treated in more detail in sections 3.1 and 3.2.

It is risky to perform measurements in autumn, winter or spring, because in these seasons the storms in the Dutch Wadden Sea area can be quite severe and are

companied by high water levels. In wintertime there is also a risk of drifting ice floes, which would certainly destroy the equipment.

Moreover it was not possible to make the measurement periods too long, because the hostile environment (at least to the equipment) made periodic maintenance inevitable.

In this chapter we first give a description of the two measurement sites. Then the temperature measurements with NTC's and their registration are discussed. The other sections in this chapter deal with the measurements of the energy fluxes. Where necessary some expansion of the theory is given.

3.1. The measurement site in Mok Bay.

The Mok Bay is a tidal inlet at the southern tip of the Isle of Texel. After a description of this area the reasons are given why this site was selected, followed by some details about the disadvantages of measurements at this place.

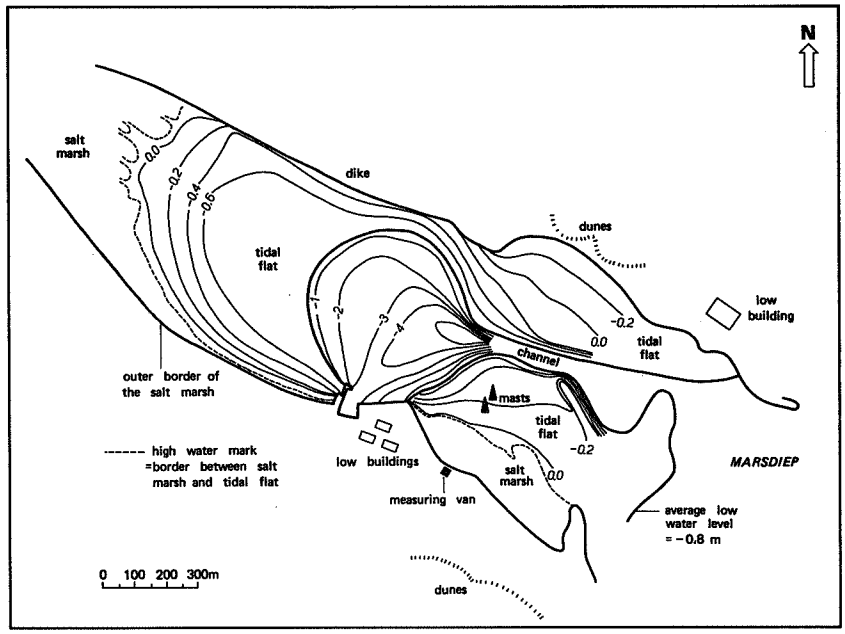

Figure 3.2: *Map of the Mok Bay area (explanation in text).*

The bay is about 2000 *m* long and 500 *m* wide. The contour lines on the tidal flats are given in figure 3.2. The bold line reflects the average low water mark and the dashed line the average high water mark. The positions of our masts and the measuring van are also marked on the map.

The tidal flats are very flat and have no plant growth at all. Earlier investigations in the Dutch Wadden Sea area have shown that the aerodynamic roughness of such a flat sandy surface does not differ very much from the roughness of a water surface (Vugts and Cannemeijer 1981). The salt marsh just above the high water mark (see figure 3.2) is covered with several types of halophyte plants typical for this environment. Most of these are less than 20 *cm* in height. This area also contains many little creeks, which are filled with water during the high tide. The rest of this area is flooded only at extreme high tide. Figure 3.2 also shows some low dunes (less than 10 *m*) to the south and to the north of the measurement masts and some low buildings located south-west and north-east of our equipment. Appendix 1 gives a more detailed map of the position of the instruments.

The reasons why the Mok Bay was selected as a measurement site are:

It has only one tidal inlet, which makes it relatively easy to calculate the heat balance.

The area is near NIOZ (Netherlands Institute for Sea Research). This institute cooperated in our research; it offered technical assistance and housing facilities.

Since previous experiments have been carried out in this area (Vugts and Zimmerman 1975), the overall experimental situation was familiar.

These tidal flats could be reached from the coast with a Land Rover. This was very convenient when heavy instruments or parts had to be moved.

The instruments were protected against vandalism because they were placed on guarded property.

The main disadvantage of doing measurements in the Mok Bay is the disturbed wind field in several directions. The largest disturbances are caused by the low buildings south-west and the dunes south of our instruments. The dunes on the other side of the bay (to the north) and the low buildings to the north-east also give disturbances. To the west and north-west the surface consists of water or tidal flat over a length of 1000 to 2000 *m*. With easterly or south easterly winds the upwind surface consists of 600 *m* of tidal flats (water at high tide) and beyond that the Marsdiep, a stretch of water which is at least 5000 *m* wide. So at westerly, northwesterly, easterly and south-easterly wind directions the roughness of the upwind surface is rather uniform.

3.2. The measurement site on Balgzand.

The Balgzand is a large tidal flat east of Den Helder (see fig. 3.1). It is about 7000 *m* wide (east-west direction) and about 7000 *m* long. It has no plant growth at all. As it can be seen from figure 3.3 the measurement site was located on the edge of the Balgzand. On the other side of the channel (Amsteldiep), which is about

400 *m* wide, there is another tidal flat. Apart from our instruments and our housing tower there were no obstacles within a circle with a radius of 5000 *m*.

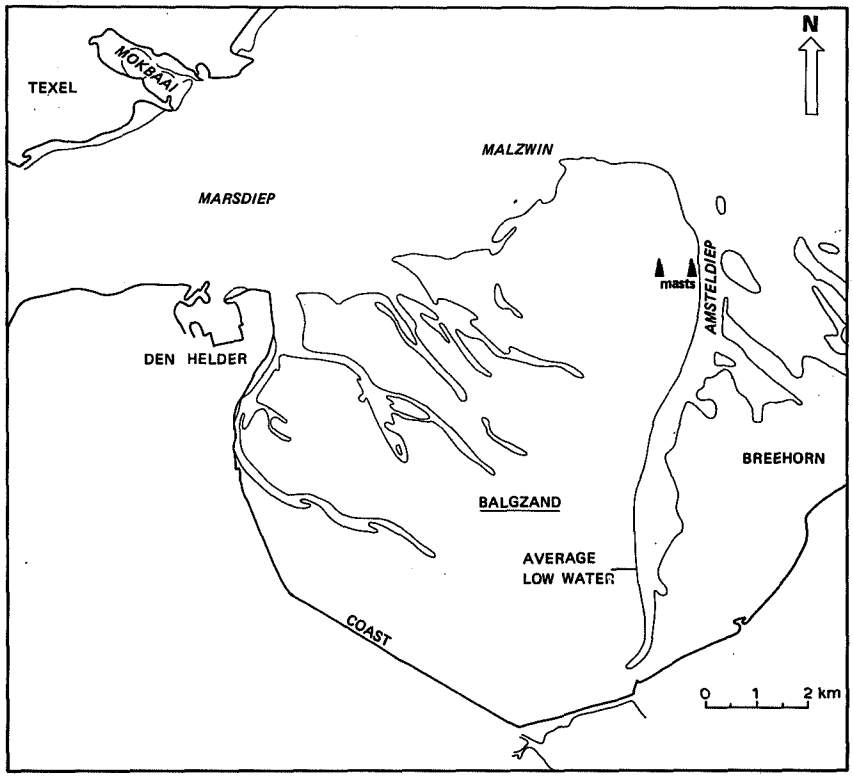

Figure 3.3: *Map of the Balgzand area.*

Appendix 2 contains a detailed map of the location of our instruments. One instrumentation mast was less than 30 *m* from the edge of the tidal flat. The other one was about 450 *m* from the edge. The housing tower (which also contained a lot of registration equipment and power source) was between the two instrumentation masts. In the vicinity of the housing tower some other measurements were carried out (mainly of radiation).

This site was selected for the following reasons:

It is free from obstacles and very uniform.

It is not very far from the NIOZ (an hour by boat), so logistical problems were not insurmountable.

In contrast to the situation in the Mok Bay the water leaves the Balgzand in various ways. With the aid of measurements published by De Boer (1978) we could however make an estimate of the flow velocity of the water on the tidal flat (see section 3.9.2.). The Balgzand area is particularly interesting because of its long undisturbed fetches.

3.3. Temperature measurements with NTC-sensors.

This item is treated in a separate section because this type of measurements is used for several purposes, such as water temperatures, soil temperatures, dry and wet bulb temperatures in the air. This section describes the NTC-sensors, the registration method, the accuracy of the measurement and some problems we met.

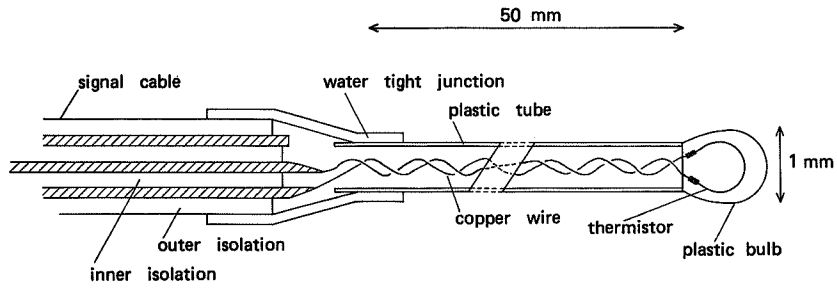

Figure 3.4: *The NTC-sensor.*

An NTC-sensor is a resistance thermometer with a negative temperature coefficient. This means that its resistance decreases with increasing temperature. The actual sensor is a thermistor temperature sensing element embedded in a solid plastic bulb of about 1 *mm* diameter. As can be seen from figure 3.4, the connection between the sensor and the signal cable is a thin hollow plastic tube with two thin insulated copper wires. This construction reduces stem conduction errors to a minimum.

Through signal cables of various lengths (mostly between 10 and 30 *m*) the NTC-sensors were connected to a small 10-channel datalogger. This datalogger measured the resistance of the sensors at fixed time intervals (usually 5, sometimes 2 minutes). The measured values were registered by means of a cassette recorder. The cassettes were later copied to computer tapes that were used for further calculations. The datalogger unit was powered by six 1.5 Volt batteries; no 220 Volt power was needed to operate this system.

In order to achieve sufficient accuracy each NTC-sensor was calibrated in the laboratory. The accuracy of the calibration was about 0.1 K. The resolution of the datalogger is about 0.02 to 0.03 K (dependent on the temperature measured), so that is well within the accuracy of the calibration.

We experienced several problems with the NTC-sensors. Corrosion of the connecting plugs (resulting in extra resistance) and the fragile construction of the sensor were the major heart aches.

Due to the fact that the experiments were carried out above the sea, high humidity and salt penetrated into almost everything and corrosion of the copper connecting plugs was almost inevitable. To avoid measuring errors due to corrosion, the plugs were cleaned once a month with steel wool.

The most fragile part in the construction of the NTC-sensor is the thin plastic tube between the sensor and the signal cable. Bending it to often leads to little holes in the tube, through which water can leak in. Also sometimes water leaks in at the point where the tubes are attached to the signal cable. Once water has leaked in, the insulation of the thin copper wires will be corroded and the presence of the (mostly salt) water reduces the resistance significantly.

For reasons of compatibility this type of NTC-sensors was also used for monitoring soil and water temperatures. It would have been wiser to use a more robust sensor for these purposes, because a lot of sensors had to be replaced.

3.4. Measurement of net radiation.

Net radiation is a very important factor in the heat balance. It was measured by means of net pyrradiometers. For comparison net radiation was also estimated from easy to measure quantities, such as incoming and outgoing short-wave radiation, surface temperature, air temperature, relative humidity and the relative duration of bright sunshine.

3.4.1. Measurement of net radiation with pyrradiometers.

Net pyrradiometers produced by Middleton Instruments were used for net radiation measurements. The main parts of the instrument are two horizontal black surfaces (one face-up, one face-down), with a thermopile between them. The instrument is protected against atmospheric influences, such as rain and wind, by two polythene hemispheres. Polythene is used because it also transmits long-wave radiation (in contrast to other materials, such as glass). The instrument has to be flushed with dry nitrogen constantly because condensated water (that might diffuse inward through the polythene) disturbs the measurement.

In 1982 (the Mok Bay experiment) one net pyrradiometer was used. The voltage produced by the thermopile was amplified by a factor of 125 and the signal was recorded on paper by a small analog recorder. The signal was also registered by a 50-channel digital datalogger. In 1983 (the Balgzand experiment) two net pyrradiometers were used. Both signals were registered directly by means of a small 10-channel (battery powered) digital datalogger. Also the signals were amplified and monitored by the 50-channel datalogger.

The manufacturer of the net pyrradiometers claims an accuracy of his calibration of 3 %. In field experiments however the accuracy is less, because the transmissivity of the polythene hemispheres reduces with time due to atmospheric influences (Jacobs 1982) and due to dust and salt particles collected on them. To avoid these errors as much as possible the polythene hemispheres were replaced monthly and cleaned regularly. Nevertheless the accuracy will be influenced and is estimated to be 5 % (using the digital registration).

Measurement of net radiation with net pyrradiometers has some drawbacks. The reduction of the transmissivity of the polythene hemispheres has already been described above. Another drawback is that the instrument has to be flushed with a slow flow of dry nitrogen. The adjustment of the slow nitrogen flow (about 1 cm^3 per minute or less) has given a lot of trouble and has not yet been resolved completely satisfactorily.

3.4.2. Estimation of net radiation from other measurements.

Net radiation can also be estimated from other measurements, such as global radiation, albedo, air humidity, air temperature, surface temperature and the duration of sunshine. These parameters can be obtained by simple meteorological measurements and are available from most meteorological stations. It is of interest, especially for further investigations, to see how much the value obtained deviates from the measured net radiation.

In order to estimate the net radiation from simple meteorological quantities De Bruin (1982) suggested the following semi-empirical formula:

$$R_n = R_{s0}(1-\alpha)(0.2+0.48p) - \sigma T_a^4(0.47-0.067\, e_a^{0.5}) * (0.2+0.8p) + \\ + 4\sigma T_a^3(T_w - T_a)\,, \qquad [W\ m^{-2}]\ (3.1)$$

where R_{s0} is the incoming short-wave radiation across a horizontal plane at the outer limit of the atmosphere, p the relative duration of bright sunshine, α the albedo, T_a the air temperature (in K), T_w the water temperature (in K) and e_a the water vapor pressure (in mb). Because in our experiments the incoming as well as the outgoing short wave radiation were measured and because the surface is not

necessarily water this equation is modified in the form:

$$R_n = R_{s1} - R_{s2} - \sigma T_a^4 (0.47-0.067\, e_a^{0.5}) * (0.2+0.8p) + \\ + \sigma T_a^3 (T_0-T_a) , \qquad [W\ m^{-2}] \ (3.2)$$

where R_{s1} and R_{s2} are the measured incoming and outgoing short wave radiation and T_0 is the surface temperature (in K).

The relative duration of bright sunshine was measured by means of a Campbell-Stokes sunshine recorder. Air temperature and humidity were taken from the registration of a thermohygrograph (an instrument which records temperature and relative humidity, see par. 3.7.2). At high tide the surface temperature was taken to be equal to the water temperature and when there was no water on the tidal flat it was extrapolated from the soil temperatures measured at a depth of 5 and 10 *cm*. Water and soil temperatures were recorded with the NTC-sensors described in section 3.3. Incoming and outgoing short wave radiation were measured by means of a double pyrradiometer (Middleton). The principle of operation of this instrument is almost the same as that of the net pyrradiometer (par 3.4.1). The polythene hemispheres have been replaced by double glass hemispheres, which absorb most of the long-wave radiation. In contrast to the net pyrradiometer, internal ventilation of this instrument is not required, because the glass prevents inward diffusion of water vapor. Also, the transmissivity of the glass does not change and it can be cleaned easily. These factors make this kind of measurement much simpler than the net radiation measurement. Incoming and outgoing short wave radiation were recorded in the same way as the net radiation measurements. The double pyrradiometer was calibrated by the manufacturer with an accuracy of 2.5 %.

3.5. Sensible and latent heat with the direct method.

According to the theory the turbulent fluxes of sensible and latent heat can be calculated directly from the measurements of the fluctuations of vertical wind speed, temperature and specific humidity. The friction velocity u_* can be calculated when also the horizontal wind speed fluctuations are measured.

The first sub-section in this section describes the measurements of horizontal and vertical wind speed together with the temperature by means of a sonic anemometer. The next sub-section deals with fluctuation measurements of specific humidity and the last sub-section treats the registration of all fast response measurements.

3.5.1. Measurements with sonic anemometers.

The two sonic anemometers were installed at a height of 4.5 m above the sand surface. For their location the reader is referred to the appendices 1 and 2.

The sonic anemometers used (Kaijo Denki, type DAT-310) have a response of 10 Hz, are accurate to 1 % (according to the manufacturer) and are free from errors caused by temperature and humidity drift (which do occur when using older types of sonic anemometers). At the end of this sub-section some remarks are made upon the accuracy, but first follows a brief description of the principle of operation of the equipment used. This description shows why they are free from errors caused by temperature and humidity drift and why they can be used to measure temperature.

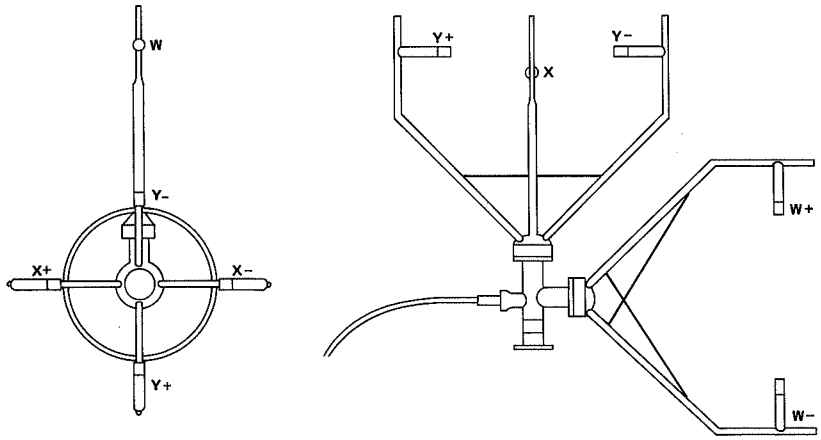

Figure 3.5: *Diagram of a sonic anemometer.*

The sonic anemometer has three pair of probe heads, each head containing a sensor which acts as an ultrasonic sound emitter, as well as a receiver. Every 0.05 seconds one of the probe heads (of a pair) sends out a sound pulse, which is detected by the opposite one. The time (t_1) the pulse needs to cross the span (d_s) is measured. The next 0.05 second a sound pulse is send back and the time (t_2) needed to reach the receiver is measured too. The times t_1 and t_2 are dependent on the span between the probe heads, the sound velocity (C_s) and the component of the wind speed in the direction of the probe heads (V_x):

$$t_1 = \frac{d_s}{C_s + V_x}, \quad t_2 = \frac{d_s}{C_s - V_x}. \qquad [s] \ (3.3)$$

Since t_1 and t_2 are measured and d_s is known, these equations can be solved to find

C_s and V_x:

$$V_x = \frac{d_s}{2} * \frac{t_1 - t_2}{t_1 * t_2} , \qquad [m\ s^{-1}]\ (3.4)$$

$$C_s = \frac{d_s}{2} * \frac{t_1 + t_2}{t_1 * t_2} . \qquad [m\ s^{-1}]\ (3.5)$$

The sound velocity depends on the air temperature and humidity:

$$C_s = 20.067\ [\ T\ (1 + 0.3192\ e_a/P\ )\ ]^{0.5}, \qquad [m\ s^{-1}]\ (3.6)$$

where T denotes the absolute temperature, e_a the water vapor pressure and P the atmospheric pressure. Combination of equations 3.5 and 3.6 leads to:

$$T = \frac{1}{1 + 0.3192\ e_a/P} * (\frac{d_s}{2*20.067} * \frac{t_1 + t_2}{t_1 * t_2})^2 . \qquad [K]\ (3.7)$$

When a suitable average for e_a/P is chosen this equation can be used to calculate the absolute temperature. The inaccuracy in the calculated temperature caused by deviations of e_a/P from the used average are less than 0.5 % (under normal atmospheric conditions), which is about 1.5 K. Although this is rather inaccurate, this error is usually disregarded, because the sonic is mainly used to measure the temperature fluctuations, and not the absolute temperature itself. However it is shown in appendix 3 that an error is introduced when temperature fluctuations measured by the sonic anemometer are used to calculate the sensible heat flux, because humidity fluctuations are included. This error is much greater than would be expected from equation 3.7. It will also be shown that the measured sensible heat flux (Q_{hs}) can be expressed in the real sensible heat flux (Q_h) and the latent heat flux (Q_w) by the following simple relation:

$$Q_{hs} = Q_h + 0.061\ Q_w . \qquad [Wm^{-2}]\ (3.8)$$

From this equation it follows that when sensible and latent heat flux have the same value (Bowen ratio equal to 1) the error in the measured sensible heat flux is 6 %, and the error in the sum of Q_h and Q_w is 3 %. This error is particularly disturbing when measurements are taken above a rapidly evaporating surface. Because this was the case in this investigation it was necessary to compensate for this error.

Concerning the wind speed the manufacturer claims an accuracy of 1 %. A calibration in a windtunnel (see figure 3.6, taken from Vugts 1980b) showed that this is true when the wind is not blowing along the line from one probe head through the opposite one. If the wind is blowing along that line, the error can be more than 10 %. During field experiments this error is reduced by the wind direction fluctuations. Anyway it was tried to avoid the error by adjusting the sonics in

such a way that the mean wind direction made an angle of 45° with the plain of the w-sensor.

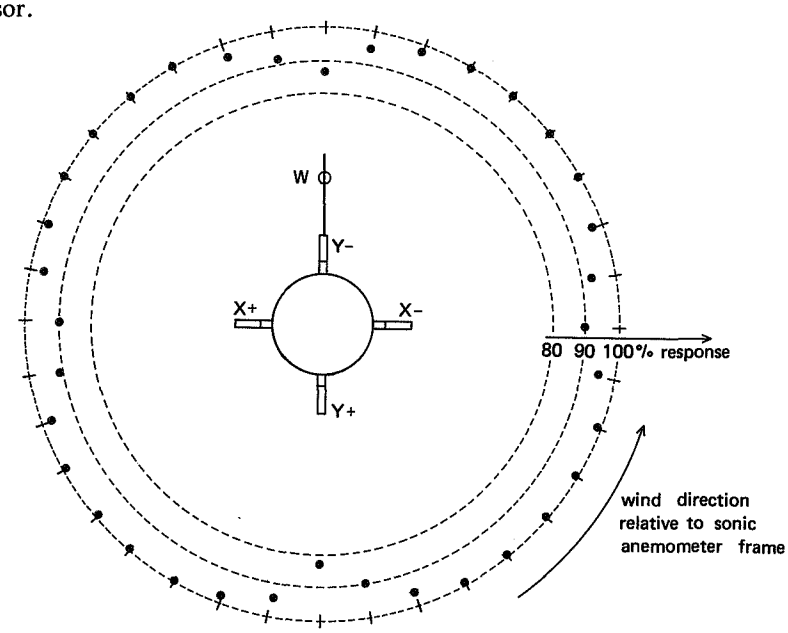

Figure 3.6: *Influence of the sonic anemometer frame on the measured horizontal wind speed.*

3.5.2. Fast response measurements of specific humidity.

Near the sonic anemometers also fast response measurements of specific humidity were carried out by means of a pair of thermocouples (one dry and one wet). The thermocouples were of the type E chromel-constantan sensors and were 25 μm thick. They had an electronic cold junction at $15^{o}C$ (that is an electronic circuit that simulates a cold junction of $15^{o}C$). One thermocouple was kept wet by means of a cotton thread, connected to a reservoir of distilled water. The amplifier, directly behind the thermocouple, multiplied the thermo-voltage by a factor of 4166, which results in a response of 250 mV per K temperature difference.

The specific humidity was calculated with the psychrometer equation (eq. 3.10, section 3.6.2). Because the response of the dry thermocouple is faster than that of the wet one, both signals had to be modified in such a way that their response time became the same (Shaw 1980). Modification has not been done in the field (the signals were registered unmodified), but back at the office with the aid of a computer. Appendix 6 shows how this can be done. The response time of the wet thermocouple was established with spectral analysis.

3.5.3. Registration of the fast response measurements.

Fast response measurements were registered by an apparatus to which we usually refer as FSK (which stands for Frequency Shift Keying) and an audio tape recorder. The FSK has 16 analog input lines (range from $-5000\ mV$ to $+5000\ mV$) which are scanned with a frequency of 25 Hz. The analog voltages are converted to digital values. Because only 12 bits were used to represent these values, the resolution was 2.5 mV. The digital values, in turn, are converted to a serial bit pattern and extra bits are added to make channel recognition possible. The bit pattern is converted to sound pulses, which were registered by the tape recorder.

In the laboratory the tapes were decoded by the FSK and fed into a computer. This system of data registration is rather safe: the loss of data is less than 0.1 %.

3.6. Sensible and latent heat flux with the profile method.

According to the theory (par. 2.2.2), profile measurements of wind speed, temperature and specific humidity can be used to calculate the turbulent fluxes of sensible and latent heat. Profile measurements were performed from two 24 m high masts. Their location is indicated in appendices 1 and 2. The dimensions etc. of the masts are described in the first sub-section of this section, the one about wind profile measurements. The next sub-sections treat the measurement of temperature and specific humidity profiles with ventilated psychrometers (equipped with NTC-sensors) and the measurement of temperature profiles with thermocouples. The last sub-section of this section describes the iteration procedure which is needed when applying the profile theory to non-neutral atmospheric conditions.

3.6.1. Wind profile measurements.

Wind speed measurements were carried out with rotating cup anemometers in two masts at levels of 24, 12, 6, 3 and 2 m above the sand surface. At the Balgzand experiment (1983) the cup anemometers at the 2 m-level were omitted because on the Balgzand the tide and the waves were too high to perform measurements at 2 m above the sand surface; they certainly would have destroyed the instruments. Also at each mast wind speed measurements were done from a raft at a level of approximately 60 cm above the water level, or 70 cm above the sand surface at low tide. At each level there were two cupanemometers, mounted on posts with a length of 60 cm, pointing in opposite directions. The cupanemometers which were upwind of the mast were used for the measurements.

The masts are of a triangular type with sides of 25 cm. The pipes at the angles have a diameter of 2.5 cm and are connected with steel plates (2 cm wide with a vertical spacing of approximately 40cm) and thin steel pins. Although these masts have a open construction, their influence on the wind-speed measurements

downwind of the mast is high, as is shown in figure 3.7.

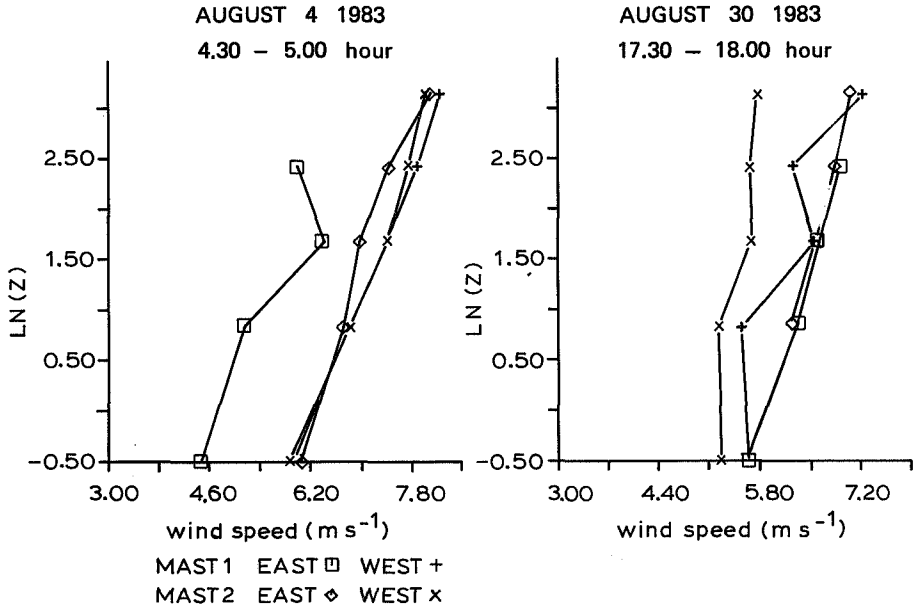

Figure 3.7: *The influence of the mast on wind-speed measurements.*

The rafts which were used in the Mok Bay experiment moved too much in the waves. The constant motion caused a great strain to the cupanemometers, their supports and the signal cables and could lead to overspeeding errors. Also the splashing of sea water on the edge of the raft was a problem because the water penetrated into the bearings of the cupanemometers and corroded them. Before the Balgzand experiment, the construction of the rafts was changed in such a way that the movement due to the waves was reduced to a minimum. Also a slight change was made in the construction of the cupanemometers, preventing water to leak into the bearings.

The cupanemometers used have cups with a diameter of 53 *mm* mounted on arms of 36 *mm*. Their distance constant is about 1.3 *m*. The rotation of the cups is detected frictionless by means of a little light bulb, a light-dependent transistor and a perforated disk. A small electronic circuit built in the cupanemometer house converts the pulses to a neat block signal, which can be send over a long cable. In the field lab the pulses were counted by an electronic counter system. The initial velocity of the anemometers is about 0.3 $m\ s^{-1}$. The cupanemometers were calibrated with an accuracy of 1 % and errors in the pulse transport and the pulse counting can be neglected.

3.6.2. Temperature and humidity profiles with psychrometers.

In the Mok Bay ventilated psychrometers for the measurement of temperature and specific humidity were mounted in the instrumentation masts at heights of 12, 6, 3 and 2 m. In the Balgzand experiment levels of 24, 12, 6 and 3 m were used. At both experiments an additional psychrometer was mounted on a raft near the masts at a height of 40 cm above the water level. However the psychrometers on the rafts gave very poor results because they were 'polluted' by water and salt. The psychrometers are a home built type and are equipped with NTC-sensors (see section 3.3).

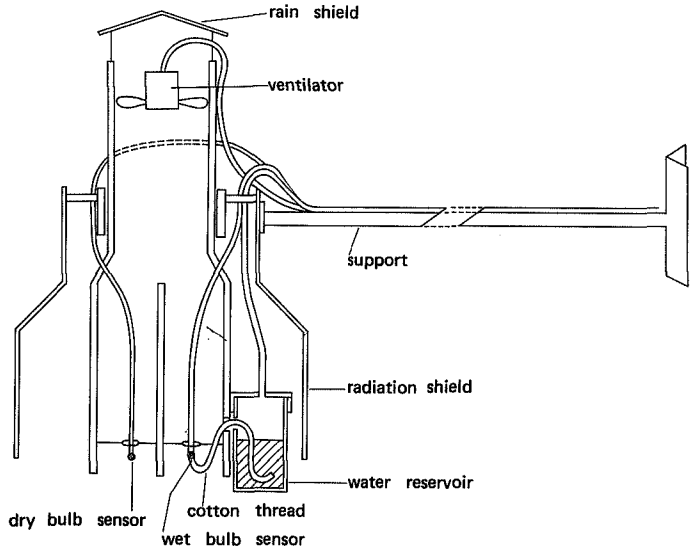

Figure 3.8: *Intersection of the ventilated psychrometer.*

The potential temperature was found by correcting the measured dry bulb temperature for the height above the surface. The specific humidity had to be calculated from the dry and the wet bulb temperature. This was done with the following set of equations:

$$q = \epsilon \frac{e_a}{P} \qquad [-] \ (3.9)$$

$$e_a = e_n - \gamma P (T_d - T_n) \qquad [mb] \ (3.10)$$

$$\gamma = \frac{M_d \, c_p}{M_w \, L_e} \qquad [K^{-1}] \ (3.11)$$

$$e_n = 6.131 + 0.467 \, T_n + 0.00898 \, T_n^2 + 0.000527 \, T_n^3 \,, \qquad [mb] \ (3.12)$$

where $\epsilon = M_d/M_w$, M_w is the molecular mass of water, M_d is the molecular mass of dry air, P the atmospheric pressure, e_n the saturated water vapor pressure at the wet bulb temperature T_n (in $^\circ C$), T_d is the dry bulb temperature, γ is the psychrometer constant, c_p the specific heat of air at constant pressure and L_e is the latent heat of vaporization of water. In order to use these equations the temperatures have to be expressed in $^\circ C$ and the pressures in *mbar*. Equation 3.10 is called the psychrometer equation.

The inaccuracy in the temperature registration (0.1 K) can lead to errors in the specific humidity of 1 to 2 %.

3.6.3. Temperature profiles measured with thermocouples.

Temperature measurements with thermocouples were carried out at levels of 24, 12, 6, 3 and 2 m above the sand surface. During the Balgzand experiment (1983) the 2 m level was omitted (see section 3.6.1). The rafts were also equipped with thermocouples, but these did not yield reliable temperatures, because the thin thermocouple wires were corroded by the sea water and because water leaked into the connecting plugs and signal cables.

The thermocouples used were type E chromel-constantan sensors with a diameter of 25 μm. The cold junctions of the thermocouples were mounted in an oil bath. The temperature of the oil bath was measured by means of a thermocouple with an electronic cold junction of 15 $^\circ C$.

The thermovoltage was amplified by a factor of 4166, resulting in a response of 250 $mV\ K^{-1}$. The thermocouple signal was passed through a low pass filter with a cut off frequency of 0.11 Hz. Amplifiers and oil bath were placed in an isolated box near the mast. Long cables (about 250 m) transported the amplified signals to a 50-channel datalogger with an adjustable sample interval. The sample interval was adjusted on 15 to 120 seconds, depending on atmospheric stability. The accuracy of the measured temperature was about 0.1 K.

3.6.4. The iteration procedure.

The theory needed to calculate the sensible and the latent heat flux with the profile method is described in section 2.2.2. Here the required iteration procedure is discussed.

When u_*, θ_* and q_* are known the sensible and latent heat flux can be calculated with equations 2.13 and 2.14. u_*, θ_* and q_* have to be calculated from equations 2.24 through 2.32 with the least squares method. However it is a problem that in these equations ψ_m, ψ_h and ψ_w are a function of z/L, which is on its turn a function of u_*, θ_* and q_*. Therefore the problem has to be solved iteratively. At

the first iteration step, atmospheric neutrality is assumed ($z/L = 0$) and therefore $\psi_m = \psi_h = \psi_w = 0$. Now u_*, θ_* and q_* can be calculated from equations 2.24 through 2.26 with the least squares method. From these calculated values, L can be found with equation 2.36. This L can be used in equations 2.24 through 2.32 to calculate new values of u_*, θ_* and q_*, which on their turn can be used to calculate a new Monin-Obukhov length, and so on. The iteration is proceeded until the Monin-Obukhov length changes less than 0.1 % (usually within 5 iterations). The values of u_*, θ_* and q_* obtained are used to calculate the fluxes of sensible and latent heat.

In stable cases the above described iteration sometimes was divergent. Therefore an extra point was added to the wind speed measurements, namely $u = 0.0\ m\ s^{-1}$ at $z = 10^{-5}\ m$. From profile calculations that did converge, it was found that the roughness length was in the order of $10^{-5}\ m$. A factor 5 error in the used roughness length causes an error of circa 10 % in the calculated u_* and therefore also approximately 10 % in the calculated fluxes. The values of θ_* and q_* are hardly influenced by errors in the roughness length.

Sometimes errors in the measurements also caused the iteration to be divergent. These errors were detected by using a criterion that was checked after each iteration. The criterion was a weighted sum of

- the average of the squares of the relative deviation of the wind speed measurements from the values that were obtained from the calculated profiles (weight factor 10), and
- the relative difference between the calculated Monin-Obukhov length and the one that was used to obtain the values for u_*, θ_* and q_* (weight factor 1).

Increase of this criterion during the iteration usually indicates one or two bad wind measurements. When this happened the run was not omitted because the sensible and latent heat flux are only one part of the heat balance calculations. What we did in those cases was minimizing to relative difference between the calculated Monin-Obukhov length and the one that was used to obtain the values of u_*, θ_* and q_*. This procedure was seldom necessary.

3.7. Sensible and latent heat flux with the bulk method.

The bulk method is attractive because the measurements needed are simple and the calculation procedure is not complicated. This section describes the wind, temperature and humidity measurements that were used to calculate the heat fluxes with the bulk method.

3.7.1. Wind speed measurements with the Lambrecht anemograph.

The Lambrecht anemograph is a cup anemometer with mechanical registration. The wind direction is also registered mechanically.

In the Mok Bay experiment the Lambrecht anemograph was mounted at a height of 3 m, about 30 m east of mast 1 (see app. 1). In the Balgzand experiment The Lambrecht anemograph was situated in the neighbourhood of the registration tower between the masts at a level of 3.8 m above the sand surface (see app. 2).

Wind speed and direction were registered continuously on paper. The threshold wind velocity for the instrument is about 0.4 $m\ s^{-1}$ and the accuracy about 0.2 $m\ s^{-1}$. The Lambrecht anemograph has a rather slow response, but since only time averages of the wind speed are needed, this is not a disadvantage.

3.7.2. Temperature and humidity measurements with a thermohygrograph.

In the Mok Bay experiment one thermohygrograph was mounted in a Stevenson screen 2.5 m above the ground. At the Balgzand the masts stood further apart and a Stevenson screen was placed at the foot of each mast, 3 m above the ground.

The temperature sensor of the thermohygrograph consists of a strip of bimetal and the hygrometer consists of hair. Temperature and humidity were registered mechanically, with ink on paper. The temperature readings were checked with the temperatures measured with a minimum, a maximum and a normal thermometer, which were also mounted in the Stevenson screen. Corrections were made if necessary. The recording of relative humidity was checked with the aid of periodic measurements of relative humidity with an Assmann psychrometer.

The accuracy of the temperature measurements with the thermohygrograph is about 0.3 $^{\circ}C$. This causes an absolute error in the calculated sensible heat flux of the order of $5 W\ m^{-2}$ (the error is dependent on wind speed and stability). The accuracy of the relative humidity readings is approximately 3 % relative humidity, which cause an absolute error in the latent heat flux of the order of $20 W\ m^{-2}$.

3.7.3. Estimate of surface temperature and humidity.

When the tidal flat was flooded the surface temperature was taken equal to the water temperature. When there was no water on the flat the surface temperature was extrapolated linearly from the soil temperatures at depths of 5 and 10 cm. Water and soil temperatures have been measured with NTC-sensors (see par. 3.3).

The surface humidity was found by assuming that the air at the surface was saturated with water vapor (at surface temperature). This assumption is not unrealistic, because the surface remained very wet, even when the tidal flats were not flooded.

3.8. Measurement of the soil heat flux.

The soil heat flux was measured in four ways, with soil heat flux plates, with the profile integration method, with the gradient method and with the Fourier method. The last two make use of soil and water temperatures, which were measured with NTC-sensors (see section 3.3). Soil temperatures were measured at depths of 5, 10, 15, 30 and 50 *cm* and water temperatures at levels of 2, 15 (20 on the Balgzand) and 50 *cm* above the sand surface.

The first sub-section in this section describes the measurements with the soil heat flux plates. The next three sub-sections show how the gradient method (see sub-section 2.3.1), the profile integration method (see sub-section 2.3.2) and the Fourier method are used to calculate the soil heat flux. At the end of this section there are three sub-sections, one concerning the in situ measurement of the thermal conductivity of the soil, the second describing the method of estimating the soil heat capacity and the last one about the thermal diffusity of the soil. This estimate is needed for the thermal conductivity measurements and for the measurement of the soil heat flux with the profile integration method.

3.8.1. Measurements with the soil heat flux plates.

The soil heat flux plates used (produced by Middleton Instruments) consist of a material with known heat conductivity and dimensions of 48*28*5 mm^3 (5 *mm* high). The upper and lower surface are covered by thin metal plates and between the metal plates there is a thermopile. The voltage produced by the thermopile is a measure for the soil heat flux. The flux plate was mounted at a depth of 2.5 *cm* in the Mok Bay and at a depth of 5 *cm* at the Balgzand experiment.

The soil heat flux plates were calibrated by the manufacturer to an accuracy of 5 %. The output signal is about $1.9 \mu V\ W^{-1}m^2$. The produced voltage was amplified by a factor 1250 and recorded on a small analog datalogger and on the 50-channel digital datalogger.

3.8.2. The gradient method.

Equation 2.42 was used to calculate the soil heat flux with the gradient method. When there was water on the tidal flat the gradient $\partial T_b / \partial z$ was calculated from the soil temperature at the surface (which was assumed to be equal to the water temperature) and the soil temperature at a depth of 5 *cm*. When the flat was not flooded the gradient was calculated from the soil temperatures at depths of 5 and 10 *cm*.

Water and soil temperatures were measured with NTC-sensors (see section 3.3) with an accuracy of 0.1 *K*. The thermal conductivity of the soil of the investigated

tidal flats is of the order of 3 $W\ m^{-1}K^{-1}$. Thus a temperature difference of 2 K over 5 cm yields a soil heat flux of 120 $W\ m^{-2}$. Since the temperature difference is calculated from two temperatures (each measured with an accuracy of 0.1 K) the accuracy of the difference (in this case) is 10 %. The error in the distance between two sensors can be 0.5 cm, which also leads to a relative error in the gradient of 10 %. When the tidal flat is flooded the exact position of the sand surface is uncertain due to sand movement. This leads to additional errors in the calculated gradient. When there is no water on the tidal flat, an extra error is introduced, because the gradient is measured at a depth of 5−10 cm, instead of just below the surface. It can be concluded that the error is in the order of 25 % when Q_b is about 100 $W\ m^{-2}$ and larger when Q_b is smaller.

3.8.3. The profile integration method.

The basis for the calculation of the soil heat flux with the profile integration method is equation 2.44. In order to use this equation the soil has been divided into seven layers (0−1 cm, 1−7.5 cm, 7.5−12.5 cm, 12.5−20 cm, 20−40 cm, 40−60 cm and deeper than 60 cm). The temperature changes in these layers are represented by the temperature changes measured at depths of 0, 5, 10, 15, 30 and 50 cm, respectively. The temperature change of the layer deeper than 60 cm is neglected. The surface temperature is assumed to be equal to the water temperature when the tidal flat is covered with water and is extrapolated linearly from the temperatures at a depth of 5 and 10 cm otherwise. Soil and water temperatures were measured with NTC-sensors (see section 3.3).

Since the temperature change with time at a specific level is calculated from measurement with the same sensor, errors in the calibration hardly influence the calculated heat flux. Here the resolution of the datalogger (0.02−0.03 K) becomes the limiting factor. Restrictions in the resolution did have an effect on the temperature registrations of the −50 cm level. The temperatures measured at that level did not change for some hours and could then "suddenly" change 0.03 K and then stay constant again. To avoid peaks in the soil heat flux caused by these sudden changes the temperatures measured at 50 cm depth were filtered with a computer simulation of a low pass filter with a time constant of two hours.

Beside the insensitivity to calibration errors (of the NTC's), the profile integration method has the advantage (above the gradient method), that errors in the measured temperature change have a tendency to average out and that it is less sensitive to the position of the sensors.

When the soil heat flux is 100 $W\ m^{-2}$ the measurement error when using the profile integration method is estimated less than 10 %.

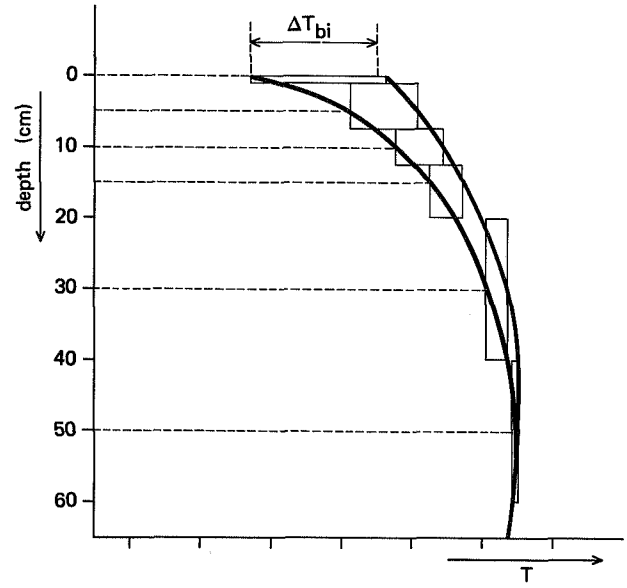

Figure 3.9: *Division of the soil into layers.*

3.8.4. The Fourier method.

The soil heat flux at the surface is obtained from temperature measurements at only one level in the soil (at 5 *cm* depth) using the Fourier method. From half hourly averages a Fourier series is calculated for the soil temperature at this depth. Then the Fourier series (a sum of sine and cosine functions) is written as a sum of sine functions solely. Finally the surface temperature is calculated, also as a series of sine functions and the soil heat flux is calculated from the course of the temperature at the surface. This process is worked out in detail below.

The Fourier series describing the temperature course at a depth of 5 *cm* is of the form (compare with equation 2.54):

$$T_b(Z,t) = \overline{T_b} + \sum_{n=1}^{N} [a_n \cos(n\,\omega_1 t) + b_n \sin(n\,\omega_1 t)], \qquad [K]\ (3.13)$$

where Z is the depth at which the temperatures were measured ($-0.05\ m$) and N is the number of harmonics used. The Fourier coefficients a_n and b_n are found from Fourier analysis. Equation (3.13) can be written as a series of sine functions:

$$T_b(Z,t) = \overline{T_b} + \sum_{n=1}^{N} A_n(Z)\, \sin(n\,\omega_1 t + \phi_n), \qquad [K]\ (3.14)$$

with:

$$A_n(Z) = b_n \left[(\frac{a_n}{b_n})^2 + 1 \right]^{0.5} \qquad [K]\ (3.15)$$

$$\phi_n = arctan(a_n/b_n) \ . \qquad [-] \ (3.16)$$

With the aid of (2.55) through (2.58) we can now write the temperature course at any depth z as:

$$T_b(z,t) = \overline{T_b} + \sum_{n=1}^{N} A_n(z) \sin(n\omega_1 t + \phi_n + (z-Z)/D_n) \ , \qquad [K] \ (3.17)$$

$$A_n(z) = A_n(Z)\, e^{+(z-Z)/D_n} \qquad [K] \ (3.18)$$

and D_n is given by (2.58). (Note that the depths are taken negative in the downward direction.)

When we take the derivative of (3.17) with respect to the time and integrate the result over the depth (after multiplication with $\rho_b c_b$) this yields the following equation for the soil heat flux at the surface:

$$Q_b(t) = \sum_{n=1}^{N} [\, n\omega_1 \lambda \rho_b c_b \,]^{0.5} A_n(Z) e^{-Z/D_n} \sin(n\omega_1 t + \phi_n - Z/D_n + \pi/4) \ [K] \ (3.19)$$

When this theory was applied to the measurements, a separate Fourier series was calculated for each day of observations. It was observed that at the beginning and the end of the day the calculated soil heat flux sometimes showed unrealistic fluctuations. These were removed by including the last five hours of the preceding day and the first five hours of the following day. So the Fourier series was calculated for a period of 34 hours (68 points) yielding 34 harmonic oscillations. We used half of the harmonics (the first 17) to calculate the soil heat flux. The higher harmonics were excluded because they contained too much of the noise in the temperature signal.

3.8.5. In situ measurement of thermal conductivity.

In situ measurements of the thermal conductivity of the soil have been carried out with specially designed needles, which were provided by the Agricultural University in Wageningen. A needle consists of a hollow steel cylinder (length 210 *mm* and diameter varying per needle from 1 to 2 *mm*), which contains a manganin-constantan-manganin thermocouple junction and a constantan resistance wire. The needle is filled with silicon. The cold junction of the thermocouple was mounted in a Dewar vessel filled with water. Before the measurement the needle was placed horizontally in the ground at a known depth. Then the needle was heated by applying a constant current to the resistance wire and the temperature increase of the needle was measured with the aid of the thermocouple.

The thermal conductivity of the soil can be calculated from the course of the needle temperature. A detailed description of the needles and the theory for

calculating the thermal conductivity is given by Van Haneghem (1981). Appendix 4 summarizes the calculation procedure used for the determination of the thermal conductivity of the soil.

For the thermal conductivity of the tidal flat in Mok Bay we found 2.96 $W\ m^{-1}K^{-1}$ with a standard deviation of 0.24 $W\ m^{-1}K^{-1}$ from 16 measurements at various depths between 0.05 and 0.50 m. There is a slight dependency of the thermal conductivity on the depth. At 10 cm below the surface 5 measurements yielded a thermal conductivity of 3.12 $\pm$ 0.21 $W\ m^{-1}K^{-1}$, whereas 4 measurements at 50cm depth yielded 2.75 $\pm$ 0.17 $W\ m^{-1}K^{-1}$. This difference is significant up to the 97.5 %-level (using the student-t test). On the Balgzand a thermal conductivity of 2.46 $\pm$ 0.06 $W\ m^{-1}K^{-1}$ was measured at a depth of 50cm. These values are in agreement with thermal conductivities found by other investigators. Van Wijk (1966) gives a thermal conductivity of 2.2 $W\ m^{-1}K^{-1}$ for a sandy soil which is saturated with water and Andrews (1980) found 2.5 $W\ m^{-1}K^{-1}$ for the thermal conductivity of a sandy tidal flat.

3.8.6. Estimation of the soil heat capacity.

Although the calculation of the thermal conductivity, which is described in appendix 4, does not depend strongly on the heat capacity of the soil, it is necessary to make an estimate. This estimate is also used where the soil heat capacity is needed in the calculation of the soil heat flux with the profile integration method or the Fourier method.

The estimate is made by assuming that the soil of the tidal flats consists of sand with a pore volume of 40 % and is saturated with water. With the properties of quartz (ρ_q = 2660 $kg\ m^{-3}$ and c_q = 787 $J\ kg^{-1}K^{-1}$) and water (ρ_w = 1000 $kg\ m^{-3}$ and c_w = 4180 $J\ kg^{-1}K^{-1}$) and the formula:

$$\rho_b c_b = 0.6\ \rho_q c_q + 0.4\ \rho_w c_w\ , \qquad [J\ m^{-3}K^{-1}] \quad (3.20)$$

it follows that $\rho_b c_b = 2.93*10^6\ J\ m^{-3}K^{-1}$. When a part of the solid fraction consists of chalk (ρ_c = 2710 $kg\ m^{-3}$, c_c = 870 $J\ kg^{-1}K^{-1}$) the result for $\rho_b c_b$ is almost the same. At the places where our measurements were carried out the soil hardly contained any organic matter.

3.8.7. The thermal diffusity of the soil.

Now that the thermal conductivity is known and an estimate is made of the volumic heat capacity of the soil, it is possible to calculate the thermal diffusity of the soil with eq. 2.46. For the Mok Bay this results in a value of 1.02 m^2s^{-1} and for the Balgzand 0.84 m^2s^{-1}. Vugts and Zimmerman (1985) used eq. 2.53 to calculate the thermal diffusity of the soil of the Mok Bay and found an average value

of 1.06 m^2s^{-1}, which coincides very good with our result. Andrews (1980) calculated a thermal diffusity of 0.79 m^2s^{-1} for a sandy tidal flat and about 0.5 m^2s^{-1} for a muddy tidal flat. The value for a sandy tidal flat corresponds with what we found for the Balgzand soil. Harrison (1981), Harrison and Phizacklea (1985) and Harrison (1985) measured thermal diffusities varying from 0.4 to 0.5 m^2s^{-1} in muddy intertidal sediments. These values are in agreement with those found by Andrews (1980) on muddy tidal flats.

3.9. Measurement of the heat advection through the water.

The measurement of the advection through the water will be discussed for three cases: at one point in the Mokbay, at one point on the Balgzand and for the entire Mokbay. In all cases two different aspects are important, namely temperature measurements and current velocity measurements.

3.9.1. Advection at mast 1 in Mok Bay.

The basis for the calculation of the advection of heat through the water at one point in the Mokbay is equation 2.64. The point for which the advection is calculated is the position of mast 1 (point A in figure 3.10). The water level is registered by means of a tide gauge at point G in figure 3.10. From the measured water level at the tide gauge, 0.38 *m* was subtracted because of the slope of the terrain between points A and G. The water temperature was measured by means of NTC-sensors (see section 3.3) at a level of 2 *cm* above the bottom surface near mast 2, near the radiation measurements and the the Lambrecht anemograph (see appendix 1). From these measurements the temperature gradient at mast 1 was calculated.

The current velocity at mast 1 (point A) was not measured directly. It was calculated from the water level and a section of the tidal flat from the measuring van (M) to the tide gauge (G) (see figure 3.10).

It was observed during the field measurements that the water flow at mast 1 was approximately parallel to the cross section. It is assumed that at a given moment t the water depth at mast 1 is h meter. Then the volume of water, V, south of mast 1, per unit length, l, (perpendicular to the cross section), is equal to the area, A, that is enclosed by the lines indicating the bottom profile and the water level south of mast 1 (hatched area in figure 3.10).

The volumes V_1 and V_2 at time t_1 and t_2 are considered. The difference between the volume V_1 and V_2 has passed point A through the area $l^*(h_1+h_2)/2$, since the water flow is approximately parallel to the cross section. Therefore the flow velocity at mast 1 is given by:

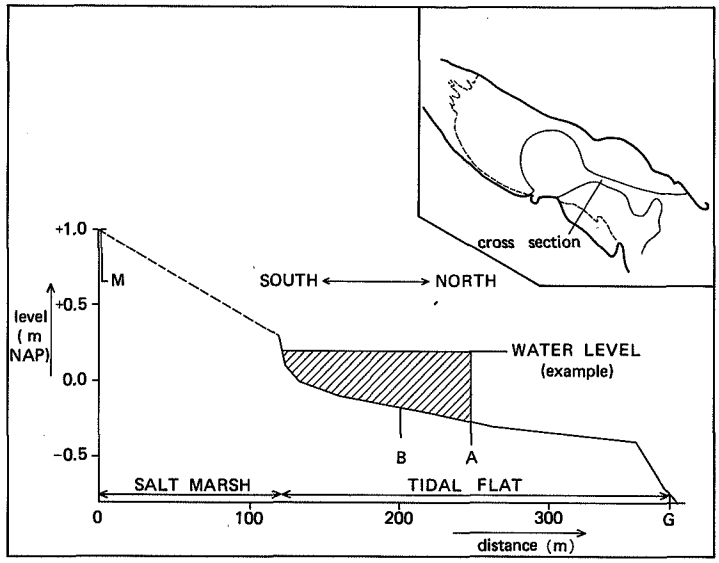

Figure 3.10: *Cross section of the Mokbay (A = mast 1, B = mast 2, G = tide gauge, M = measuring van).*

$$U = \frac{V_2 - V_1}{l * \frac{h_2 + h_1}{2} * (t_2 - t_1)} \quad [m\ s^{-1}] \quad (3.21)$$

Elimination of the unit length, l, gives:

$$U = \frac{2 * (A_2 - A_1)}{(h_2 + h_1) * (t_2 - t_1)} \quad [m\ s^{-1}] \quad (3.22)$$

3.9.2. Advection of heat at one point on Balgzand.

The advection of heat through the water at one point on the Balgzand can be calculated from the horizontal water temperature gradient, the flow velocity and the water depth (see equation 2.64).

Water temperatures were measured with NTC-sensors at levels of 2, 20 and 50 *cm* above the soil surface at the same place, where the soil temperatures were measured. Water temperatures were also measured at a level of 2 *cm* above the soil surface 50 *m* north and 50 *m* south of that spot. Since the flow direction was approximately north-south when the water level was rising and south-north when the water was falling, the temperature gradient was measured parallel to the flow direction.

For the water level, measurements were used which had been taken by the Governmental Department of Public Works with the aid of a tide gauge. These were taken at their Wierbalg station, which is a few kilometers south of our location. During the last measurement periods we placed a pipe on the tidal flat with marks at every 10 *cm*. From this pipe we could estimate the water level near our observation tower. Comparison with the Wierbalg measurements showed that the highest water level is reached at the tower half an hour before it is reached at Wierbalg. Since the tidal wave passes our location about half an hour before it reaches Wierbalg, all Wierbalg measurements were shifted half an hour in advance.

The current velocity is difficult to determine, because no direct flow velocity measurements were carried out and because the hydrological situation on the Balgzand is rather complicated. In 1977 the Governmental Department of Public Works carried out extensive hydrological measurements on the Balgzand. From these measurements (reported by De Boer 1978) the flow velocity is estimated as a function of the rate at which the water level changes. The following empirical relation has been derived for the local flow velocity at our observation tower on the Balgzand:

$$U = 0.01 + 20 * \left| \partial H / \partial t \right| . \qquad [m\ s^{-1}] \ (3.23)$$

where H is the water level in meters relative to NAP. When the water level is not changing there is a small residual current estimated at 0.01 $m\ s^{-1}$.

3.9.3. The advection term for the entire Mok Bay.

Due to the continuous tidal movement enormous amounts of water are moved in and out the bay, carrying huge quantities of heat with them. This advection of heat for the entire bay is calculated with equation 2.67. The term is a function of the water temperature in the tidal channel, T_g, the average water temperature in the bay, T_w, and the water flow through the tidal channel, which is expressed as the change of the Mok Bay water volume $\partial V_w / \partial t$. The water temperature in the tidal channel was measured continuously with the aid of three NTC-sensors (see section 3.3) at levels of about 1, 2 and 3 meter above the bottom (measuring depths change slightly with the tide). The average Mok Bay water temperature follows from successive heat balance calculations.

Vugts and Zimmerman (1985) used a relaxation time to calculate the influence of the inflowing water. We did not used this technique, since the relaxation time is a parameter which is difficult to determine.

In order to get a good estimate for the water flow through the tidal channel a height map of the bay was constructed. The part of the bay which was not inundated during the ebb-tide was measured with a theodolite. The other part was measured by echo sounding. From these measurements the following empirical relation

was derived for the Mok Bay volume:

for $H \leqq -1.0$ $V_w = 1000 * (33\ H^2 + 282\ H + 639)$ $[m^3]$ (3.24a)

for $-1.0 < H < 0.0$ $V_w = 1000 * (282\ H^2 + 780\ H + 888)$ $[m^3]$ (3.24b)

for $H \geqq 0.0$ $V_w = 1000 * (282\ H^2 + 780\ H + 888)$ $[m^3]$ (3.24c)

The water level, H (in m NAP), was measured continuously with a tide gauge, which was located very close to the tidal channel (see appendix 1). Now the water flow follows from:

$$F_w = \partial V_w / \partial t \ . \qquad [m^3 s^{-1}] \ (3.25)$$

Water flows calculated from equation 3.25 have been verified with flow velocity measurements in the tidal channel during a few days, yielding a good agreement.

CHAPTER 4

COMPARISON OF METHODS

Some terms of the heat balance are measured in two or more different ways. In this chapter the various methods are compared. This comparison serves two purposes, first it is used to make a choice about which method should be used in the actual heat balance calculations and second it can be used for developing a measurement strategy for further investigations.

Comparisons are discussed for sensible and latent heat flux, soil heat flux and net radiation.

4.1. Sensible and latent heat flux.

The sensible and latent heat flux are measured with the direct method, the profile method and the bulk method. First the effect is shown of neglecting the moisture influence on the Monin-Obukhov length, when using the profile method. Then the profile method is compared with the bulk method and the direct method.

4.1.1. Effect of the moisture gradient on the Monin-Obukhov length and the heat fluxes.

When the profile method is used to calculate the sensible and the latent heat flux, the effect of the moisture gradient on the Monin-Obukhov length is often neglected. During this research measurements were always taken above water or very wet surfaces. In these cases the Bowen ratio is small (mostly between -0.25 and 0.25), so the effect of the moisture on the Monin-Obukhov length is expected to be considerable (see eq. 2.37). Which effect this will have on the sensible and latent heat fluxes can only be found by calculating the heat fluxes from measured profiles. Therefore profile calculations were carried out in the correct way (calculating the Monin-Obukhov length with eq. 2.36) and with neglection of the moisture influence (calculating L with eq. 2.34), using the same set of input data. In both cases L was computed from profile data (see 3.6.4).

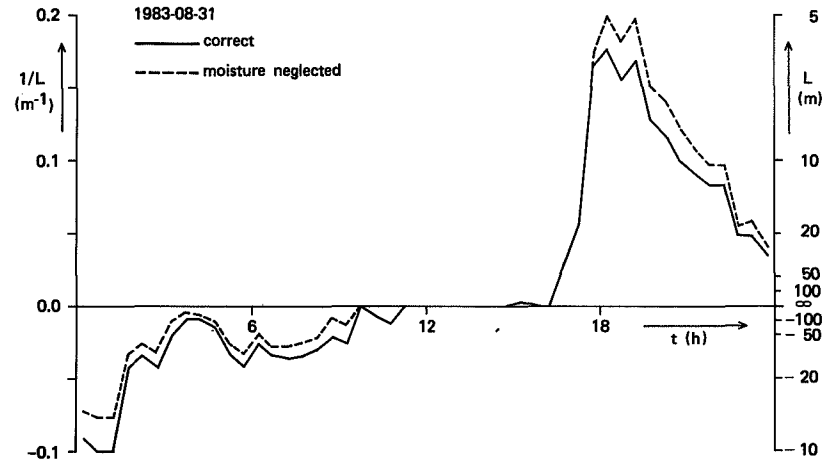

Figure 4.1: *Course of the (reciprocal) Monin-Obukhov length during one day. (explanation in text).*

The course of the (reciprocal) Monin-Obukhov length during one day, August 31, 1983, at mast 1 on the Balgzand has been plotted in figure 4.1. The full line represents the correctly calculated Monin-Obukhov length and the dashed line the Monin-Obukhov length calculated by neglecting the moisture influence. During the day shown, the neglect of the moisture influences always increased $1/L$, because the latent heat flux was always upwards (evaporation). When atmospheric stability is neutral the effect of the moisture neglect is small. However when the surface layer is stable or unstable the effect on $1/L$ is considerable. Only in the beginning of the stable period (15.30−18.00 hour) the effect is small because the moisture gradient is small.

For the same day figure 4.2 shows the calculated sensible (Q_h) and latent (Q_w) heat fluxes. It can be seen that the neglection of the moisture influence has a very small effect when the atmosphere is neutral and when the latent heat flux is small. In all other cases the effect is considerable. For this day the error in the daily average of the latent heat flux is 14 %. The average error in the sensible heat flux is 12 %.

The same exercise has been done for a six day period (July 28 to August 2, 1982) during the Mokbay experiment. In this period neglect of the moisture influence on the Monin-Obukhov length results in a latent heat flux which is too low by a factor 0.85 (on the average). For the sensible heat flux this factor is about 0.87. Also these numbers illustrate that the moisture influence on the Monin-Obukhov length cannot be neglected when the profile theory is used to calculate the sensible

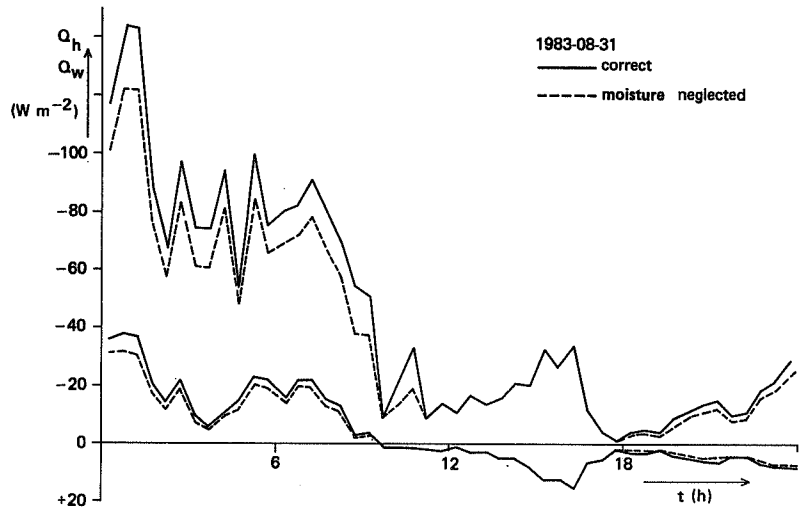

Figure 4.2: *Course of the heat fluxes during one day. (explanation in text)*

or latent heat flux above wet surfaces.

The errors in the calculated sensible and latent heat flux, due to the neglect of the moisture influence on the Monin-Obukhov length, which are found above, are slightly larger than those obtained by Blanc (1983). Blanc found an error which was typically less than 10 % when the humidity flux was upwards. The difference between our results and Blanc's can be explained by the fact that the measurements were taken under different circumstances. In Blanc's case the fetch was always over the ocean and waves were rather high (about 2.0 meters on the average 15.6 *km* north-west of the location). Relative humidity was always high (about 80 %) and most of the time the water temperature was 1 to 2 degrees above the air temperature at 10 *m* (see also Blanc 1981). During our experiments the waves near the measurement site were always low (less than 0.30 *m*) and there was hardly any breaking of the waves near the masts. So surface roughness during our experiments was smaller than the roughness during the experiments reported by Blanc. During our investigations the difference between the 12 *m* air temperature and the surface temperature was positive as well as negative (between -2.6 and $1.8\ ^{\circ}C$ on August 31, 1983). During the Balgzand experiment relative humidity was high most of the time (80 to 90 % on August 31, 1983). In the time of the Mokbay study the relative humidity was sometimes as low as 50 %.

4.1.2. Sensitivity analyses of the profile method.

In this section the sensitivity of the sensible and latent heat fluxes derived from the profiles to errors in the temperature measurement is evaluated. Therefore three tests were carried out on the measurements obtained on August 31, 1983 (the Balgzand experiment). These are discussed below.

The first test was to decrease all temperatures (dry and wet bulb at all levels) by 0.5 K. This was done to see whether radiative errors or errors in the calibration of the sensors could have influenced the results. The effect of this action on the calculated sensible heat fluxes was hardly noticeable. From 96 observations there were three with a difference of 1 $W\ m^{-2}$, whereas the others showed no difference (all fluxes were rounded to the nearest $W\ m^{-2}$). The latent heat flux was reduced by 2 − 3 % because all specific humidities decreased and so did the specific humidity gradients.

At the second test the temperatures measured at 24, 12, 6 and 3 meter were reduced by 0.45, 0.48, 0.52 and 0.55 K respectively. So the temperature gradient was tilted. Height dependent reductions were applied because radiative errors usually are less for the higher levels due to the fact that the wind speed changes with height. The effects were small in stable cases, because then the gradients were already large and 0.1 K did not make much of a difference. In unstable cases, however, the sensible heat flux was reduced about 50 %, due to the combined effect of the reduced temperature gradient and the less unstable atmosphere. In near neutral cases there was a difference of about 3 $W\ m^{-2}$ between the sensible heat flux calculated in this way and the one derived from the unchanged profile. The humidity gradient was not greatly affected by reducing both the dry and the wet bulb temperature. However due to the changed (calculated) stability the derived latent heat flux was reduced by 60 % to 70 % in unstable cases. In stable situations the influence was small.

At the third test the 24 m level temperatures and humidities were omitted. The effect thereof is different for both masts. For mast 2 the sensible and latent heat fluxes decrease by about 15 %. For mast 1 the difference is small for stable cases, but in unstable situations the sensible heat flux increases about 45 % and the latent heat flux about 35 %. This different influence on the profiles is mainly caused by errors in the temperature measurements at mast 1, which are due to errors in the laboratory calibration of the sensors. From visual observation of the temperature profiles the errors are estimated to be in the order of 0.05 K. Excluding the 24 m level also changes the geometric mean height of the profile from 8.5 m to 6 m, which possibly has also played a role.

It can be concluded that in unstable cases the profile derived fluxes are very sensitive to errors in the temperature measurement. Errors in the order of 0.1 K in

the measured temperature gradient can change the sensible heat flux by 50 % and the latent heat flux by about 30 %. That these relatively small errors have such large effects is caused partially by the fact that (in an unstable atmosphere) about 90 % of the temperature gradient lies below the lowest measurement level. That such a large fraction of the total gradient lies below 3 meter is due to the very low surface roughness. In stable situations errors in the temperature measurement have little effect because then the temperature gradients are large.

4.1.3. Comparison between profile and bulk method.

The comparison is based on measurements in the Mok Bay in the period from July 28 to August 3, 1982. In all cases we compare half hourly averages of the sum of latent and sensible heat flux, calculated with the various methods. In order to be able to be more conclusive about which method yields the best results, we used a third method, to which we will refer as the balance method. This method calculates the sum of latent and sensible heat flux from the heat balance (only when the tidal flat is not flooded).

When using the bulk method we did not use a constant bulk aerodynamic transfer coefficient, but one that was dependent on stability and surface roughness. Equation 2.41 was used to calculate the coefficient assuming a surface roughness of 10^{-4} m.

The correlation between the bulk method and the balance method (correlation coefficient $r = 0.90$) is better than the correlation between the bulk and the profile method ($r = 0.74$) and better than the correlation between the balance and the profile method ($r = 0.70$). This indicates that the bulk method yields more reliable results than the profile method. The average sum of sensible and latent heat fluxes over the period from July 28 to August 3 is overestimated by about 20 % by the bulk method, compared to the profile method as well as the balance method. This problem can be overcome by using a surface roughness of circa $3*10^{-5}$ m. This value also is in agreement with the surface roughness which was estimated from the profile method.

At first sight it is surprising that a simple method like the bulk method, for which rather inaccurate measurement techniques were used, yields more reliable results than a rather sophisticated method like the profile method. The better behaviour of the bulk method can be explained by the fact that with application of the bulk method one uses the gradient between the surface and 2.5 m, whereas with the profile method one uses the gradient between 2 and 12 m (at the Mok Bay experiment). On tidal flats with their very low surface roughness 80 to 90 % of the total gradient between the surface and 12 m lies below 2.5 m (under unstable or neutral conditions). In a stable atmosphere a larger fraction of the gradient lies

between 2 and 12 m, but then the fluxes are small and the absolute differences between the methods are small too.

4.1.4. Comparison of direct and profile method.

In order to compare the results from the sonic anemometers with those obtained with the profile method, covariances have been calculated for 10 half hour runs on August 31, 1983 (the Balgzand experiment). Since two sonics were installed this yields 20 data points. August 31 was a day with bright sunshine and weak winds ($2-6\ m\ s^{-1}$) from easterly directions. The highest water level occurred around 14.00 h (LST). The 10 runs were selected in such a way that the data set contains several conditions (low/high water level, day/night, stable/neutral/unstable).

The values obtained for the friction velocity (u_*) by the use of the direct method corresponds very good with those obtained from the profiles. The agreement between the sensible heat flux calculated using the profile method and the flux that resulted from the covariance of vertical wind speed and the temperature measured with the sonic anemometer or the dry bulb thermocouple is reasonable. For the latent heat flux the direct method yielded less negative fluxes than the profile method. These items are treated below.

- Similarity of friction velocities.

When a linear regression was performed between the friction velocity calculated with the profile method and that obtained from the direct method we found:

$$u_*(profile) = 0.00 + 0.97\ u_*(direct)\ , \qquad [m\ s^{-1}]\ (4.1)$$

with a correlation coefficient of $r = 0.96$. When we omitted one point (the point that deviated the most from the line $u_*(profile) = u_*(direct)$), the result became:

$$u_*(profile) = 0.00 + 1.01\ u_*(direct)\ , \qquad [m\ s^{-1}]\ (4.2)$$

with a correlation of $r = 0.98$. The offset of $0.00\ m\ s^{-1}$ and the regression coefficient of 1.0 indicate that on the average $u_*(profile) = u_*(direct)$. The high correlation indicates that the deviations from this average are small (see also figure 4.3). So the profile method and the direct method yield the same friction velocities.

- Sensible heat fluxes from the sonics.

The measured sensible heat fluxes are shown in figure 4.4. On the vertical axis are the fluxes obtained by the direct method (w and T from the sonic anemometer) and on the horizontal axis those from the profile method. As it can be seen from the figure there are some points for which the profile method gives a sensible heat flux of about 0 $W\ m^{-2}$, whereas the direct method yields something in the

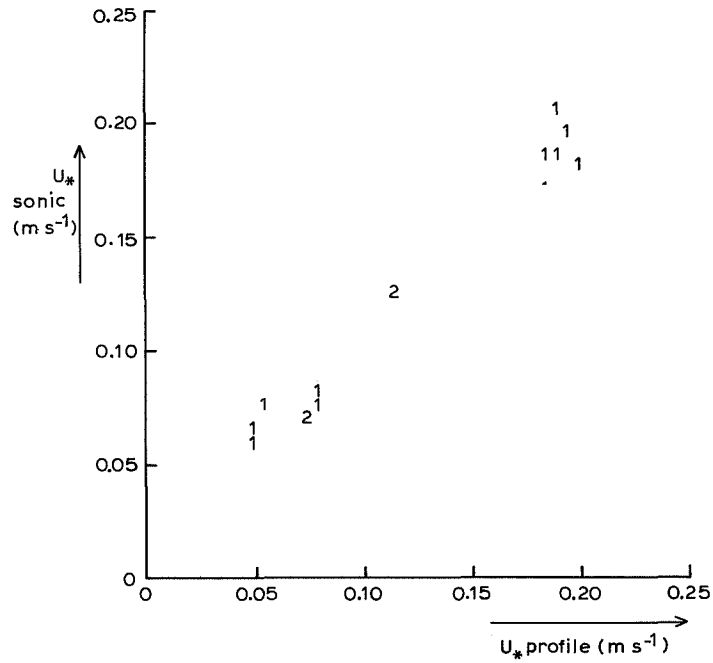

Figure 4.3: *Comparison of friction velocities from the direct method (vertical) and the profile method (horizontal), (a '1' indicates a measurement point, a '2' indicates two coinciding points, and a '*' indicates a point more than 2 standard deviations away from the line $x = y$).*

order of $-10\ W\ m^{-2}$. The other points lie more or less on a straight line through the origin with an angle of tangent 0.7.

Although the relative differences in the sensible heat fluxes are large, the absolute magnitude of these differences is small compared to the total heat balance, therefore the cause of the differences was not examined in full detail.

A small part of these differences can be explained by the fact that the temperature fluctuations measured by the sonic anemometer also contain humidity fluctuations (see appendix 3). For the points near $(0,-10)$ in figure 4.4, the latent heat flux was in the order of -50 to $-20\ W\ m^{-2}$. So with the aid of equation A3.7 we find that 1 to 3 $W\ m^{-2}$ is caused by the humidity influence on the measured sonic virtual temperature.

In near neutral conditions errors in the measured temperature gradient might cause an error of about 5 $W\ m^{-2}$ in the sensible heat flux obtained with the profile method (assuming an error of at most 0.2 K in the total profile and u_* about 0.1 $m\ s^{-1}$). Systematic errors in the measurement of the temperature profile, however, cannot explain all the differences since in near neutral cases the sign of the

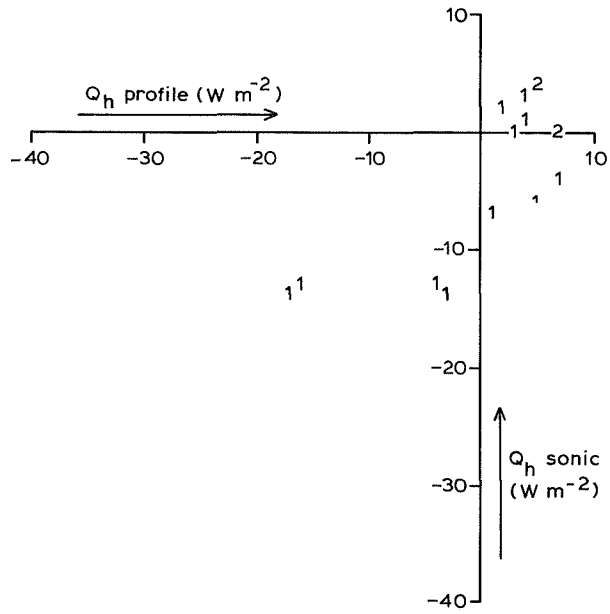

Figure 4.4: *Comparison of sensible heat fluxes calculated from the sonic anemometer measurements with those derived from the profiles (for more explanation see figure 4.3).*

difference is opposite to that in unstable cases.

The runs for which the direct method gives about $-10\ W\ m^{-2}$ and the profile method about $0\ W\ m^{-2}$ fell in the period when the water level was rising. Possibly not completely adapted boundary layers have influenced the profile results. Also the fact that the geometric mean height of the profile ($8.5\ m$) is not equal to the height on which the sonic anemometer was installed ($4.5\ m$) can become important in situations where the boundary layer is not adapted.

- **The latent heat fluxes.**

With the direct method the latent heat flux is derived from the eddy correlation product of the vertical wind speed, which was measured with the sonic anemometer and the specific humidity, which was found from a dry and a wet bulb temperature with the psychrometer equation (3.10). The wet bulb temperature was measured with a wet thermocouple. For the dry bulb temperature we used a thermocouple or the sonic virtual temperature. The wet bulb thermocouple however, reacts slower to temperature changes than the dry thermocouple or the sonic anemometer due to the presence of a cotton thread saturated with water. To avoid unrealistic humidity fluctuations to be calculated, one can filter the dry bulb temperature or one can artificially accelerate the measured wet bulb temperature signal.

In all cases it made only a little difference whether the dry thermocouple was used or the sonic virtual temperature. The usage of the sonic virtual temperature yielded a latent heat flux which was 3 to 6 $W\ m^{-2}$ less (more negative) than the usage of the dry thermocouple. In stable situations, with a latent heat flux of 0 to 20 $W\ m^{-2}$ the relative error is large, but in all cases 3 to 6 $W\ m^{-2}$ can be neglected in the heat balance.

The agreement between the directly obtained latent heat fluxes and those derived from the profiles is much worse. In stable and neutral cases both methods yield fluxes of approximately the same magnitude (using the sonic virtual temperature as dry bulb in the direct method). Under unstable atmospheric conditions, however, the profile derived fluxes are about 2 times those found with the direct method. In section 4.1.1. it was shown that in unstable situations the profile method is very sensitive to errors in the temperature measurement. Nevertheless the latent heat fluxes obtained with the profile method are estimated to contain errors less than 30 %.

Even if the magnitude of the profile derived latent heat fluxes was 30 % to high due to systematic errors in the measurement of the temperature profile, this leaves a factor 1.5 unexplained. Therefore we will have a closer look at the effect of accelerating the measured wet bulb temperature signal which is used in the direct method, and the effect of filtering the other signals used in the direct method.

When the wet bulb signal is to be accelerated, or the other signals are filtered in such a way that their response characteristics resemble those of the wet bulb sensor, one has to know the cut off frequency, or the response time of the wet bulb thermocouple. For a definition of the response time, the cut off frequency and how they are related, the reader is referred to appendix 6. From a comparison of the various temperature spectra the cut off frequency of the wet bulb thermocouple was estimated to $0.4 \pm 0.1\ s^{-1}$, which corresponds with a response time of 0.4 s. For the same type of wet bulb sensor Shaw & Tillman (1980) also found a cut off frequency of $0.4\ s^{-1}$ by minimizing the variance in the calculated specific humidity.

The latent heat fluxes calculated by accelerating the wet bulb signal are slightly less (more negative) than those obtained by filtering the other signals. The difference is 2 to 4 $W\ m^{-2}$, which is about 8 % of the calculated latent heat flux in unstable cases. When nothing was done to match the response characteristics of the wet bulb and the other signals, the latent heat fluxes were reduced by a factor 0.8. It was also observed that filtering reduced the calculated sensible heat flux by about 17 % (in unstable cases), so probably even the latent heat flux obtained by accelerating the wet bulb signal is about 10 % to low.

When accelerating the wet bulb signal the cut off frequency was assumed to be $0.4\ s^{-1}$. When this value is changed to $0.3\ s^{-1}$, the calculated latent heat fluxes

increase by about 6 %. So changing the cut off frequency within reasonable margins does not affect the results greatly. To obtain latent heat fluxes in the order of 0.7 times those derived with the profile method, one should use a cut off frequency of 0.1 s^{-1}, which is a very unlikely value.

Taking into account all errors discussed so far, there remains under unstable conditions a difference of at least 30 % between the latent heat fluxes found by applying the direct method and those derived from the profiles. Therefore all possible causes of errors are summarized below.

Errors in the profile derived latent heat fluxes due to inaccuracies in the measured temperature profiles have already been excluded by applying a 30 % margin.

There have been problems in translating the profile method in computer programs, but these problems only apply to stable atmospheric conditions.

Theoretically the profile method cannot be used if terrain conditions are not homogeneous. Some of the unstable runs were taken during the night with more than one meter water on the tidal flats. Under these conditions the gradients in the surface temperature and roughness length are very low. Since these runs show no better agreement between profile and direct method than the other unstable runs, inhomogeneity cannot explain the difference.

There are some indications that the stability dependence of the profile method is to strong during unstable conditions. Possibly the low surface roughness played a role, since the experimentally established parameters in the profile method have been derived for terrains with a surface roughness which is about three orders of magnitude larger. It would however take a more thorough study of the profile method and perhaps an experiment especially dedicated to this, to be more certain about this.

The problem of the different response time of the various sensors used to measure the latent heat flux with the direct method seems adequately solved by accelerating the wet bulb temperature signal.

The spatial separation of 0.5 to 1.0 m between the sonic anemometer and the thermocouples has some influence in stable situations, but in unstable situations little influence could be observed.

The results of the direct method can also have been inflicted by a poor water supply to the wet bulb thermocouple. Also the collection of salt particles on the wet bulb thermocouple can have reduced the evaporation of water from it. If the evaporation from the wet bulb thermocouple is reduced due to an inadequate water supply, or due to the presence of salt, the wet bulb temperature will follow the dry bulb temperature closer than in the ideal situation, causing the calculated

specific humidity fluctuations to be less than what they are in reality. Measures should be taken to assure an adequate water supply and to avoid pollution of the wet bulb sensor.

As a conclusion we can state that under stable conditions the latent heat flux obtained with the direct method agrees well with values obtained by the profile method, whereas in unstable situations there is a large difference between the two methods. This difference cannot be completely explained by errors in the measurement of the temperature profiles. Probably it was largely caused by pollution of the wet bulb sensor, which was used in the direct method, by salt particles or an insufficient water supply to the wet bulb sensor. The possibility that the profile method reacts to strong to changes in stability can however not be excluded totally.

4.2. Comparison of soil heat flux measurement.

Soil heat fluxes have been measured by four methods: the integration method, the gradient method, the Fourier method and by the use of soil heat flux plates (see section 3.8). The results from these methods are compared below. Comparisons are based upon measurements during the 1983 Balgzand experiment. However for the comparison between the profile integration and the Fourier method we used data from the 1982 Mok Bay experiment. It is found that the integration method and the Fourier method yield the best results, mainly because these methods provide a way to measure the soil heat flux at the surface, while the other methods always measure the flux at some depth. Other reasons are that the gradient method is very sensitive to errors in the calibration of the NTC-sensors and that the plates have a conductivity which is not well adapted to that of the soil of the tidal flat.

4.2.1. Integration method versus gradient method.

With the integration method it is possible to determine the soil heat flux at the surface, which is not possible with the gradient method. When the temperatures at the surface and at a depth of 5 *cm* are used to calculate the gradient, the gradient method yields the soil heat flux at a depth somewhere between 0 and 5 *cm* (about 2.5 *cm* depth). When there is no water on the tidal flat the problem is even worse, because then the surface temperature is difficult to measure. In this case the temperatures on a depth of 5 and 10 *cm* are used, yielding the flux at approximately 7.5 *cm*.

In order to make the two methods more comparable, the integration method was also used to calculate the flux at a depth of 2.5 *cm* when the tidal flat was inundated and at a depth of 7.5 *cm* when it was dry. It was found from the measurements on the Balgzand that on the average the heat flux at the surface is about 1.2 times the flux calculated in this way. Since on the Balgzand most of the time

the surface temperature was available, this factor of 1.2 applies to a depth of 2.5 *cm*. This value of 1.2 can also be found from theory (appendix 5)

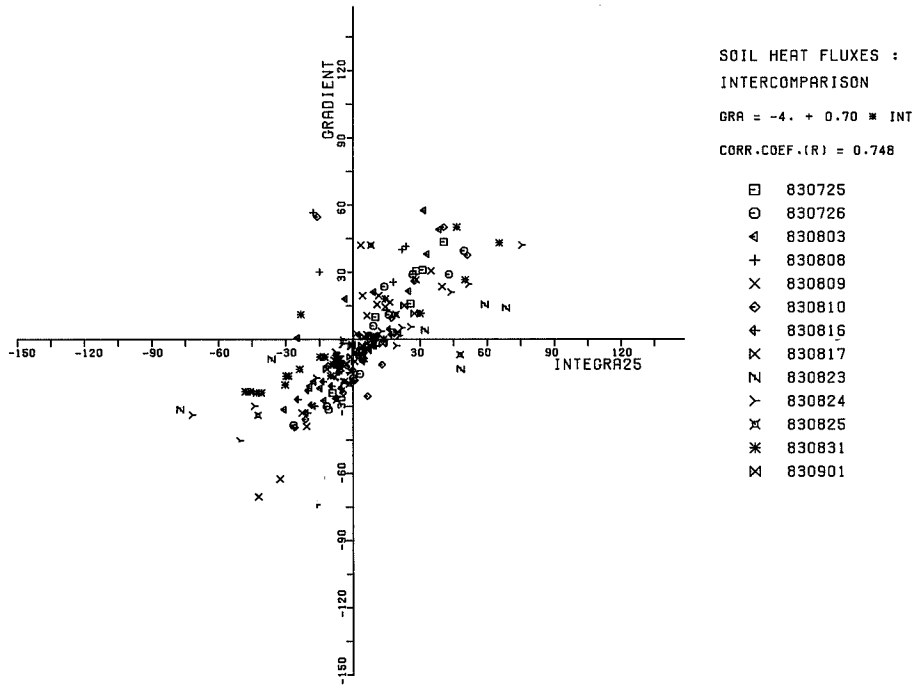

Figure 4.5: *Comparison of soil heat fluxes from the gradient method with those from the integration method (more explanation in text).*

In figure 4.5 the fluxes measured with the gradient method are compared with those calculated with the integration method (for the same depth). The comparison is based on hourly averages. Almost all data gathered at the 1983 Balgzand experiment are used, only days with to few observations are excluded. For each day a different symbol is used. Extreme differences between the two methods are caused by rapid changes of the surface temperature (for example when relatively cold water inundates the tidal flat which is heated by the sun). The basic condition for the use of the gradient method, stationarity, is not fulfilled when the surface temperature changes rapidly.

The gradient method is also very sensitive to errors in the temperature measurement, because two temperatures measured with different sensors are subtracted. Probably some systematic errors (for example on the 31^{st} of august) are caused by a drift in the calibration factors of the sensors. Since NTC-sensors are resistance thermometers oxidation of the connecting plugs adds extra resistance and therefore changes their temperature response.

Another disadvantage of the gradient method is that it is (almost) impossible to extrapolate the calculated heat flux to the soil heat flux at the surface. Although the rate of these two fluxes is on the average 1.2, it can be anything in the range from 0.5 to 2.0 and even outside this range in extreme cases. The integration method however is sensitive to noise in the temperature registrations of the lowest levels, because they represent the temperature of a thick layer. Also the resolution of the NTC-sensors ($0.02-0.03\ K$) caused some noise in the calculated soil heat fluxes. This is due to the fact that the deepest sensors represent the temperature in a layer of 20 cm thickness. When this layer changes 0.03 K in temperature, its contribution to the soil heat flux at the surface is about 9 $W\ m^2$, which is high compared with values in the order of 50 $W\ m^2$. This resolution problem has been solved by filtering the temperature registrations of the $-50\ cm$ level with a first order filter which has a time constant of two hours. This filtering also reduces the noise in the temperature signal. Filtering is legal because fast temperature fluctuations at the surface hardly reach the $-50\ cm$ level. For example when the surface temperature should vary sinusoidally with a period of four hours and an amplitude of ten degrees Celcius, the amplitude at $-50\ cm$ will be less than $0.001\ ^oC$ (assuming $\underline{a} = 1.07 * 10^{-6}\ m^2 s^{-1}$). This is well below our measuring accuracy.

The integration method is almost insensitive to (small) calibration errors or drift in the calibration factors, because it always subtracts temperatures which are measured with the same sensor.

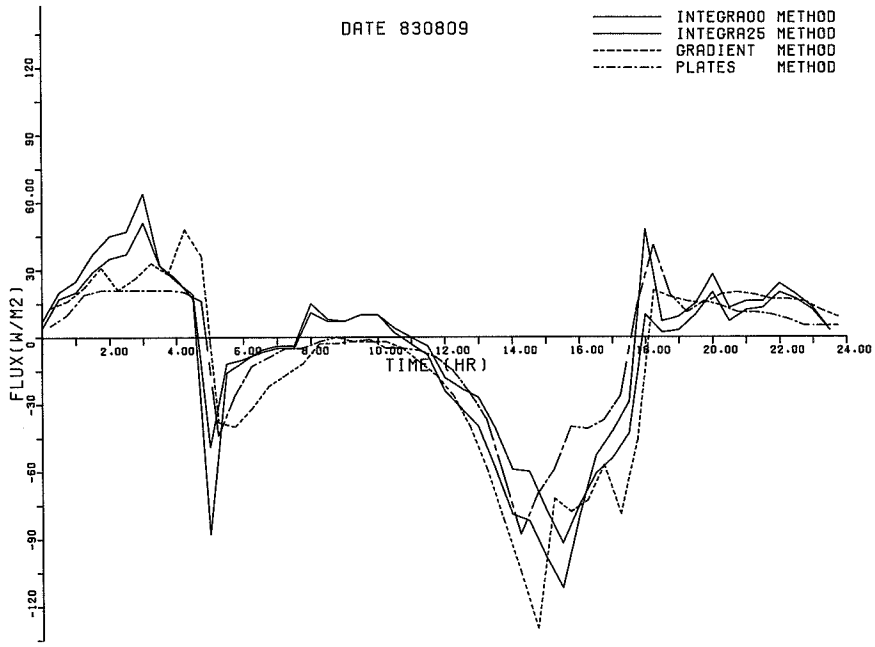

Figure 4.6: *Course of the soil heat flux during a day. (explanation in text)*

In figure 4.6 the course of the soil heat flux measured with the gradient and with the integration method during a day is shown. For the integration method two lines are drawn, one indicates the soil heat flux at the surface (integra00) and the other one indicates the flux at the same depth as for which the flux is calculated with the gradient method (integra25).

4.2.2. Plate versus integration method.

The soil heat flux plate was mounted at a depth of 5 *cm* (during the Balgzand experiment). With the integration method also the soil heat flux was calculated for a depth of 5 *cm* in order to make the two methods comparable. Figure 4.7 compares hourly averages of the soil heat fluxes measured with the flux plate and those calculated from the integration method (for a depth of 5 *cm*).

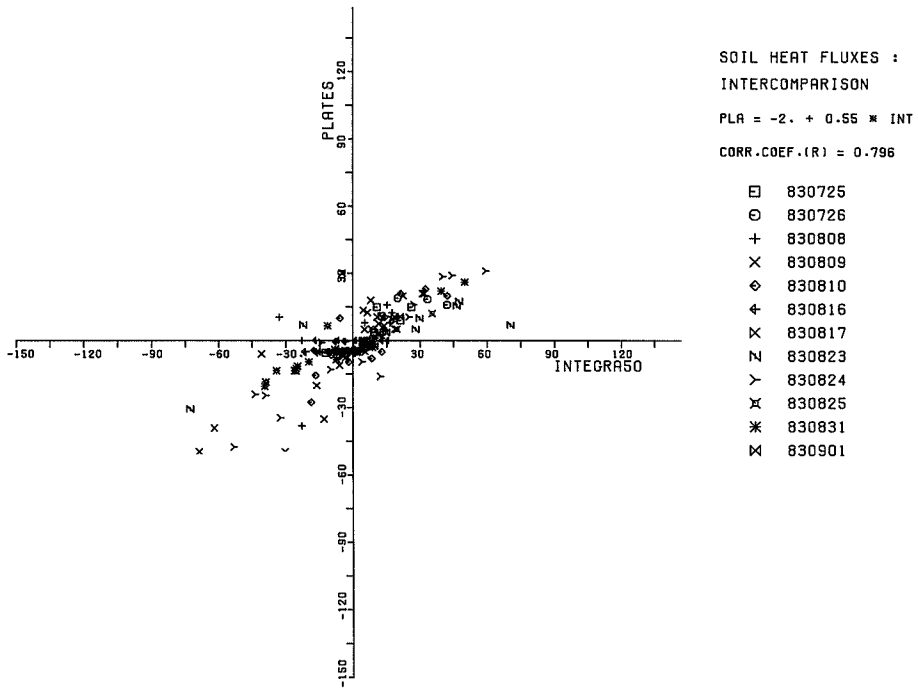

Figure 4.7: *Comparison of soil heat flux measured by the flux plate with that calculated from the integration method.*

On the average the flux measured with the flux plate is about 45 % to low, which is almost a factor of 2. Andrews (1980) also mentioned that the calibration factors for Middleton soil heat flux plates, which are supplied by the manufacturer, do not yield good results when the plates are used in the wet soil of a tidal flat. The difference can be explained by assuming that the thermal conductivity of the flux

plates differs to much from that of the soil. Overgaard-Mogensen (1970) derived a formula which describes the ratio of actual and measured soil heat flux as a function of the dimensions of the flux plate and the ratio of the thermal conductivities of the flux plate and the soil:

$$\frac{Q_b}{Q_{bp}} = \frac{1}{1 - a_p \frac{d_p}{A_p^{0.5}} (1 - \frac{\lambda_b}{\lambda_p})}, \qquad [-] \ (4.4)$$

where a_p is a meter constant (approximately 1), d_p is the thickness of the flux plate (5 mm), A_p is the area of the flux plate (48*29 mm^2), λ_b is the thermal conductivity of the soil (2.9$W\ m^{-1}K^{-1}$) and λ_p is the thermal conductivity of the flux plate.

This formula is used to make an estimate of the thermal conductivity of the flux plate. With $Q_b/Q_{bp} = 1/0.55$ it follows that the thermal conductivity of the flux plate should be about 0.4 $W\ m^{-1}K^{-1}$. This is a very reasonable value for flux plates when they are used in dry sand, but it is not very suitable when the plates are used in a water saturated soil. A correction could be made by multiplying the heat fluxes measured with the flux plates with a factor of 1.8. The measurement with plates at a finite depth causes a loss of information. On the average the soil heat flux at a depth of 5 cm is only about 0.65 times that at the surface, but again this figure is not a constant, so there is no way of finding the flux at the surface accurately from the measurements with the plates. The integration method is preferred, because it yields the soil heat flux at the surface.

4.2.3. Fourier method versus integration method.

The Fourier method (described in section 3.8.4) provides a way to calculate the soil heat fluxes at the surface, like the integration method. It only needs temperature measurements at one depth not too far below the surface (preferably less then 5 cm) and the thermal properties of the soil (conductivity and volumic heat capacity). The comparison in figure 4.8 (based on hourly averages) shows that the correlation between the two methods is good. There are a few values for which the calculated soil heat flux obtained by the Fourier method differs far from the integration method. During these hours the soil heat flux changes very fast because the water starts inundating the tidal flat. The Fourier method is better capable of following these very fast changes (as can be seen in figure 4.9 at 22.00 h).

Figure 4.9 shows the course of the soil heat flux during 1 day calculated with different methods. In this figure it can also be seen that the Fourier and the integration method compare well. The fluctuations between 4.00 and 8.00 h of the values

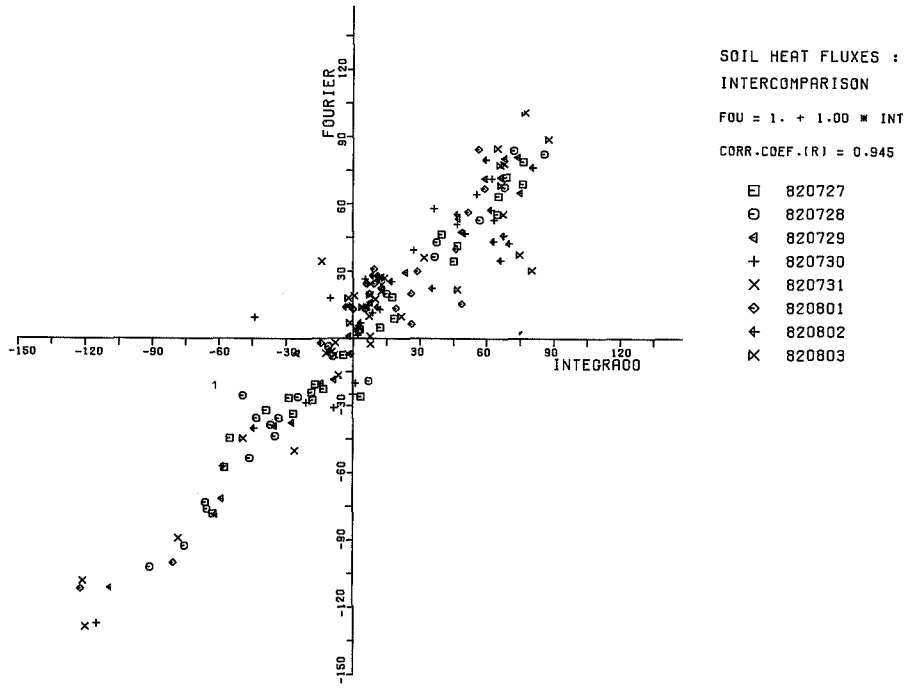

Figure 4.8: *Comparison between the soil heat fluxes calculated with the Fourier method and those calculated with the integration method.*

calculated with the Fourier method are an artefact of the method. This artefact can be removed by measuring the temperature closer to the surface. Possibly the results from the Fourier method can also be improved by using the separate observations (12 per hour) in stead of half hourly averages.

4.3. Comparison of estimated and measured net radiation.

The radiation data collected at the 1982 Mok Bay experiment were evaluated statistically by Lambooy (1985). In this evaluation estimated net radiation is included too.

When using equation 3.2 to estimate hourly averages of net radiation the estimates correlate well with the observed net radiation (correlation coefficient $r = 0.98$). The offset of the regression line was small (2.5 $W\ m^{-2}$) and the slope of the regression line close to unity (0.98). The standard error of estimate was found to be 34 $W\ m^{-2}$, whereas on the average the net radiation was overestimated by 5 $W\ m^{-2}$. The standard error of estimate which was found is low when we bear in mind that measured net radiation, as well as the measured incoming and reflected short wave radiation are subject to measurement errors. Moreover the net long

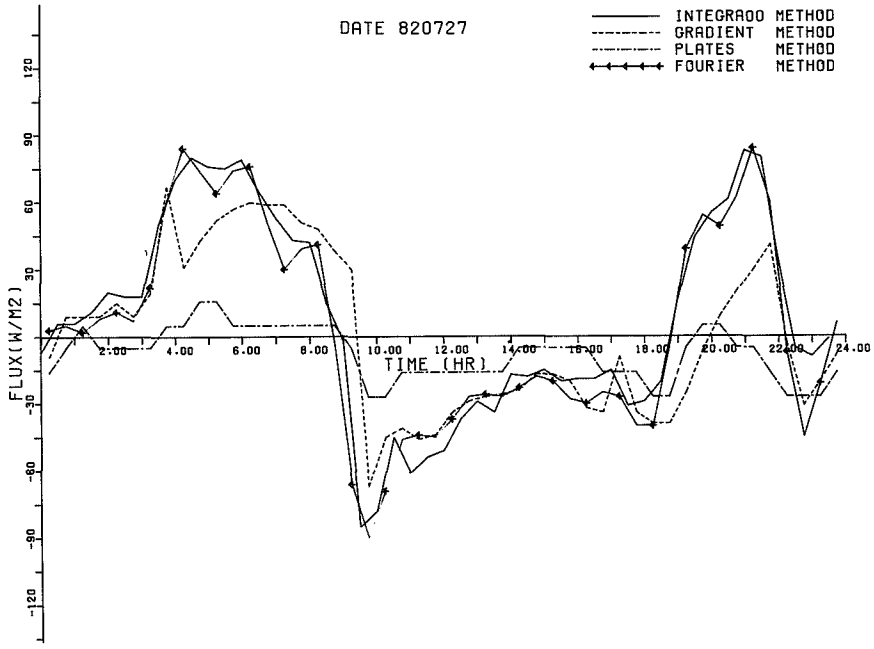

Figure 4.9: *Course of the soil heat flux during 1 day, calculated with different methods.*

wave radiation was found by a rough estimate from surface temperature, air temperature, humidity and the relative duration of bright sunshine (or effective cloudiness during the night).

Equation 3.1 does not make use of the measured incoming and reflected short wave radiation, but estimates the net short wave radiation from the incident angle of the sunshine, the solar constant and the relative duration of bright sunshine. When this equation was used in stead of 3.2 the correlation became less (r = 0.96) and the standard error of estimate larger (53 $W\ m^{-2}$).

Also tested were two other equations. The first equation calculates net radiation as the sum of the measured net short wave radiation ($R_{s1}-R_{s2}$), the long wave radiation emitted by the surface (σT_0^4), the clear sky radiation according to Swinbank (1963) and the long wave radiation emitted by clouds (if present) as proposed by Paltridge (1973), resulting in:

$$R_n = R_{s1}-R_{s2} - \sigma T_0^4 + a_s T_a^6 + b_p N \ , \qquad [W\ m^{-2}] \ (4.5)$$

where T_0 is the surface temperature, T_a is the air temperature, $a_s = 5.31*10^{-13}\ W\ m^{-2}\ K^{-6}$ (Swinbank 1963), $b_p = 60\ W\ m^{-2}$ (Paltridge 1976) and N is the fractional cloud cover. In the second equation the clear sky radiation according to Idso (1983) was used, which gives:

$$R_n = R_{s1} - R_{s2} - \sigma T_0^4 + (a_i + b_i e_a * e^{c_i/T_a})\ \sigma T_a^4 + b_p N\ , \qquad [W\ m^{-2}]\ (4.6)$$

where $a_i = 0.660$, $b_i = 5.95 * 10^{-5}\ mb^{-1}$ and $c_i = 1500\ K^{-1}$ (Idso 1983). Equation 4.5 underestimates the observed net radiation by 11 $W\ m^{-2}$ on the average, whereas (4.6) overestimates by $7W\ m^{-2}$ on the average. The standard error of estimate of both methods was 29 $W\ m^{-2}$, which is slightly better than what was found by applying (3.2).

The net short wave radiation could be parameterized by (Holtslag 1983):

$$R_{s1} - R_{s2} = a_h + b_h \sin(S_e)(1 + c_h N^{d_h})(1 - \alpha)\ , \qquad [W\ m^{-2}]\ (4.7)$$

where $a_h = -69\ W\ m^{-2}$, $b_h = 1041\ W\ m^{-2}$, $c_h = -0.75$, $d_h = 3.4$ (Holtslag 1983), S_e is the solar elevation and α is the surface albedo. When this was substituted in (4.5) or (4.6) the standard error of estimate became approximately 53 $W\ m^{-2}$ in both cases. The combination of (4.5) and (4.7) yielded on the average an overestimation of the net radiation of 16 $W\ m^{-2}$, whereas the combination of (4.6) and (4.7) gave an underestimation of 2 $W\ m^{-2}$ on the average.

equation	*short wave*	*long wave*	$R_e - R_o$	*SEE*	*R*	*A*	*B*
3.2	*measured*	*De Bruin*	*5*	*34*	*0.98*	*-2.5*	*0.98*
4.5	*measured*	*Swinbank Paltridge*	*-11*	*29*	*0.99*	*13.6*	*0.97*
4.6	*measured*	*Idso Paltridge*	*7*	*29*	*0.99*	*-4.8*	*0.98*
3.1	*De Bruin*	*De Bruin*	*-2*	*53*	*0.96*	*-0.4*	*1.02*
4.5+4.7	*Holtslag*	*Swinbank Paltridge*	*-2*	*52*	*0.96*	*6.3*	*0.95*
4.6+4.7	*Holtslag*	*Idso Paltridge*	*16*	*54*	*0.96*	*-10.5*	*0.96*

Figure 4.10: *Statistical result for equations for estimating net radiation. (R_e is the estimated net radiation, R_o is the observed net radiation, SEE is standard error of estimate, R is correlation coefficient, A is offset of regression line and B is slope of regression line, units $W\ m^{-2}$* if appropriate).

The table in figure 4.10 summarizes the most important results of a statistical analysis of the six equations for estimating net radiation which were discussed.

CHAPTER 5

THE HEAT BALANCES

In this chapter the results of the heat balance calculations are discussed and the importance of the separate terms is weighed. The heat balance is also used to determine the course of the water temperature. Comparison of the course of the calculated water temperature with the measured water temperature gives information on the accuracy of the measured meteorological parameters and the validity of the formulas used for calculating the heat balance terms.

5.1. Heat balance at one point on the Mok Bay tidal flat.

When the water temperatures were calculated from the heat balance (eq. 2.3), for a point near mast 1 on the tidal flat in Mok Bay (see app. 1), large problems were encountered. These problems were mainly due to errors in the advection calculation, which were caused by a wind driven current in a direction perpendicular to our measurement line. Possibly the calculation of sensible and latent heat fluxes from profiles, which were measured in a not completely adapted boundary layer, also played a role. In the calculations we used net radiation which was measured directly and soil heat fluxes derived with the profile integration method.

Since there is only a restricted amount of time available for this research, a choice had to be made from the available data. From the Mok Bay measurements, the period from July 28 to August 3, 1982 was selected, because this was a long period with fine weather, i.e. large heat fluxes.

Below follows a brief description of the weather for the chosen period, a description of the heat balance during low tide and an explanation of the errors in the calculation of the water temperatures from the heat balance.

5.1.1. The weather.

The following description covers the period from July 26 to August 4, 1982, this weather description is also used in section 5.2, in which the heat balance for the entire Mok Bay is discussed.

Most of this period fine weather prevailed, with little cloud cover. The wind was blowing moderately from easterly directions and maximum temperatures above the tidal flats sometimes were as high as $25-26\ ^oC$. Inland (De Bilt) there were several days with a maximum temperature above $30\ ^oC$.

This fine weather was caused by a high pressure system, located west of Ireland on July 26, above Scotland on July 28 and moving slowly towards Scandinavia. July 27 was a clouded day due to the vicinity of a front, but there was no rainfall. On July 30 cirrus clouds, belonging to a frontal system, reached the Dutch Wadden area from the south. Also July 31 was partly clouded with cirrus. In the afternoon of August 1 there was also some altostratus. The front, which was highly deactivated by the vicinity of the high pressure system, passed our location on August 1. Nevertheless the weather stayed warm and dry. The wind changed more or less gradually from south easterly in the morning to north westerly in the afternoon. At about 17.00 h (LST) that day, the wind veered from almost north (340°) to east (100°) within 5 minutes. The wind speed decreased gradually from 8 $m\ s^{-1}$ in the early morning to 2.5 $m\ s^{-1}$ at 17.00 h.

August 2 and 3 were almost unclouded with light to moderate winds from the east. The afternoon of August 4 was partly clouded and in the evening the wind turned to the west.

5.1.2. The heat balance during ebb-tide.

To illustrate the problems we met, a few days have been selected, namely July 31, August 1 and August 2. We will turn to the heat balance during the periods that the tidal flat was submerged in the next section. This section treats the heat balance for one point on the Mok bay tidal flat during the periods with no water on the tidal flat.

During the low tide in the morning of July 31 the sum of the fluxes was close to zero (see fig. 5.1). Although there is some discrepancy during separate runs, the average deficit over the whole dry period is $-15\ W\ m^{-2}$, which is very low.

During the dry period in the evening of July 31 it is obvious (from figure 5.1) that the terms do not balance. This is caused by the fact that during that night the datalogger, which monitored the soil temperatures, stopped. Therefore it was necessary to use the soil heat flux measurements from the flux plates, which are very inaccurate, as was shown in section 4.2.2. During the dry periods in other nights,

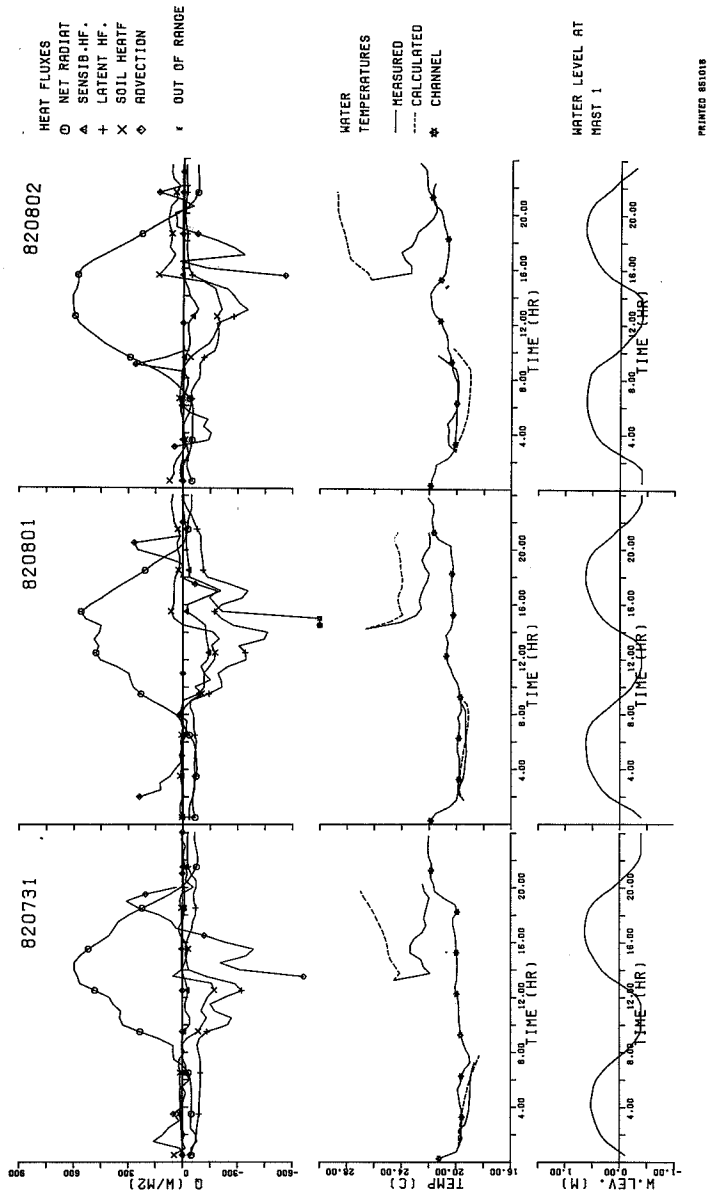

Figure 5.1: *Heat balance on the Mok Bay tidal flat.*

the sensible and latent heat flux become very small and the loss of net radiation is compensated by the soil heat flux.

During the dry period in the morning and early afternoon of August 1, there is a large deficit in the heat balance, about 150 $W\ m^{-2}$ on average. When we used

the bulk method in stead of the profile method, for calculating the fluxes of sensible and latent heat, these fluxes were on average only half of the values which were calculated with the profile method and the deficit in the heat balance became $+38\ W\ m^{-2}$. The large errors in the fluxes calculated with the profile method can be explained by the fact that, during this day, the weather situation was not stationary and the upwind terrain inhomogeneous. This day, the wind veered gradually from 170° at 9.00 h to 300° at 15.00 h. In the same period the wind speed decreased from 4.6 to 2.5 $m\ s^{-1}$. Most of the time the wind was south to southwest, so the border between the salt marsh and the tidal flat was between 100 and 200 m from our masts. The roughness length of the salt marsh is in the order of 1 cm, whereas that of the tidal flat is at least a factor 100 lower. This (upwind) roughness step might have had implications for the measured profiles (measured from $2-12\ m$). The bulk method uses estimated surface temperatures and humidities and wind speeds, temperatures and humidities measured at a height of approximately 2.5 m. Most (if not all) of the gradient used for the bulk method lies within the inner (adapted) boundary layer, whereas the measurements used for the profile method lie, at least partly, outside the adapted part of the boundary layer.

During the dry period around noon August 2, the deficit in the heat balance is $+88\ W\ m^{-2}$ on average. This is about 18 % of the largest term (net radiation) and about 10 % of the sum of the absolute values of all terms. The wind speed was about 6 $m\ s^{-1}$ and the wind direction east. So the edge of the tidal flat was about 300 m upwind. Possibly the discontinuity in the surface temperature at the edge of the tidal flat influenced the measurement of the profiles. The temperature of the water surface was about 21 $°C$, whereas the temperature of the surface of the tidal flat changed from 21 $°C$, just after falling dry, to 30 $°C$ just before flooding.

5.1.3. The calculated water temperatures.

Figure 5.1 depicts the heat balance for one point on the Mok bay tidal flat and the observed and calculated (with eq. 2.3) water temperatures. As can be seen the calculated water temperatures deviate largely from the measured temperatures during daytime, except on August 1. Other days in the period from July 28 to August 3 are similar to July 31. During the nights the differences between the calculated and observed temperatures are less, so we will concentrate on the daytime.

Errors in the calculation of the sensible and latent heat fluxes were not large enough to have caused the differences between the observed and calculated temperatures. It was seen in the previous section that during the dry periods there can be errors in the calculated fluxes of sensible and latent heat, which were probably caused by the inhomogeneity of the upwind terrain. During high water periods this inhomogeneity was less; there was no change in the roughness length of the upwind

terrain and the change in surface temperature was at most 3 K and at a distance of at least 300 m. So during high water periods the errors in the calculated sensible and latent heat fluxes will be less than during the dry periods. The error in the sum of the latent and the sensible heat flux is estimated to be at most $50 W\ m^{-2}$, which is far too small to cause the large discrepancies between the calculated and observed temperatures.

The discrepancies cannot have been caused by errors in the soil heat fluxes. The soil heat flux, calculated with the profile integration method, is reasonably accurate, but even if it was wrong by a factór 2, it can not have caused the large errors in the calculated water temperatures.

Since net radiation was also measured with reasonable accuracy this leaves only one term to explain the errors, namely the advection term. The advection term was calculated from the temperature gradient, measured in a direction perpendicular to the tidal channel, and a flow velocity, which was estimated from the change of the water level and local topography. Now that we have seen the results of the heat balance calculations we conclude that probably there was a wind driven current over the tidal flat parallel to the tidal channel. When there is a temperature gradient in the direction of this current this causes advection of heat. In the afternoon of August 1, when there was a weak westerly wind, this advection probably was less important, so the water temperature was calculated more accurately. On other days, when the wind was stronger and blowing from the east, this advection contributed more to the local heat balance of the water on the tidal flat.

As an example we examine the situation in the afternoon of August 2. From figure 5.1 it can be seen that the temperature difference between the water on the tidal flat and the water water in the channel was typically in the order of 3 K. Since the wind was east the distance to the tidal channel in the upwind direction was approximately 300 m, resulting in a temperature gradient of $0.01\ K\ m^{-1}$. When we assume a flow velocity, parallel to the channel, of $0.02\ m\ s^{-1}$ and a water depth of 0.5 m we find an advection of heat (parallel to the channel) of $-420 W\ m^{-2}$ (using eq. 2.64). Together with the advection perpendicular to the tidal channel this is more than enough to compensate the net radiation and to cause a cooling of the water instead of the warming which was calculated.

During the nights the temperature gradient between the tidal channel and the tidal flat is small, so the advection is less important. The errors in the calculated water temperature, during the first hours of the high tide in the early morning of August 2, however, may also have been caused by errors in the advection calculation.

5.2. Heat balance for the entire Mok Bay.

The heat balance for the water in the entire Mok Bay (eq. 2.5) will be discussed for the period from July 26 to August 4, 1982. The weather in this period has already been described in section 5.1.1. In the heat balance calculations the bulk method was used to calculate the fluxes of sensible and latent heat in the air, because with the bulk method it is possible to calculate the fluxes above the water surface of the bay (we used the water temperature as surface temperature). With the profile method on the other hand the fluxes on the tidal flat are calculated (position of mast 1 and 2 in appendix 1.). When the tidal flat is emerged, these fluxes are not necessarily representative for the fluxes above the water surface. In section 5.2.2 it will be discussed what the consequences for the heat balance and the calculated water temperatures will be when the profile method is used in stead of the bulk method. In all cases directly measured net radiation was used.

5.2.1. The heat balance using the bulk method.

With the aid of the heat balance for the entire Mok Bay (eq. 2.5) the average water temperature for the bay was calculated. As input variables for the calculation of the fluxes of sensible and latent heat with the bulk method we used the temperature, relative humidity and wind speed measured above the tidal flat near mast 1 and the water temperature which was calculated for the Mok Bay. Further it was assumed that the air just above the water surface had been saturated with water vapor and that the roughness length of the water surface was 10^{-4} m.

The heat balance of the water in the bay is illustrated by figure 5.2. The upper part of the figure shows the amount of heat that the various processes contribute to or retrieve from the water. Therefore net radiation, evaporation and the exchange of sensible heat with the air, which are usually given per unit area, have been multiplied with the water surface of the bay, which is strongly dependent on the tide. Also the soil heat flux is integrated over the part of the bay which is flooded.

It is clear that net radiation is the largest term in the heat balance. The evaporation also is very important. Another important contribution is the input of warm or cold water through the tidal channel, but its influence is far less than that of the advection when calculating the heat balance at one point on the tidal flat. The soil heat flux can be of some significance during the first hours after the tidal flats are flooded, because then the heat which is stored in the bottom during the dry period is released (see for example August 1 12.30−16.00 h). The sensible heat flux is almost always much smaller than the evaporation. On the average the heat balance is determined for about 50 % by net radiation, 30 % by evaporation, 10 % by the input of water through the tidal channel, 7 % by the sensible heat flux and for about 3 % by the soil heat flux. During the daylight hours net radiation,

evaporation and to a less extent the input of water during the flood dominate the heat balance. During the night net radiation is of the same order of magnitude as the evaporation, or less (in absolute sense).

The middle part of figure 5.2 shows the water temperatures measured in the tidal channel (drawn line) and those calculated for the Mok Bay, assuming that the bay water has completely mixed (dotted line). When this assumption is true and the fluxes have been measured accurately, the calculated Mok Bay water temperature should be equal to the water temperature measured in the tidal channel during the ebb-tide (see lowest part of the figure for the tide).

During the period shown in figure 5.2 the overall agreement between the calculated and observed temperature is fairly good. When the calculated water temperatures are averaged over the 19 ebb-tides in this period, the difference with the measured average is only 0.02 K. The standard deviation of the difference between the observed and calculated water temperatures (averaged per ebb-tide) is 0.4 K. This means that in 65 % of the ebb-tides the average water temperature is predicted within 0.4 K. On the basis of this standard deviation we can expect an error of more than 0.8 K in about 5 % of the ebb-tides. These errors are caused by the combined effect of incomplete mixing of the bay water and errors in the calculation of the heat fluxes. That the water in the bay is not completely mixed is shown below.

On several days the calculated and the measured temperatures are essentially different during the first hours of the ebb-tide, due to incomplete mixing of the Mok Bay water. The water which is leaving the bay in those hours is the last water which has entered the bay. During its stay in the bay it has resided in the tidal channel and the central basin only. It did not stay long enough in the bay to mix with the rest of the water. During the first two hours of the ebb-tide on the average about $15*10^4$ m^3 of water leaves the bay (about 20 % of the total tidal discharge). The volume of the tidal channel and the central basin is about $40*10^4$ m^3 (when the water level is -0.8 m NAP), so this is well enough to contain the amount of water which leaves the bay in the first hours.

Incomplete mixing can also be observed in the water that enters the bay (for example in the evening of July 29). In the first two hours of the flood-tide water, which did not yet leave the tidal channel, passes our measurement point, followed by water from the Marsdiep. If the temperature difference between the bay and the Marsdiep is large this transition is marked by a fast temperature change of the water passing the measurement point (for example at 23.30 on July 29).

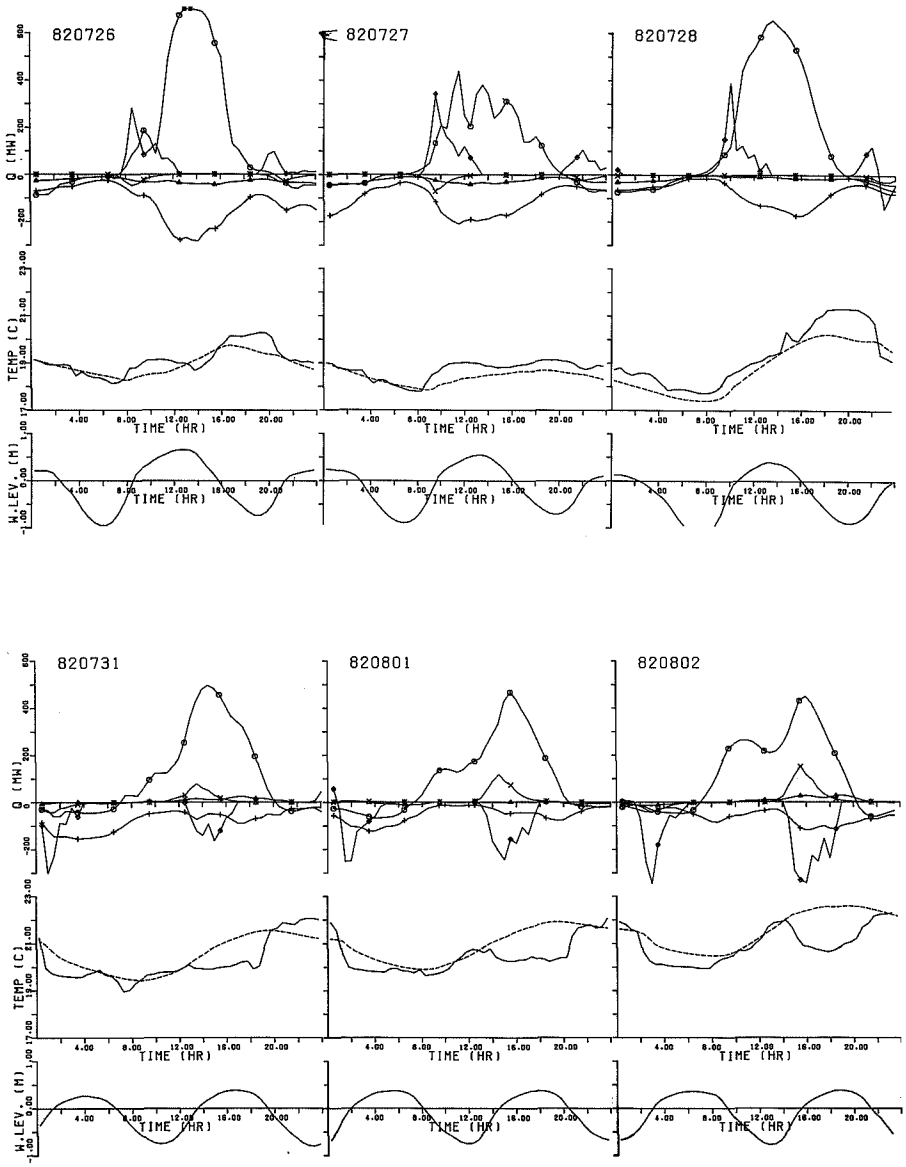

Figure 5.2A: *Heat balance for the entire Mok Bay.*

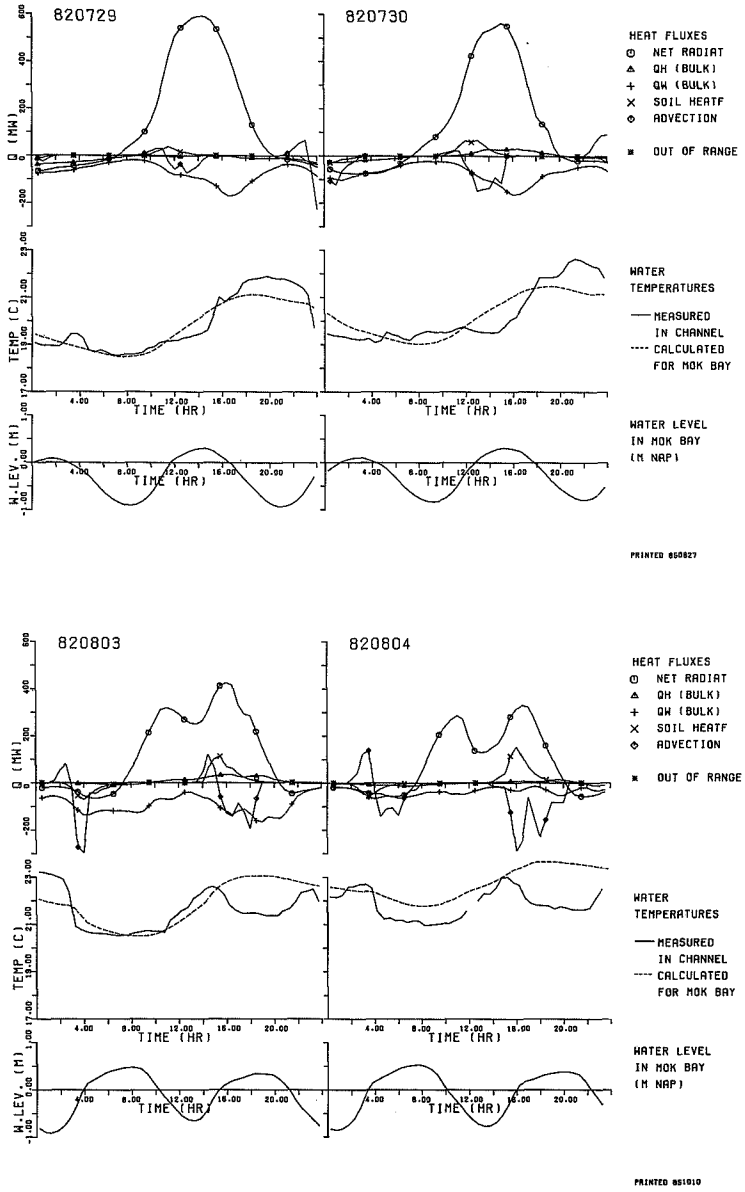

Figure 5.2B: *Heat balance for the entire Mok Bay.*

5.2.2. Using the profile method.

To evaluate the effect of using the profile method in stead of the bulk method to calculate the fluxes of sensible and latent heat we carried out heat balance calculations for the period from July 28 to August 3. When the profile method was used in the heat balance calculations, the water temperature was on the average 0.20 K overestimated, whereas the bulk method yields an overestimation of 0.02 K for the same period. The standard error of the difference between the observed and calculated water temperature (averaged per ebb-tide) is slightly larger than when using the bulk method (0.46 K, compared with 0.42 K when using the bulk method).

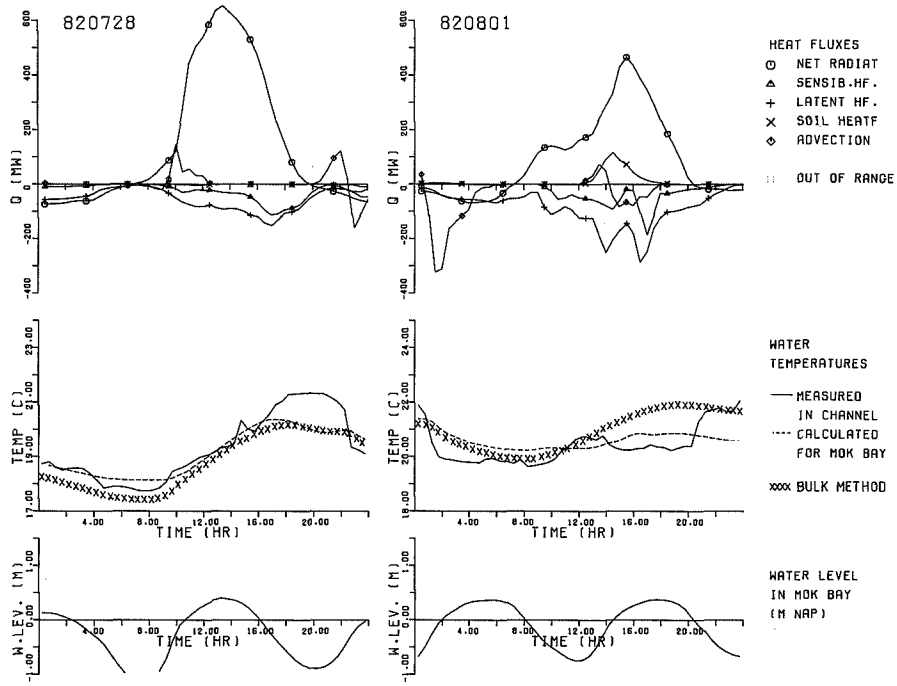

Figure 5.3: *Calculated water temperatures for the Mok Bay from the heat balance with the profile method (dotted line) and with the bulk method (crosses) compared with the measured temperature in the tidal channel (drawn line).*

On most days it makes little difference for the heat balance whether the profile or the bulk method is used. On some days the heat balance with the profile method yields bad water temperatures. As an example the calculated water temperatures are shown for two days in figure 5.3. Also indicated are the water temperatures obtained from the heat balance with the bulk method. The use of the profile method on July 28 slightly improves the agreement between observed and calculated

temperatures. For August 1 the heat balance with the profile method yields bad results, mainly because in the afternoon the evaporation is strongly overestimated. The reason for this overestimation has already been discussed in section 5.1.2.

Since the results obtained with the bulk method are better and the bulk method it simpler to use, the fluxes of sensible and latent in the heat balance can best be calculated with the bulk method. The bulk method also has the advantage that one can use the water temperatures and the air temperature and humidity measured above or very close to the water, whereas the profile method can only calculate the fluxes for the place where the masts are positioned.

5.3. The heat balance for one point on the Balgzand.

The heat balance for one point on the Balgzand (eq. 2.3) is mainly dominated by the net radiation, the advection of heat by the water which flows over the tidal flat and the evaporation. The soil heat flux can be of some importance during short periods, but is small during most of the time. In our situation the sensible heat flux is only of minor importance. These features will be shown in the discussion of three measurement periods during the 1983 Balgzand experiment.

The fact that the advection term plays an important role makes the modeling of the heat balance difficult, because the advection term is hard to measure and extremely sensitive to errors in the measurement of the water temperature (as it will be shown in section 5.3.4). In the heat balance calculations we used net radiation which was measured directly, sensible and latent heat fluxes determined with the profile method and soil heat fluxes which were found with the profile integration method.

5.3.1. The period from August 16 to August 17, 1983.

In the morning of the August 16 there was little cloud cover (1/8 of cumulus) and the wind was blowing from the west with a speed of $7-8\ m\ s^{-1}$. In the afternoon cirrus and later altostratus came over, announcing the approach of a front from the north. The next day the sky was completely clouded with low stratus and there was a small amount of rain in the morning. The actual front passage took place at about 13.30 h LST (11.30 h GMT). At the front passage the wind veered from north-west to east within an hour. Air temperatures were mostly in the range from 16 to 18 ^{o}C with a maximum of 19.4 ^{o}C in the afternoon of the 16^{th}. The weather situation in western Europe is shown on the surface map in figure 5.4.

The heat balance of the Balgzand will be discussed with the aid of figure 5.5. The calculated water temperature in the figure is found from the sum of the terms of the heat balance and the water depth with equation 2.3.

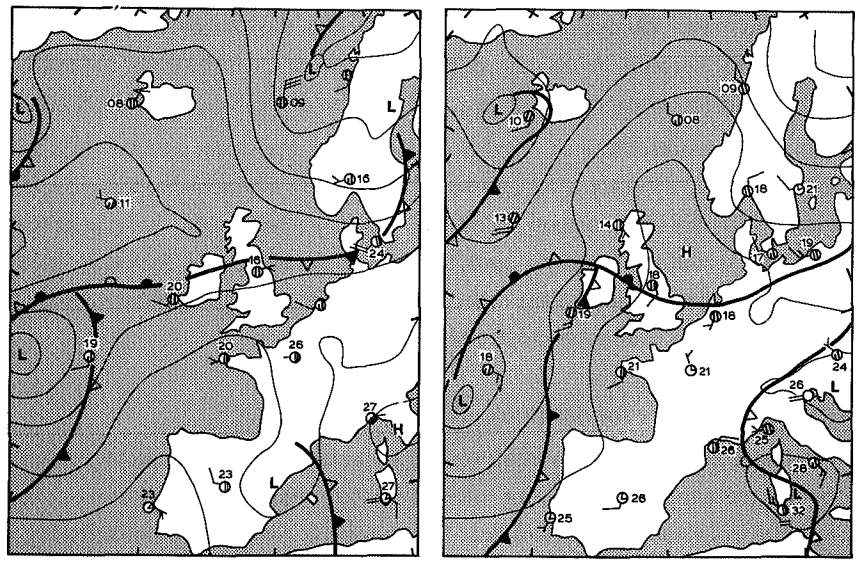

Figure 5.4: *Surface maps: to the left 14.00h LST August the 16th, to the right 14.00h LST August the 17th. (data for these maps are taken from the KNMI daily weather report.)*

In the afternoon of the 16th the water temperature rises gradually, mainly due to solar radiation. This behaviour is also shown in the calculated water temperature. The small peak at 11.15 h is not found in the model calculations. Also in other cases short during peaks and rapid changes are not calculated properly. The decrease in the evening is also seen in the calculated temperatures, although it seems that the model predicts the start of the cooling one hour later than in reality and the decrease is less steep. Probably this is due to an overestimation of the advection between 16.00 and 19.00 h. The peak at the end of the day and the rather sudden rise of the measured water temperature just before midnight are not found in the calculated temperatures. These temperature variations are due to sudden changes in the advection, as will be discussed in section 5.3.5.

The next day changes in the water temperature are very small. The changes which occur are also calculated by the model. Between 9 and 11 hour the model predicts a temperature rise, whereas in reality the temperature rises only slightly. This difference might be due to errors in the water level registration. Also errors in the calculation of the advection or evaporation can cause rather large temperature changes when the heat balance is applied to a thin layer of water.

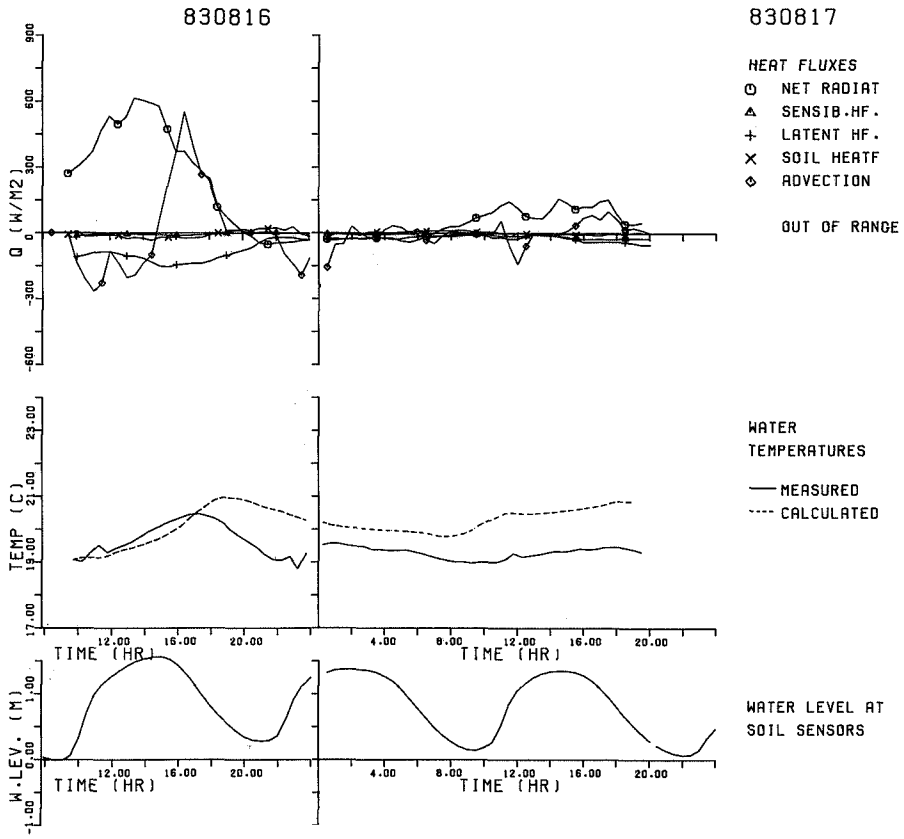

Figure 5.5: *Heat balance from August 16 to August 17.*

5.3.2. The period from August 23 to August 25, 1983.

The 23^{rd} was a sunny day with some cirrus and cirrostratus clouds. In the evening of the 23^{rd} and the following night cumulus and stratocumulus clouds covered the sky almost completely. In the afternoon of the 24^{th} the clouds disappeared, as it can be seen from the net radiation measurements shown in figure 5.6. The 25^{th} was a cloudy day again. The wind in this period was not very strong, $5-7\ m\ s^{-1}$ from the north east. The air temperatures varied from 17 to 20 ^{o}C with a maximum of 20.3 ^{o}C in the afternoon of the 23^{rd}. Relative humidity was high , between 80 and 90 %. Only from 16.00 h till 22.00 h on the 24^{th} it was between 70 % and 80 %.

The strong cooling of the water in the evening of the 23^{rd} (shown in figure 5.6) is also found from heat balance calculations. However the total cooling is underestimated by the calculations. Probably this is due to an overestimation of the advection, caused by inaccuracies in the temperature measurements or errors in the water level correction procedure. The high peak in the water temperature is not

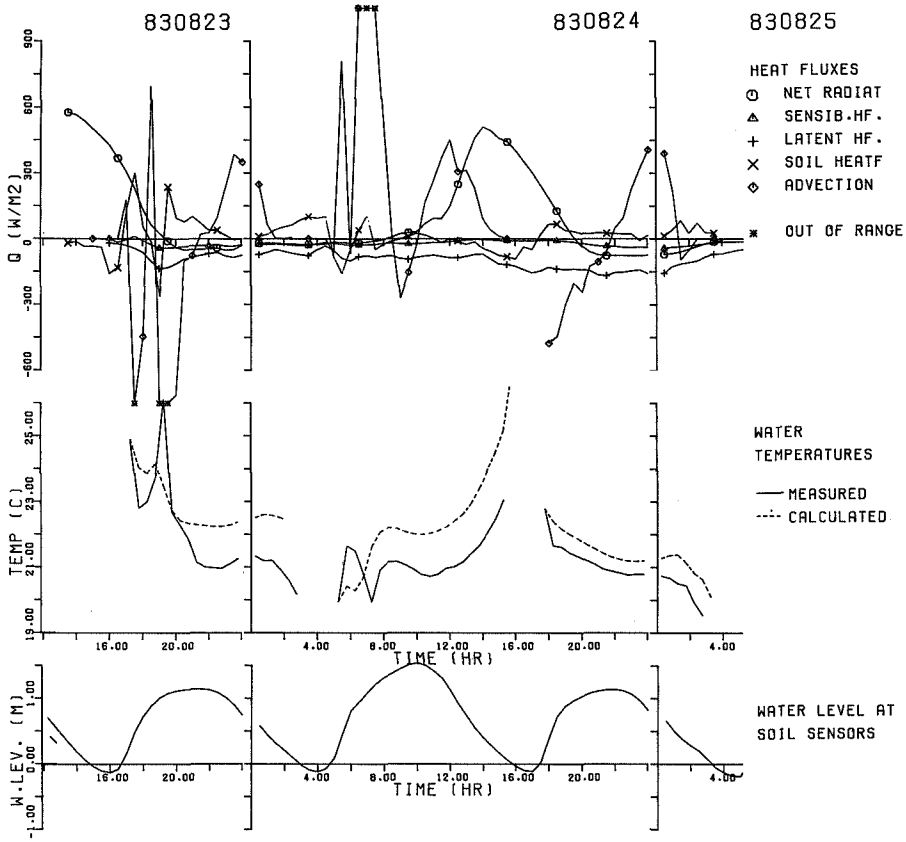

Figure 5.6: *The heat balance from August 23 to August 25, 1983.*

predicted correctly. It will be shown in section 5.3.5 that the calculation of advection, using hourly averages of water temperatures, is not useful for predicting these short peaks. By a more detailed observation of the water temperature measurements it was seen that the high peak, with a maximum of 26.1 ^{o}C lasted only 20 minutes. The peak is caused by water which has been heated on the tidal flat during daytime, has flowed to the deeper tidal channel during the ebb-tide and which is now returning.

It is interesting to see how the soil heat flux responds rapidly to the changes in the water temperature (examine the period from 4 to 8 hour the 24^{th}). This rapid response is due to the fact that the upper layers of the soil follow the changes in water temperature rather quickly. Also the sensible and the latent heat flux respond to changes in the water temperature.

The course of the water temperature in the morning and early afternoon is well calculated from the heat balance. The calculated dip in the water temperature at 7.00 h shows a greater discrepancy with the measured one.

During the evening of the 24^{th} the decrease of the water temperature is very well predicted.

5.3.3. The period from August 30 to September 1, 1983.

In the beginning of this period the weather was dominated by a high pressure system, which had its center above the north-sea in the afternoon of the 30^{th}. The sky was almost clear, apart from some cirrus (1/8) in the evening of the 30^{th} and some clouds at the horizon during both nights. The wind was weak ($2-7\ m\ s^{-1}$) and was predominantly south-east. Air températures varied from 15 to 21 ^{o}C and relative humidity was in the range from 70 to 90 %. At the end of the period the influence of the high pressure system decreased due to the approach of a front. In the morning of September 1 the sky was clouded with stratocumulus, which was formed in a trough.

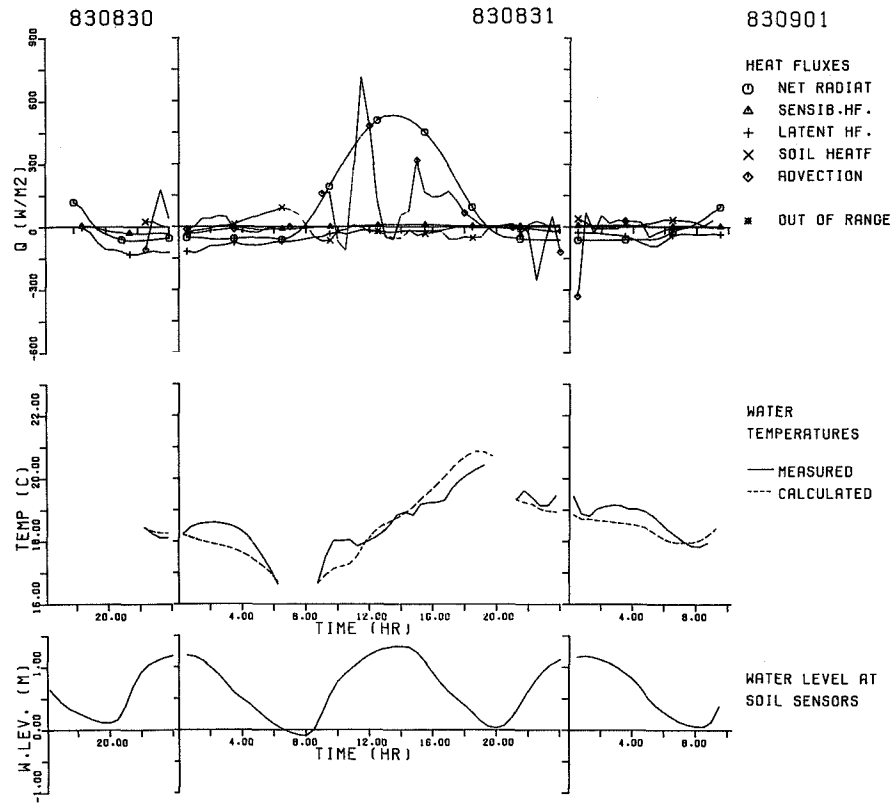

Figure 5.7: *The heat balance from August 30 to September 1, 1983.*

During the night from the 30^{th} to the 31^{st} the heat balance calculations do not predict the temperature rise of the water around midnight because advection is

underestimated. This might be due to covering of one of the sensors with seaweed. Also the subsequent temperature decrease is underestimated.

During the second high tide, in the morning and afternoon of the 31^{st}, the course of the water temperature is predicted rather well by the heat balance calculations. Only between 11.00 h and 12.00 h the model predicts a temperature rise, while in reality the temperature stays more or less constant (there is a small temperature drop). This can be explained by an error in the calculated advection, which should be negative in stead of positive.

During the night of August 31 to September 1, the course of the water temperature is predicted very well by heat balance calculations. Only the short term temperature variations are not calculated. Note however that the peaks in the advection are in the right place, only the response of the calculated water temperature is too low. So it seems that advection is underestimated.

5.3.4. Sensitivity analysis of advection calculation.

In this sub-section the extreme sensitivity of the calculation of the advection term (and thereby of the heat balance) to systematic errors in the measurement of the water temperature will be discussed.

The advection term is calculated from the water level, the water flow velocity and the temperature difference between two sensors which have a horizontal separation of 100 meters (eq. 2.64). In order to investigate the sensitivity of the advection term and the calculated water temperature to systematic temperature measurement errors the following test was performed. The same calculations as shown in figure 5.5 were carried out, but now with a systematic error of 0.05 K in one of the temperatures used to calculate the advection. The results are shown in figure 5.8. Figure 5.8A and B display the calculated heat fluxes and water temperatures when the water temperature measurements 50 m south (landward) of the location are increased by 0.05 K. Figure 5.8C and D shown the results when that temperature is decreased by 0.05 K.

Increasing the measured water temperature on the landside causes a decrease in the calculated advection when the water level is rising (because then the water flow direction is landward) and an increase when the water level is falling. Figure 5.8A clearly shows these features (compare with figure 5.5). The opposite effect is achieved by decreasing the water temperature on the landside, as is shown in figure 5.8C. Figure 5.8B and D show how grave the effects of such small measurement errors can be on the calculated water temperature. Increasing the water temperature on the landside (with 0.05 K) causes a delay in the calculation of the temperature rise in the afternoon of the 16^{th} (see figure 5.8B); the temperature fall in the evening is overestimated and also the course of the temperature during the 17^{th} of

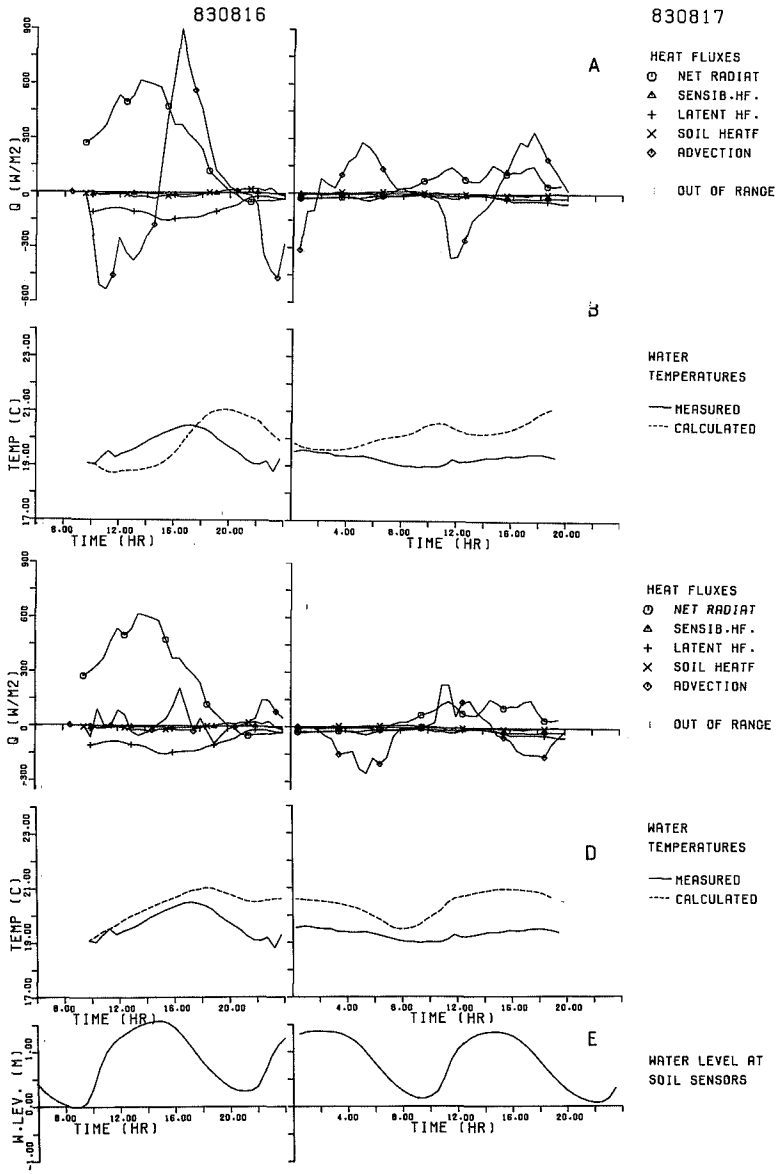

Figure 5.8: *Sensitivity of the heat balance to errors in the temperature measurement.*

august is not correctly calculated. Decreasing the temperature measured with the sensor on the landside causes an oscillation in the calculated temperature the 17^{th}.

This reveals that an accurate calculation of the advection term is an absolute necessity for adequate modeling of the water temperature. However, in order to

calculate the advection term well, the temperature difference in the water over a horizontal distance of 100 *m* should be measured with an accuracy near to 0.01 *K*. This is not possible with the NTC-sensors and registration equipment we used. The reasons for this are:

- First: the resolution of the dataloggers is only 0.03 *K*. This can be improved by changing the method of registration. Also the resolution of time averages of the water temperatures can be improved by increasing the sample frequency (which was 12 samples per hour).
- Second: the accuracy of the laboratory calibration of the NTC-sensors is 0.1 *K*. This is far too inaccurate for advection calculations. In order to obtain the results shown in figure 5.5, the calibration factors of the sensors measuring the water temperatures north and south of the location had to be "tuned" to each other carefully under circumstances with little advection. This was done by evaluating the measurements of August 10, which were taken after the sensors had been replaced. This was a clouded day (7/8 to 8/8 stratus) with high relative humidity (about 90 %), so the heat fluxes, including the advection through the water, were small.
- Third: for the sensors used in the experiment 1 *Ohm* extra resistance is equal to a change in the value of the measured temperature of about 0.01 *K*. Oxidation of the connecting plugs can easily add a few Ohms of extra resistance, causing the temperature to be a few hundreds of a degree lower. As shown in figure 5.8, this causes large errors. Although the plugs were cleaned regularly, oxidation could not be prevented completely.

It can be concluded that for a good calculation of the advection term the water temperature measurements should have been taken more accurately and more frequently.

Other weak spots in the calculation of the advection term are the used water level and the calculation of the water flow velocity.

During the period described above the water level was measured in a tidal channel (Wierbalg) a few kilometer south of our location. During later periods we also measured the water level near our tower at the measurement site on the Balgzand. Because of the spatial separation between the Wierbalg and our location, a time correction was made for the Wierbalg measurements. However, at the end of the ebb-tide and at the beginning of the flood-tide the form of the tidal wave on the Balgzand and at the Wierbalg are different. This difference is caused by the fact that at low water levels the tidal wave is delayed on the shallow Balgzand. The form difference has been included in the water level correction procedure (as good as possible).

The water flow velocity was calculated from measurements some years earlier by Rijkswaterstaat (De Boer 1978). It would have been better to carry out velocity measurements regularly during the experiment, (for example following the path of floating objects might be a way to estimate the flow velocity).

However, the advection term is less sensitive to an error in these parameters than to errors in the temperature measurement.

5.3.5. Why fast changes are not always correctly predicted.

Fast changes of the water temperature on the tidal flat usually occur at the end of the ebb-tide, or in the first hours of the flood-tide. The temperature changes at the end of the ebb-tide and in the very beginning of the flood-tide are well predicted most of the time. Sometimes there are extreme peaks or drops in the measured water temperature a few hours after the water has covered the tidal flat. These sudden changes are responsible for the relatively large errors.

These peaks and drops are very clearly present August 23 at 19.15 hour and the 24^{th} at 7.15 hour (see fig. 5.6). The drop at 23.15 hour August 16 is less destinctive (see fig. 5.5). They can be explained by assuming that water which is heated on the tidal flat during daytime (or cooled during nighttime) accumulates in the tidal channels during the ebb-tide and returns when the water level rises again.

The peaks and drops are not correctly predicted because the advection is miscalculated due to errors in the interpretation of the temperature measurements. Other terms in the heat balance can never be big enough to cause these strong temperature variations in a layer of water of about 1 meter depth (see figure 5.6). The errors in the interpretation of the temperature measurement are caused by horizontal and vertical inhomogeneity of the water temperature in combination with a relatively long sample interval and a relatively fast sensor. This causes errors in the calculated half hour averages. Probably accumulation of sea weed on the sensors has given rise to errors in the temperature measurement. These items will be discussed below.

The part of the tidal flat where our measurements were carried out had hardly any relief. Therefore horizontal temperature gradients in the water were usually low. Turbulent movements also removed vertical temperature gradients. However vertical gradients do exist under conditions with strong horizontal temperature advection. These features are shown in figure 5.9. The temperatures used to calculate the advection were measured at a height of *approximately* 2 *cm* above the soil surface. It can be seen from the figure that the temperature measured at that depth is not always representative for the whole layer of water of about 1 *m* thickness. It can also be seen that it makes a difference whether the sensor is at a height of 1 *cm* or 4 *cm* above the soil (which is about the range in which the sensor height varied due

to the displacement of sand on the tidal flat).

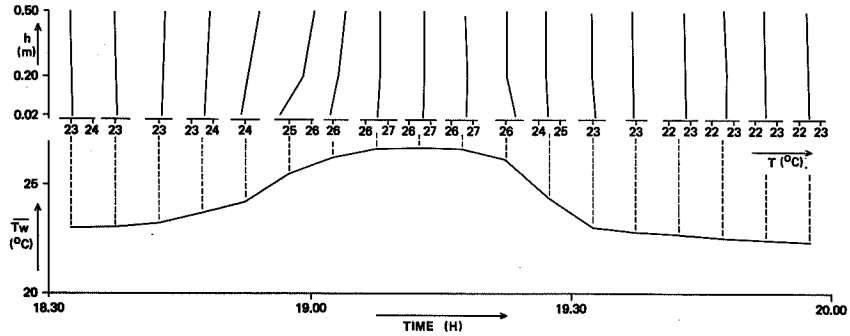

Figure 5.9: *Vertical water temperature distribution during a passage of an amount of warm water*

Calculating hourly averaged temperatures from twelve samples (5 minutes sample interval) taken with relatively fast sensors (circa 5 seconds relaxation time) yields accurate results when the temperature fluctuations are small (within 0.3 K). However when temperature gradients become larger and turbulent motion causes temperature fluctuations, one needs more samples or slower sensors to get a good average.

During the high water period, sea weed accumulated on the sensors used to calculate the advection. This causes a decrease in the response of the sensors. The accumulation of sea weed was different on both sensors, because the accumulation was dependent on the orientation of the sensor relative to the flow direction of the water. Since the errors in both temperatures were different, the accumulation of sea weed has probably contributed to the miscalculation of the advection (the extreme sensitivity to errors in the temperature measurement was already shown in section 5.3.4). When the water temperature changes slowly, the accumulation of sea weed does not cause significant errors, because then the polluted (and therefore slower) sensor registeres the temperature correctly.

CHAPTER 6

SUMMARY AND CONCLUSIONS

Although the heat balance of the earth's surface has been the subject of many meteorological studies, the heat balance of tidal flat areas has only been investigated a few times. The heat balance of a tidal area is very different from that of any land or sea surface. A good insight in the heat balance of tidal areas is necessary to understand the ecology of the area and many meteorological processes. The purpose of the present research is to provide a better understanding of the thermal conditions and the heat balance of tidal areas and to describe the heat fluxes above tidal flats and tidal waters. This was done by developing models which describe the course of the water temperature in a tidal area, by carrying out measurements during two summer seasons in the Dutch Wadden sea and by testing the models with the aid of these measurements.

In chapter 2 it was shown how the heat balance can be used to obtain the water temperature. The theory needed to calculate the terms of the heat balance was developed there. Chapter 3 described the measurements and how they are used in the theory. For some terms of the heat balance a number of different calculation methods were compared (chapter 4). Chapter 5 described the test of the heat balances with the aid of the measurements.

In the following the most important conclusions from the chapters 4 and 5 are summarized. Since this research focuses on the heat balance, the conclusions regarding the heat balance will be discussed first, followed by some remarks on the measurement of the separate terms in the balance.

All conclusions are based on the observations during the summer of 1982 in Mok Bay and during the summer of 1983 on the Balgzand. In other seasons or under other circumstances some of them may not be valid.

6.1. Heat balance of the entire Mok Bay.

In 1982 extensive measurements were carried out in the Mok Bay, which is a tidal inlet at the southern tip of the isle of Texel. In figure 5.2 the heat balance for the entire Mok Bay is shown for a period of 10 days. The heat balance is almost entirely dominated by net radiation, evaporation and the accumulation of heat in the bay water. During the flood-tide the inflow of relatively warm or cold water through the tidal channel is also important. The sensible heat flux and the soil heat flux are of minor importance. The amount of heat stored in the bay water is considerable. Under favourable conditions the change of the average temperature of the bay water over a period of one tide (about 12 h) was observed to be as large as 2.3 K. Taking the average volume of the bay about 1.0 * 10^6 m^3 and the average water surface about 0.8 * 10^6 m^2, this means that averaged over the 12 hour period and over the total wet surface of the bay the storage of heat in the water equals about 270 $W\ m^{-2}$, which means an accumulation of heat of about 1 $kJ\ cm^{-2}$. During shorter intervals it was observed to be as much as 400 $W\ m^{-2}$.

In a model of the Mok Bay the heat balance was used to calculate the water temperature in the bay. It was assumed that the bay water was completely mixed. During the ebb-tide the model could be validated by comparing the calculated temperatures with those observed in the tidal channel. From this comparison it was clear that the water was not completely mixed. During the first hours of the ebb-tide the temperature of the water which was leaving the bay often deviated from the average water temperature. This water had only entered the tidal channel and the central basin recently and the duration of its stay in the bay had been to short to assure good mixing with the rest of the water. Nevertheless the average water temperature during the ebb-tide was predicted fairly well. In 80 % of the cases the average calculated ebb-tide water temperature was within 0.5 K of the observed value. Averaged over 19 successive ebb-tides the deviation was only 0.02 K. Probably the model can be improved by taking into account that the bay water is not completely mixed.

6.2. Heat balance for one point on the Mok Bay tidal flat.

In the preceding section the heat balance for the entire Mok Bay was treated. This section discusses the heat balance for one point on the Mok Bay tidal flat. The reference point for which the heat balance was calculated was the position of mast 1 (indicated in appendix 1).

When the tidal flat was above the water during the night the sensible, as well as the latent heat flux became very small and the loss of heat by radiation was compensated by the soil heat flux (see figure 5.1). During the day when the tidal flat was above the water, the heat balance was dominated by the incoming solar radiation.

During midday net radiation was sometimes as high as 600 $W\ m^{-2}$. Among the other terms in the balance the latent heat flux is the most important one. The sensible heat flux is always much smaller (Bowen ratios were typically 0.25 or less), but sometimes to large to be neglected. The soil heat flux often was only slightly smaller than the latent heat flux. It was observed to be in the order of 100−200 $W\ m^{-2}$ during periods of several hours.

When the profile method was used to calculate the sensible and latent heat flux during the periods that the tidal flat was above the water, the local heat balance was not always in equilibrium. Probably this was due to the fact that some conditions needed to apply the profile method (stationarity and homogeneity) were not met. Most of the imbalance was removed by using the bulk method instead. The bulk method uses (in our case) the lowest 2.5 m of the profiles and therefore is less sensitive to upwind inhomogeneities. Since the temperature, humidity and wind speed gradient are largest below 2.5 m, the bulk method is less sensitive to disturbances than the profile method.

When the tidal flat is submerged there is another very important term in the local heat balance, which is the horizontal advection of heat in the water. This term is especially important during the first hour of the flood-tide, but also remains considerable afterwards. Unfortunately we have not been very successful in parameterizing this term on the Mok Bay tidal flat. There were water currents (probably wind driven) perpendicular to our line of measurements. The contribution of these currents to the advection could not be taken into account, because no information was available on the temperature gradients in that direction. The problem was least disturbing in situations with small water temperature gradients (during the night and probably also overcast days). In those cases the heat balance calculations yielded fairly accurate water temperatures on the tidal flat. A reasonable estimate of the water temperature was also obtained on days with little wind. On days with a wind speed more than circa 4 $m\ s^{-1}$ (especially from easterly directions) the model calculations yielded unrealistic water temperatures. In future investigations it would be worthwhile to pay more attention to the advection of heat in the water. Then the water temperature gradients should be measured in several directions and water flow velocity as well as direction should be measured constantly. This will be difficult, since flow velocities of a few $cm\ s^{-1}$ can be important and sea weeds are liable to disturb the measurement.

6.3. Heat balance on the Balgzand.

The part of the Balgzand where our experiment took place was situated at a lower level than the Mok Bay tidal flat. Therefore the periods with water on the tidal flat were longer and the periods during which the tidal flat was above the water were shorter. Some parts of this tidal flat did not emerge completely; for example at mast 2 the bottom surface was always covered with a layer of water of at least 10−20 *cm*.

The most important term in the heat balance on the Balgzand was net radiation (see figures 5.5 to 5.7). A large portion of the heat gained by radiation (during the day) was stored in the water. The advection of heat through the water also gave a significant contribution. During short intervals this term was found to be much larger than the largest value observed for the net radiation term. The latent heat flux attributed considerably to the heat balance, although its influence seemed to be less than on the Mok Bay tidal flat. In all cases which were examined the sensible heat flux was so small that it could easily be neglected without influencing the heat balance, or the calculated water temperatures significantly. Most of the time the soil heat flux was not very important, partly because the periods during which the tidal flat was above the water were short. When rapid changes of the water temperature occurred, the soil heat flux was large during short periods of time.

When the heat balance was used to calculate the water temperatures, this yielded reasonable results. The main trends in the water temperature were followed by the model calculations, but in details differences between the model and the reality remain. The first hour of the flood-tide (or more in general when the water layer was thin) the calculations were not very accurate. Also the model was not capable of "predicting" the rapid changes in the water temperature which were sometimes observed. This misbehaviour can only be solved partly by measuring water flow and temperature more accurately (resulting in a better estimate of the advection term). The largest problem is that these changes are to fast to be treated in terms of half hourly means.

6.4. The measurement of sensible and latent heat flux.

For the measurement of the sensible and latent heat flux three methods were tested: the direct method, the profile method and the bulk method. Furthermore we tested the sensitivity of the profile method to errors in the measured temperature profile and to whether or not the moisture term was included in the calculation of the Monin-Obukhov length.

For practical purposes the bulk method was the most useful of the methods which were tested. The sensible and the latent heat fluxes calculated with the bulk method (using bulk aerodynamic transfer coefficients which are dependent on

stability and surface roughness) are more reliable than those obtained with the profile method. This is caused by the fact that the bulk method uses the gradient from 0 to 2.5 m, whereas the profile method uses the gradient from 2 (or 3 on the Balgzand) to 24 m. A large fraction of the total gradient from 0 to 24 m lies below 3 m, especially in situations when the fluxes are large; i.e. unstable situations (see section 4.1.3).

When using the profile method the influence of the moisture term in the Monin-Obukhov length cannot be neglected. Neglecting the moisture term leads to underestimates of the sensible and the latent heat fluxes by 10–20 % (see section 4.1.1).

Under unstable atmospheric conditions the fluxes calculated with the profile method are very sensitive to errors in the measured temperature gradient. An error of 0.1 K in the gradient between 3 and 24 m can change the calculated sensible heat flux by 50 % and the latent heat flux by 30 %. In stable situations errors in the measured temperature gradient have little influence, since the gradient is already large in that case (see section 4.1.2).

The friction velocities obtained from the profile method correspond very well with those obtained from the direct method. The average absolute difference between the two methods was 1.1 $cm\ s^{-1}$, for an average friction velocity of about 12 $cm\ s^{-1}$.

The sensible heat fluxes calculated with the direct method were (in most situations) about 0.7 times those derived with the profile method. However, there were some runs for which the profile method yielded a sensible heat flux near 0 $W\ m^{-2}$, whereas the direct method gave fluxes that were about 10 $W\ m^{-2}$ less. This difference can be attributed to:

- the humidity component in the temperature of the sonic anemometer ($1-3\ W\ m^{-2}$),
- errors in the measured temperature profile (up to 5 $W\ m^{-2}$),
- unadapted boundary layers and
- a difference between the geometric mean height of the profiles (8.5 m) and the installation height of the sonic anemometers (4.5 m).

The latent heat flux found from the direct method is on the average about a factor 2 smaller than that yielded by the profile method. The main cause for this difference is a bad measurement of the wet bulb temperature used in the direct method. It is almost certain that the collection of salt on the wet bulb sensor and an inadequate water supply to it has influenced its measurements. The results would have been better if we had regularly replaced the wet bulb thermocouples.

6.5. The measurement of the soil heat flux.

Four ways of measuring the soil heat flux were examined. Of these four, both the integration method and the Fourier method yielded very good results. The correlation between these two methods was good ($r = 0.95$), On the average the Fourier method yielded a soil heat flux which was on the average 1 $W\ m^{-2}$ larger. The results from the gradient method were poor, mainly because this method is very sensitive to errors in the temperature measurement. The soil heat flux plates gave bad results. The values obtained with those devices were on the average a factor 2 too small and the correlation with for example the integration method was poor (0.80). A disadvantage of the gradient method and the flux plates is that they do not yield the soil heat flux at the surface.

6.6. Parameterizing net radiation.

Several ways of parameterizing net radiation from simple meteorological observations gave good results. When use was made of global and reflected short wave radiation which were measured at the site, the standard error of estimate for the net radiation was about 35 $W\ m^{-2}$. When the short wave component was obtained from cloud data and the solar elevation, the standard error of estimate became about 55 $W\ m^{-2}$.

HOOFDSTUK 7

SAMENVATTING EN CONCLUSIES

Alhoewel de warmtebalans van het aardoppervlak het onderwerp van vele meteorologische studies is geweest, is de warmtebalans van waddengebieden nog nauwelijks onderzocht. De warmtebalans van een waddengebied verschilt zeer sterk van die van enig land- of zeeoppervlak. Een goed inzicht in de warmtebalans van waddengebieden is onmisbaar voor het begrijpen van de ecologie van deze gebieden, alsmede van vele meteorologische processen. Het doel van dit onderzoek was het verschaffen van een beter inzicht in de thermische condities en de warmtebalans van waddengebieden, en het beschrijven van de warmtefluxen boven het wad. Er werden modellen ontwikkeld die het verloop van de watertemperatuur beschrijven als funktie van een aantal meteorologische parameters. Gedurende twee zomers werden metingen gedaan in het Nederlandse waddengebied en met behulp van deze metingen werden de ontwikkelde modellen getoetst.

In hoofdstuk 2 wordt afgeleid hoe de warmtebalans kan worden gebruikt voor het schatten van de watertemperatuur en wordt de theorie behandeld die nodig is voor het berekenen van de termen van de warmtebalans. Hoofdstuk 3 beschrijft de metingen en hoe die metingen zijn ingepast in de theorie. Voor enkele termen van de warmtebalans worden in hoofdstuk 4 een aantal verschillende berekeningswijzen vergeleken. Hoofdstuk 5 beschrijft het toetsen van de warmtebalansen aan de hand van de metingen.

In het onderstaande worden de belangrijkste conclusies uit hoofdstuk 4 en 5 samengevat. Omdat de warmtebalans van waddengebieden het primaire onderzoeksdoel was zullen de conclusies betreffende de warmtebalans eerst worden behandeld, gevolgd door enkele opmerkingen over de meting van de afzonderlijke termen.

Alle conclusies zijn gebaseerd op de waarnemingen tijdens de zomer van 1982 in de Mokbaai en gedurende de zomer van 1983 op het Balgzand. In andere seizoenen of onder andere omstandigheden zijn een aantal van de conclusies mogelijk niet geldig.

7.1. Warmtebalans van de gehele Mokbaai.

In 1982 werd in de Mokbaai, op de zuidpunt van Texel, een uitgebreide meetcampagne uitgevoerd. In figuur 5.2 is voor een periode van 10 dagen de warmtebalans van de gehele Mokbaai afgebeeld. De warmtebalans wordt vrijwel totaal gedomineerd door de netto straling, de verdamping en de opslag van warmte in het water in de baai. Tijdens het opkomend water is ook de instroming van relatief koud of warm water via de geul van belang. De voelbare warmtestroom en de bodemwarmtestroom zijn minder belangrijk. De hoeveelheid warmte die wordt opgeslagen in het water in de baai is aanzienlijk. Onder gunstige omstandigheden kwam het voor dat het water in de baai gedurende een getijperiode gemiddeld 2.3 K in temperatuur steeg. Wanneer we voor het gemiddelde volume van de baai $1.0 * 10^6\ m^3$ nemen en voor het gemiddelde wateroppervlak $0.8 * 10^6\ m^2$, betekent dit dat, gemiddeld over de periode van 12 uur en over het gehele wateroppervlak van de baai, de warmteopslag in het water 270 $W\ m^{-2}$ bedraagt, wat overeenkomt met ruim 1 $kJ\ cm^{-2}$. Gedurende kortere intervallen zijn voor deze term zelfs waarden van 400 $W\ m^{-2}$ waargenomen.

In een model van de Mokbaai is de warmtebalans gebruikt om de gemiddelde watertemperatuur in de baai te berekenen. Daarbij werd aangenomen dat het water in de baai volledig gemengd was. Tijdens het afgaand water kon het model worden gecontroleerd door de berekende watertemperaturen te vergelijken met de in de geul gemeten temperaturen. Uit deze vergelijking bleek dat het water in de baai niet volledig gemengd was. Vaak verschilde de berekende temperatuur van het water dat de baai verliet van de gemiddelde watertemperatuur gedurende de eerste uren van het afgaand water. Het water dat dan de baai verliet was slechts doorgedrongen tot de geul en het centrale bassin en de duur van het verblijf in de baai was niet lang genoeg geweest om een goede menging met de rest van het water te verzekeren. Desalniettemin werd de gemiddelde watertemperatuur tijdens afgaand water vrij goed berekend. In 80 % van de gevallen bedroeg het verschil tussen de berekende gemiddelde water temperatuur tijdens afgaand water en de gemeten waarde minder dan 0.5 K. Gemiddeld over 19 opeenvolgende perioden van afgaand water was de afwijking slechts 0.02 K. Waarschijnlijk kan het model verbeterd worden door rekening te houden met het feit dat het water in de baai niet volledig gemengd is.

7.2. Warmtebalans voor een punt op het wad in de Mokbaai.

In het voorgaande werd de warmtebalans van de gehele Mokbaai behandeld. Deze paragraaf gaat over de warmtebalans van een punt op het wad. Als referentiepunt is gekozen voor de positie van mast 1 (aangegeven in appendix 1).

Als 's nachts het wad droog stond, werden de voelbare en de latente warmteflux zeer klein, en werd het verlies aan netto straling gecompenseerd door de

bodemwarmteflux (zie figuur 5.1). Als het wad overdag droog stond werd de warmtebalans gedomineerd door de invallende zonnestraling. Omstreeks het middaguur bereikte de netto straling soms waarden van 600 $W\ m^{-2}$. Van de andere termen van de warmtebalans was de latente warmtestroom de belangrijkste. De voelbare warmtestroom was steeds aanzienlijk kleiner (de Bowenverhouding was normaliter 0.25 of minder), maar soms te groot om te worden verwaarloosd. Vaak was de bodemwarmtestroom maar een beetje kleiner dan de latente warmtestroom; Waarden van 100−200 $W\ m^{-2}$ gedurende enkele uren zijn waargenomen.

Werd, tijdens de perioden dat het wad droogstond, de profiel methode gebruikt om de voelbare en de latente warmtestroom te berekenen, dan was de warmtebalans niet altijd in evenwicht. Waarschijnlijk lag dit aan het feit dat aan een aantal voorwaarden voor het toepassen van de profielmethode (zoals een stationaire situatie en een homogeen aanstroomgebied) niet was voldaan. Dit euvel kon grotendeels worden verholpen door de bulkmethode toe te passen in plaats van de profielmethode. De bulkmethode gebruikt (in ons geval) de onderste 2.5 m van de profielen en is daarom minder gevoelig voor het inhomogeen zijn van het aanstroomgebied. Ook het feit dat het grootste gedeelte van de temperatuur-, luchtvochtigheids- en windsnelheidsgradient beneden 2.5 m valt maakt de bulkmethode minder gevoelig voor onnauwkeurigheden dan de profielmethode.

Als het wad bedekt is met water wordt er een erg belangrijke term aan de warmtebalans toegevoegd, namelijk de horizontale advectie van warmte in de waterlaag. Deze term is vooral belangrijk tijdens het eerste uur van het opkomend water, maar blijft ook daarna aanzienlijk. Helaas was de gebruikte parameterisatie van deze term op het wad in de Mokbaai niet erg geslaagd. Op het wad kwamen stromingen voor loodrecht op onze meetraai (waarschijnlijk onder invloed van de wind). Met de bijdrage van deze stromingen aan de advectie kon geen rekening worden gehouden omdat de gradienten in de watertemperatuur in die richting niet zijn gemeten. In situaties met geringe gradienten in de watertemperatuur ('s nachts en waarschijnlijk ook tijdens bewolkte dagen) kon de warmtebalans worden gebruikt om de watertemperaturen op het wad te berekenen. Ook op dagen met weinig wind was een redelijke schatting van de watertemperatuur mogelijk. Overdag, bij een windsnelheid van meer dan 4 $m\ s^{-1}$ (vooral uit oostelijke richtingen) gaf het model onrealistische watertemperaturen. In eventuele vervolgonderzoeken verdient het aanbeveling meer aandacht te besteden aan de advectiewarmte. Het is het beste de gradient in de watertemperatuur tenminste in twee onderling loodrechte richtingen te meten en tevens zowel de stroomsnelheid van het water als de richting waarin het water stroomt continu te meten (wat resulteert in een betere bepaling van de advectieterm). Dit zal echter niet eenvoudig zijn, daar stroomsnelheden van enkele $cm\ s^{-1}$ al van belang kunnen zijn en omdat mag worden verwacht dat zeewier de

metingen zal verstoren.

7.3. Warmtebalans op het Balgzand.

Het deel van het Balgzand waar ons onderzoek werd uitgevoerd lag iets lager dan het wad in de Mokbaai. Daarom waren de perioden met water op het wad langer en de droge perioden korter. Sommige delen vielen niet geheel droog; bij mast 2 bijvoorbeeld bleef altijd een laag water met een diepte van 10−20 *cm* staan.

De belangrijkste term in de warmtebalans op het Balgzand was de netto straling (zie de figuren 5.5 tot 5.7). De ingestraalde energie (overdag) werd voor een groot deel opgeslagen in het water. De advectie van warmte via het water gaf ook een behoorlijke bijdrage. Deze term was soms, gedurende korte perioden, groter dan de grootst waargenomen waarde voor de netto straling. Ook de latente warmtestroom was belangrijk, alhoewel de invloed daarvan minder leek dan in de situatie van de Mokbaai. In alle onderzochte gevallen was de voelbare warmtestroom zo klein dat die verwaarloosd kon worden zonder dat dat ernstige consequenties had voor de warmtebalans of de berekende watertemperaturen. Het grootste gedeelte van de tijd was de bodemwarmtestroom niet erg belangrijk, hetgeen deels te wijten is aan het feit dat de perioden dat het wad droog viel erg kort waren. Wanneer er snelle veranderingen van de watertemperatuur optraden, kwamen gedurende korte perioden grote bodemwarmtestromen voor.

Wanneer de warmtebalans werd gebruikt om de water temperaturen te berekenen gaf dat redelijke resultaten. De belangrijkste trends in de gemeten watertemperatuur werden gevolgd door de modelberekeningen, maar in details waren er wel verschillen. Het eerste uur van het opkomend water (of meer in het algemeen als de waterlaag erg dun is) waren de berekeningen niet erg nauwkeurig. Ook was het model niet in staat een goede beschrijving te geven van de snelle veranderingen in de watertemperaturen die soms werden waargenomen. Dit kan slechts gedeeltelijk worden opgelost door de waterstroming en de watertemperatuur nauwkeuriger te meten. Het grootste probleem is dat deze veranderingen zo snel gaan dat ze niet goed meer met halfuurgemiddelden kunnen worden beschreven.

7.4. De meting van de voelbare en latente warmteflux.

Voor de meting van de voelbare en de latente warmteflux zijn drie methoden getest: de directe methode, de profielmethode en de bulkmethode. Verder werd getest hoe gevoelig de profielmethode was voor fouten in het gemeten temperatuurprofiel en voor het al dan niet gebruiken van de vochtterm in de berekening van de Monin-Obukhovlengte.

De bulkmethode bleek de meest bruikbare van de gebruikte methoden. De voelbare en latente warmtestroom berekend met de bulkmethode (gebruikmakend

van bulk aerodynamische overdrachtscoefficienten die afhankelijk zijn van stabiliteit en oppervlakteruwheid) zijn betrouwbaarder dan die verkregen met de profielmethode. Dit wordt veroorzaakt door het feit dat de bulkmethode de gradient van 0 tot 2.5 m gebruikt, terwijl de profielmethode de gradient gebruikt van 2 m (of 3 m op het Balgzand) tot 24 m. Een groot deel van de gradient van 0 tot 24 m valt beneden de 3 m, vooral in die situaties dat de fluxen groot zijn (zie paragraaf 4.1.3).

Bij gebruik van de profielmethode kan de invloed van de vochtterm in de Monin-Obukhovlengte niet worden verwaarloosd. Verwaarlozing van de vochtterm leidt tot een onderschatting van zowel de voelbare als de latente warmteflux van 10−20 % (zie paragraaf 4.1.1).

Onder onstabiele atmosferische omstandigheden zijn de fluxen die worden berekend met de profielmethode erg gevoelig voor fouten in de gemeten temperatuurgradient. Een fout van 0.1 K in de gradient tussen 3 en 24 m kan een fout geven van 50 % in de voelbare en 30 % in de latente warmteflux. In stabiele situaties hebben fouten in de gemeten gradient weinig effect, omdat dan de gradient groot is (zie paragraaf 4.1.2).

De wrijvingssnelheden berekend met de profielmethode corresponderen erg goed met die verkregen met de directe methode. Het gemiddelde absolute verschil tussen deze twee methoden was 1.1 $cm\ s^{-1}$ bij een gemiddelde in de orde van 12 $cm\ s^{-1}$.

De voelbare warmtefluxen berekend met de directe methode waren (in de meeste gevallen) ongeveer 0.7 maal die gevonden met de profielmethode. Er waren echter enkele runs waarvoor de profielmethode een voelbare warmteflux gaf van circa 0 $W\ m^{-2}$, terwijl de directe methode fluxen gaf van ongeveer $-10\ W\ m^{-2}$. Dit verschil kan zijn veroorzaakt door:

- de vochtcomponent in de sonische virtuele temperatuur ($1-3\ W\ m^{-2}$),
- fouten in het gemeten temperatuurprofiel (tot $5\ W\ m^{-2}$),
- onaangepaste grenslagen en
- een verschil tussen de geometrisch gemiddelde hoogte van de profielen (8.5 m) en de hoogte waarop de sonics waren opgesteld (4.5 m).

De latente warmtestroom die werd gevonden met de directe methode was gemiddeld een factor twee kleiner dan wat werd berekend met de profielmethode. De belangrijkste oorzaak hiervan is dat de natte bol temperatuur die werd gebruikt in de directe methode niet nauwkeurig genoeg is gemeten. Hoogstwaarschijnlijk is de meting beinvloed door de afzetting van zout op de natte bol sensor en een slechte watertoevoer. De resultaten zouden beter geweest zijn als de natte bol thermokoppels regelmatig waren vervangen.

7.5. De meting van de bodemwarmtestroom.

Vier manieren om de bodemwarmtestroom te meten werden onderzocht. Van deze vier gaven zowel de integratiemethode als de Fouriermethode goede resultaten. De correlatie tussen deze twee methoden was zeer goed ($r = 0.95$) en gemiddeld gaf de Fouriermethode een bodemwarmtestroom die 1 $W\ m^{-2}$ groter was. De resultaten verkregen met de gradientmethode waren slechter, voornamelijk omdat deze methode erg gevoelig is voor fouten in de temperatuurmetingen. De bodemwarmtestroomplaatjes gaven zonder meer slechte resultaten. De waarden die hiermee werden verkregen waren gemiddeld een factor 2 te klein en de correlatie met bijvoorbeeld de integratiemethode was slecht (0.80). Een nadeel van de gradientmethode en de bodemwarmtestroomplaatjes is dat ze niet de bodemwarmteflux aan het oppervlak geven.

7.6. Parameterisatie van de netto straling.

Verschillende manieren voor het parameteriseren van de netto straling met behulp van eenvoudige meteorologische waarnemingen gaven goede resultaten. Als gebruik werd gemaakt van ter plekke gemeten globale straling en gereflecteerde kortgolvige straling, was de standaardafwijking van het verschil tussen de gemeten en berekende netto straling ongeveer 35 $W\ m^{-2}$. Werd de kortgolvige component geschat uit bewolkingsgegevens en de zonnehoogte, dan werd deze standaardafwijking ongeveer 55 $W\ m^{-2}$.

REFERENCES.

Anonymus, 1978,
Instruction manual DA(T)-310,
Kaijo Denki Co., LTD., Tokyo, Japan.

Andrews, R., 1980,
Warmeaustausch zwischen Wasser und Wattboden
Deutsche Gewasserkundlige Mitteilungen, 24, 57-65.

Barret, E.W. and V.E. Suomi, 1949,
Preliminary report on temperature measurement by sonic means,
J. of Meteor. 6, 273-276.

Becht, H.Y., 1976,
De Warmtehuishouding van een waddengebied,
Afstudeerverslag NIOZ/TH Delft.

Blanc, T.V., 1981,
Report and analysis of the may 1979 marine surface layer experiment at San Nicolas island, California,
Naval Research Laboratory Report 8363, Washington DC.

Blanc, T.V., 1983,
Typical influences of moisture on profile measurements in marine atmospheric surface layer,
Bound. Layer Meteor., 25, 411-415.

Boer, M. de, 1978,
Uitwisseling wadwater Balgzand, waterloopkundig onderzoek, mei 1977,
Rijkswaterstaat, Hoorn.

Bruin, H.A.R. de, 1982,
The energy balance of the earth's surface: a practical approach,
KNMI, De Bilt, WR 82-1.

Busch, N.E., 1973,
On the mechanics of atmospheric turbulence,
Workshop on micrometeorology, 1-66,
Haugen, D.A., Ed, Am. Met. Soc., Boston, Massachusetts.

Businger, J.A., J.C. Wijngaard, Y. Izumi and E.F. Bradly, 1971,
Flux profile relationships in the atmospheric surface layer,
J. Atmos. Sci., 28, 181-189.

Businger, J.A., 1973,
Turbulent transfer in the atmospheric surface layer,
Workshop on micrometeorology, 67-100,
Haugen, D.A., Ed, Am. Met. Soc., Boston, Massachusetts.

Carlslaw, H.S. and J.C. Jaeger, 1959,
Conduction of heat in solids,
Oxford University Press.

Dunkel, M., L. Hasse, L. Krugermeyer, D. Schriever and J. Wucknitz, 1974,
Turbulent fluxes of momentum, heat and water vapor in the atmospheric surface layer at sea during ATEX,
Bound. Layer Meteor., 6, 80-106.

Dyer, A.J. and B.B. Hicks, 1970,
Flux-gradient relationships in the constant flux layer,
Quart. J. R. Met. Soc., 96, 715-721.

Dyer, A.J. and E.F. Bradly, 1982,
An alternative analysis of flux-gradient relationships at the 1976 ITCE,
Bound. Layer Meteor., 22, 3-19.

Emmanuel, C.B., 1975,
Drag and bulk aerodynamic coefficients over shallow water.
Bound. Layer Meteor., 8, 465-474.

Friehe, C.A. and K.F. Schmidt, 1976,
Parameterization of air-sea interface fluxes of sensible heat and moisture by the aerodynamic formulas,
J. of Phys. and Oceanogr., 6, 801-809.

Gunneberg, F., 1976,
Abkühlungsvorgange in Gewassern,
Deutsche Gewasserkundlige Mitteilungen, 20, 151-161.

Haneghem, I.A. van, 1981,
Een niet-stationaire naaldmethode
(warmtegeleiding, warmtecapaciteit, contactweerstand),
Ph.D. Thesis, Agricultural University, Wageningen.

Harrison, S.J., 1981,
Diurnal temperature waves in muddy intertidal sediments, discussion paper,
Stirling University, Scotland, IMRP Report nr 4, 1981.

Harrison, S.J., 1985,
Heat exchanges in muddy intertidal sediments: Chichester Harbour, West Sussex, England,
Est., Coastal and Shelf Sc. 20 477-490.

Harrison, S.J. and A.P. Phizacklea, 1985
Seasonal changes in heat flux and heat storage in the intertidal mudflats of the Forth Estuary, Scotland,
J. Clim. 5: 473-485.

Heath, R.A., 1977,
Heat balance in a small coastal inlet: Pauatahanui Inlet, North Island, New Zealand,
J. Est. and Coastal Mar. Sc., 5, 783-792.

Hicks, B.B., 1975,
A procedure for the formulation of bulk transfer coefficients over water,
Bound. Layer Meteor., 8, 515-524.

Holtslag, A.A.M., and A.P. van Ulden, 1983,
A simple scheme for daytime estimates of the surface fluxes from routine weather data,
J. Clim. Appl. Met., 22, 517-529.

Idso, S.B., 1983,
On calculating thermal radiation from cloudless skies,
Arch. Met. Geoph. Biol., Ser. B, 32, 53-57.

Jacobs, P., 1982,
The thermal behaviour of a three-dimensional object placed in the open field,
Ph.D. Thesis, Agricultural University, Wageningen.

Keijman, J.Q., 1974,
The estimation of the energy balance of a lake from simple data,
Bound. Layer Meteor., 7, 399-407.

Kondo, J. and G. Naito, 1972,
Disturbed wind fields around the obstacle in sheared flow near the ground,
J. of the Meteor. Soc. of Japan, 50, 346-354.

Lambooy, E., 1985,
Meteorological field work Mokbaai 1982,
Internal report: Meteorology section Institute of Earth Sciences, Free University, Amsterdam.

Monin, A.S. and A.M. Yaglom, 1971,
Statistical fluid mechanics, mechanics of turbulence, volume 1,
MIT Press, Massachusetts.

Monteith, J.L., 1973,
Principles of environmental Physics,
Edward Arnold (publishers) LTD, London.

Overgaard-Mogensen, V., 1970,
The calibration factor of heat flux meters in relation to the thermal conductivity of the surrounding medium,
Agric. Meteor., 7, 401-410.

Paltridge, G.W. and C.M.R. Platt, 1976,
Radiative processes in meteorology and climatology, Development in atmospheric science, Vol. 5,
Elsevier, New York/Amsterdam.

Paulson, C.A., 1970,
The mathematical representation of wind speed and temperature profiles in the unstable atmospheric surface layer,
J. Appl. Meteor., 9, 857-861.

Pond, S., D.B. Fissel and C.A. Paulson, 1974,
A note on bulkaerodynamic coefficients for sensible heat and moisture flux,
Bound. Layer Meteor., 6, 333-339.

Rao, N.J., A.S. Mascarenhas and Y. Yamazaki, 1980,
Air-sea interaction studies at the station occupied by R/V Sirius,
Bound. Layer Meteor., 19, 387-391.

Robinson, G.D., 1966,
Another look at some problems of the air-sea interface,
Quart. J. R. Met. Soc., 92, 451-465.

Schotanus, P., 1982,
Turbulente fluxen in inhomogene omstandigheden,
KNMI, De Bilt, WR 82-3.

Shaw W.J. and J.E. Tillman, 1980,
The effect of and correction for different wet-bulb and dry-bulb response in thermocouple psychrometry,
J. Am. Meteor. Soc. 19, 90-97.

Swinbank, W.C., 1963,
Long wave radiation from clear skies,
Quart. J. R. Met. Soc., 89, 339-348.

Vugts, H.F., 1974,
Calculation of temperature variations of small mountain streams,
J. Hydrol., 23, 267-278.

Vugts, H.F. and J.T.F. Zimmerman, 1975,
Interaction between the daily heat balance and the tidal cycle,
Nature, 255, 113-117.

Vugts, H.F., 1980a,
A study of terrain inhomogeneity (correspondence),
Bull. the Am. Met. Soc., 61, 568-569.

Vugts, H.F., 1980b,
IJking sonische anemometer DAT-310,
Internal report, Meteorology department, Free University, Amsterdam.

Vugts, H.F. and F. Cannemeijer, 1981,
Measurements of drag coefficients and roughness length at a sea-beach interface,
J. Appl. Meteor., 20, 335-340.

Vugts, H.F. and J.T.F. Zimmerman, 1982,
Heat balance investigations of tidal flats,
First international conference on meteorology and air sea interaction,
The Hague, 277-280.

Vugts, H.F. and J.T.F. Zimmerman, 1985,
Heat balance of a tidal flat area,
Neth. J. Sea Res. 19, 1-14.

Wartena, L., 1959,
Het klimaat en de verdamping van een meer in centraal Irak,
Ph.D. Thesis, Agricultural University Wageningen,
H. Veenman & Zonen N.V. Wageningen.

Webb, E.K., 1970,
The profile relationships: The log-linear range and extension to strong stability,
Quart. J. R. Met. Soc., 96, 67-90.

Wieringa, J., 1973,
Applications of turbulence measurements over Lake Flevo,
Ph.D. Thesis, University of Utrecht.

Wieringa, J., 1980,
A revaluation of the Kansas mast influence on measurements of stress and cup-anemometer overspeeding,
Bound. Layer Meteor., 18, 411-430.

Wilde , P.A.W.J. de and E.M. Berghuis, 1979,
Cyclic temperature fluctuations in a tidal mud-flat,
Cyclic phenomena in marine plants and animals,
E. Naylor and R.G. Hartnoll, Ed, Pergamon Press, Oxford & New York p435-441.

Wijk, W.R. van and D.A. de Vries, 1966,
Periodic variations in a homogeneous soil,
Physics of plant environment,
Wijk, W.R. van, Ed, North Holland Publishing Company, Amsterdam.

Zimmerman, J.T.F., 1976,
Mixing and flushing of tidal embayments in the western dutch Wadden Sea,
Part 1: Distribution of salinity and calculation of mixing time scales,
Neth. J. Sea Research 10, 149-191.

APPENDIX 1: THE INSTRUMENTS IN MOK BAY.

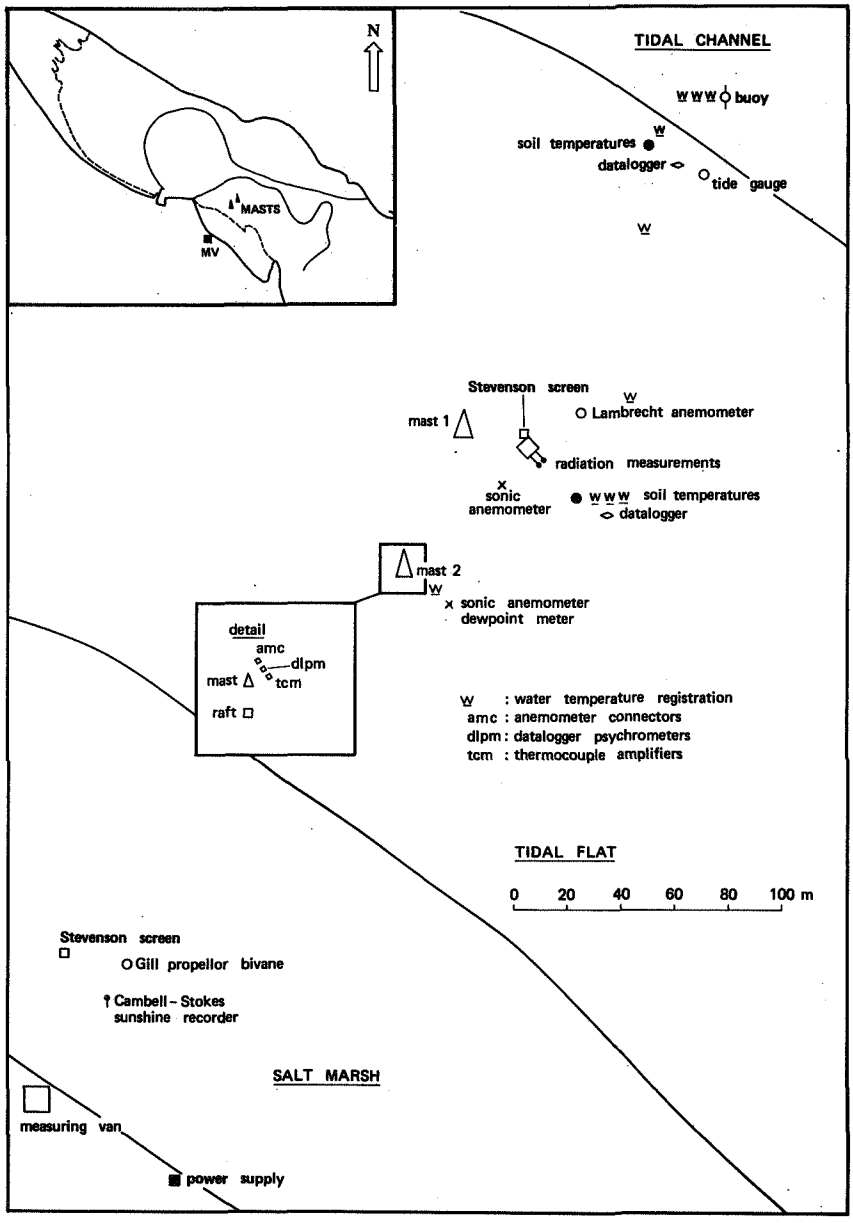

APPENDIX 2: LOCATION OF THE INSTRUMENTS ON THE BALGZAND.

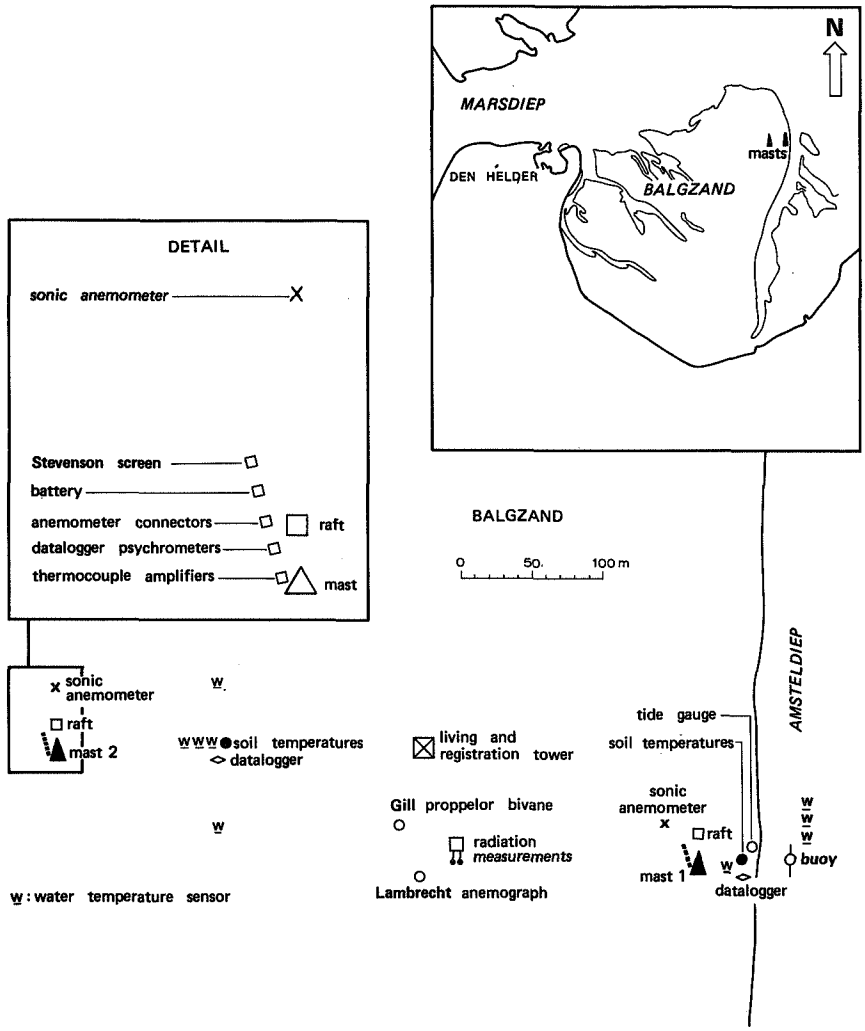

APPENDIX 3: ERRORS IN HEAT FLUX MEASUREMENTS WITH SONIC ANEMOMETERS.

The sound velocity, which is a function of temperature and water vapor pressure can be written as (Barret 1949):

$$C_s = 20.067\ [\ T(1 + 0.3192\ e_a/P)\ ]^{0.5}\ , \qquad [m\ s^{-1}]\ (A3.1)$$

where C_s is the sound velocity, T the absolute temperature, e_a the water vapor pressure and P the atmospheric pressure. With specific humidity $q = \epsilon e_a/P$ (eq. 3.9) this leads to:

$$T = (\frac{C_s}{20.067})^2 \frac{1}{1 + 0.3192q/\epsilon}\ , \qquad [K]\ (A3.2)$$

where ϵ is the ratio of the molecular masses of dry air and water vapor ($\epsilon = M_d/M_w$). Because $0.3192q/\epsilon \ll 1$, the humidity influence is usually neglected, or at best q is taken equal to some suitable average, q_a. When q_a is substituted for q in equation A3.2, it represents the temperature measured by the sonic, T_s. From the sonic manual (anonymus 1978) it is not clear whether q_a is neglected. The temperature measured by the sonic can be expressed in the real temperature by:

$$T_s = T\ \frac{1 + 0.3192\ q/\epsilon}{1 + 0.3192\ q_a/\epsilon}\ . \qquad [K]\ (A3.3)$$

As long as the specific humidity, q, does not deviate too much from q_a this seems to be a reasonable estimate. However, since T_s is an absolute temperature, small relative errors may appear to be big in absolute sense. When the range of specific humidities under normal atmospheric conditions is considered, it follows that neglection of the humidity influence, can lead to errors of 0.5 % (no matter how suitable q_a is chosen), which is about 1.5 K, in T_s. Because the sonics are mainly used for measuring fluctuations, this error can be tolerated, as long as the temperature fluctuations are measured correctly. Equation A3.3 can be used to evaluate the humidity influence on the average temperatures measured with the sonic, but it does not reveal the influence of humidity fluctuations on the measured temperature fluctuations. More useful is the following relation, derived by Schotanus (1982):

$$\overline{w'T_s'} = \overline{w'T'} + \frac{0.3192}{\epsilon}\ \overline{w'q'} - 2\frac{\bar{T}\ \bar{u}}{C_s^2}\ \overline{u'w'}\ . \qquad [K\ m\ s^{-1}]\ (A3.4)$$

When this equation is multiplied with $-\rho_a c_p$ it follows that:

$$Q_{hs} = Q_h + \frac{0.3192\ \bar{T}}{\epsilon}\frac{c_p}{L_e} Q_w + 2\rho_a c_p \frac{\bar{T}\,\bar{u}}{C_s^2}\overline{u'w'}\ , \qquad [W\ m^{-2}]\ (A3.5)$$

where Q_{hs} is the uncorrected sensible flux found from the sonic measurements, Q_h is the correct sensible heat flux and Q_w is the latent heat flux.

In order to get a rough estimate of the importance of the last two terms, equation A3.1 is substituted for C_s (with neglection of the moisture part) and $\bar{T}$ is fixed on 290 K. This results in:

$$Q_{hs} = Q_h + 0.061 Q_w + 6.27\ \bar{u}\ \overline{u'w'}\ . \qquad [W\ m^{-2}]\ (A3.6)$$

Above the tidal flat the sensible heat flux is usually far less than the latent heat flux (Bowen ratio far less than unity) and the surface is rather smooth. A situation with $Q_h = -75\ W\ m^{-2}$, $Q_w = -300\ W\ m^{-2}$, $\bar{u} = 10\ m\ s^{-1}$ and $\overline{u'w'} = -4*10^{-2}\ m^2 s^{-2}$, could be a typical situation of a dry tidal flat under bright sunshine. In this case the influence of the second term in eq. A3.6 is about 24 % and the influence of the third term is about 3 %. So in this example, with an unstable atmosphere, the third term has only a minor influence. In stable cases the sensible and latent heat flux are smaller, but also $\overline{u'w'}$ is much smaller (less stress). In near neutral cases the third term becomes important in comparison with the sensible heat flux. In absolute sense however, this term is always small, when measuring above a relatively smooth surface, such as a tidal flat. The estimate is that, during our measurements, it was always less than 10 $W\ m^{-2}$, so it justified to neglect this term.

Now equation A3.6 is reduced to:

$$Q_{hs} = Q_h\ (\ 1 + 0.061/\beta)\ , \qquad [W\ m^{-2}]\ (A3.7)$$

where β is the Bowen ratio. This formulation is useful to evaluate the moisture influence on the sensible heat flux measured with the sonic anemometer. A Bowen ratio of 0.25 or less is quite normal above the tidal flats (also when they are inundated), so the influence of the second term is estimated in the order of 25 % or more.

APPENDIX 4: CALCULATION PROCEDURE AT THERMAL CONDUCTIVITY MEASUREMENTS.

For a detailed description of the theory the reader is referred to Van Haneghem (1981). In this appendix the essential steps in the calculation are summarized.

Since the set of equations is rather complicated it has to be solved iteratively. The procedure is as follows: First two constants are calculated, namely Q_l (the heat production in the needle per unit length) and α_j (a parameter which compares the heat capacity of the soil with that of the needle). Then a first estimate of thermal conductivity, λ, and two variables, A_j and B is made and the iteration procedure starts.

The heat production in the needle per unit length follows from:

$$Q_l = \frac{I^2}{R_l} , \qquad [W\ m^{-1}]\ (A4.1)$$

where I is the current through the resistance wire and R_l is the resistance of the wire per unit length. α_j is calculated from:

$$\alpha_j = \frac{2\ \pi\ r^2\ \rho_b c_b}{c_l}, \qquad [-]\ (A4.2)$$

where r is the radius of the needle, $\rho_b c_b$ is the heat capacity of the soil per unit volume and c_l is the heat capacity per unit length of the needle.

The first estimate of λ, A_j and B is made by assuming:

$$T_j(t) = A_j\ ln(t) + B , \qquad [K]\ (A4.3)$$

where T_j is the needle temperature and A_j and B are found by regression analysis. λ is calculated from:

$$\lambda = \frac{Q_l}{4\ \pi\ A_j} . \qquad [W\ m^{-1}K^{-1}]\ (A4.4)$$

The complete equation which describes the needle temperature according to the modified Jaeger model (Van Haneghem 1981) is:

$$T_j(t) = A_j\ ln(t+t_0) + B + E\ \frac{ln(t)}{t} . \qquad [K]\ (A4.5)$$

This equation is fitted to the measured temperature course in the needle with the iterative procedure described below.

The constant E is calculated from:

$$E = \frac{Q_l}{4\,\pi\,\lambda}\,\frac{(\alpha_j - 2)\,r^2}{2\,\alpha_j\,\underline{a}} \qquad [K\ s]\ (A4.6)$$

where $\underline{a}$ is the thermal diffusity of the soil given by:

$$\underline{a} = \frac{\lambda}{\rho_b c_b} \qquad [m^2 s^{-1}]\ (A4.7)$$

Then another constant, γ_j, is calculated from:

$$\gamma_j = \frac{\frac{B}{A_j} - ln\left(\frac{4\,\underline{a}}{r^2\,C_E^*}\right)}{2} \qquad [-]\ (A4.8)$$

where C_E^* is the e-power of the constant of Euler ($C_E^* = 1.78107...$). The time delay, t_0, is found from:

$$t_0 = \frac{(\alpha_j - 2)\,r^2\ ln(4\underline{a}/r^2 C_E^*) + r^2\,(\alpha_j - 4\gamma_j)}{2\,\alpha_j\,\underline{a}} \qquad [s]\ (A4.9)$$

For each time a corrected temperature is calculated from:

$$T_j^*(t) = T_j(t) - E\,\frac{ln(t)}{t} \qquad [K]\ (A4.10)$$

The new constants A_j and B now follow from linear regression between the corrected temperature T_j^* and $\ln(t+t_0)$ (compare with equations A4.5 and A4.9). The new thermal conductivity is calculated with equation A4.4 and the procedure (starting from equation A4.6) is repeated until the thermal conductivity changes less than 0.001 $W\ m^{-1}K^{-1}$. This usually takes about 5 iterations.

APPENDIX 5: CHANGE OF THE SOIL HEAT FLUX WITH DEPTH.

From measurements with the integration method it was found that the mean ratio between the soil heat flux at the surface and at a depth of 2.5 *cm* is about 1.2. In this appendix this factor will be derived theoretically in two different ways, first by assuming a sinusoidally varying surface temperature and secondly by assuming a step function in the soil heat flux at the surface.

The sine wave

The soil heat flux at any depth z can be found by integrating the temperature change in time:

$$Q_b(z_1,t) = -\int_{-\infty}^{z_1} \rho_b\, c_b\, \frac{\partial T(z,t)}{\partial t}\, \partial z\ , \qquad [W\ m^{-2}]\ (A5.1)$$

where ρ_b is the density of the soil and c_b the specific heat of the soil (compare with eq. 2.43). When the surface temperature varies sinusoidally the temperature (T) as a function of depth (z) and time (t) is described by eq. 2.50. Substitution of $T(z,t)$ in eq. A5.1 by eq. 2.50 leads to:

$$Q_b(z_1,t) = -\int_{-\infty}^{z_1} \rho_b c_b A(0)\ \omega e^{z/D} cos(\omega t + z/D)\, \partial z\ . \qquad [W\ m^{-2}]\ (A5.2)$$

This integral was solved with the aid of partial integration, resulting in:

$$Q_b(z,t) = -\frac{1}{2^{0.5}}\ \rho_b c_b A(0) D\ \omega e^{z/D} sin(\omega t + z/D + \pi/4)\ [W\ m^{-2}]\ (A5.3)$$

When the time delay of the soil heat flux between 0 and 2.5 *cm* is neglected it follows that:

$$\frac{Q_b(0,t)}{Q_b(0.025,t)} = e^{0.025/D}\ , \qquad [-]\ (A5.4)$$

with $D=(2\underline{a}/\omega)^{0.5}$ [m]. For the tidal flat soil $\underline{a}$ is circa $1.07 \times 10^{-6}\ m^2 s^{-1}$. When it is assumed that the variation of the surface temperature is dominated by the tidal cycle (period is 12.5 hr) it follows that the ratio of the soil heat flux at the surface and that at a depth of 2.5 *cm* is about 1.22. When it is assumed that the daily cycle dominates the temperature variation at the soil surface it follows that the ratio is about 1.16. Neither of these values conflict with the experimentally found number of 1.2 (see section 4.2.1).

The step function.

In order to be able to evaluate the ratio between the surface soil heat flux and the soil heat flux at a depth of 2.5 *cm*, we will consider a theoretical case. It is assumed that initially the soil temperature is homogeneous and equal to $\overline{T_b}$. The surface soil heat flux is assumed 0 when $t < 0$ and equal to Q_{b0} for times after $t = 0$. For this case the soil temperature is described by:

$$T(z,t) = \overline{T_b} - \frac{2}{\pi^{0.5}} \frac{Q_{b0}}{[\lambda_b \rho_b c_b]^{0.5}} t^{0.5} [e^{-x^2} - x\pi^{0.5}(1-erf(x))] \qquad [^\circ C] \text{ (A5.5)}$$

where $erf(x)$ is the well known error function:

$$erf(x) = \frac{2}{\pi^{0.5}} \int_0^x e^{-y^2} \partial y \qquad [-] \text{ (A5.6)}$$

and $x = -z/2(at)^{0.5}$. When eq. A5.5 is substituted in eq. A5.1 and the integration is carried out it follows that:

$$Q_b(z,t) = Q_{b0}(1 - erf(x)) \qquad [W\ m^{-2}] \text{ (A5.7)}$$

In figure A5 the ratio $Q_b(z,t)/Q_{b0}$ as follows from eq. A5.7 is plotted against x. Along the horizontal axis also the time is given assuming that $z = -0.025m$ and $\underline{a} = 1.07x10^{-6}\ m^2 s^{-1}$. Also shown in the figure is a horizontal line at $Q_b(z,t)/Q_{b0} = 1/1.2$, which is what was found experimentally. It can be seen that the experimentally obtained value is valid for sudden changes in the surface soil heat flux which last one to three hours.

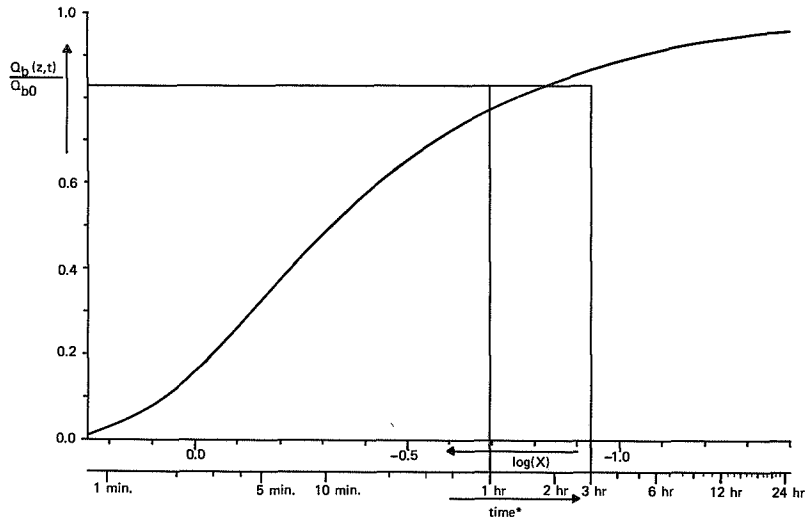

Figure A5: $Q_b(-0.025,t)/Q_b(0)$ versus time (explanation in text).

APPENDIX 6: ACCELERATING OR DECELERATING SIGNALS.

In order to be able to compare two signals measured by sensors with different response times, one can either decelerate (filter) the faster signal or accelerate the slower signal. An example in which this is necessary is the fast response thermocouple psychrometry, where the specific humidity is calculated from measurements with a dry and a wet bulb thermocouple, which usually have different response characteristics.

In this appendix the formula for the first order response of a sensor to a step function will be used as a basis for the derivation of the other formulas. The first order response to a step function is given by:

$$s(t) = S_1 - (S_1 - S_0) * e^{-t/t_r} , \qquad \text{(A6.1)}$$

where s denotes the measured signal, S_0 the real signal before the step and S_1 after the step, t is the time (since the step) and t_r the response time of the sensor. The *response time* is defined as the time after a step change in the signal to be measured, in which an instrument measures 63 % (fraction $1-1/e$) of the total step.

When an arbitrary signal is represented as a series of step changes, it can be proved with the aid of mathematical induction that (A6.1) corresponds with:

$$s_i = \alpha_f \, s_{i-1} + (1 - \alpha_f) \, S_i , \qquad \text{(A6.2)}$$

where i denotes the step number and the filter constant α_f is given by:

$$\alpha_f = e^{-\Delta t/t_r} , \qquad \text{(A6.3)}$$

where Δt is the length of a time step.

When the *cut off frequency* is defined as the frequency at which the square of the amplitude of a sine shaped signal is reduced to 50 % due to the inertia of the instrument, it can be shown that it is related to the response time by:

$$f_c = \frac{1}{2 \pi t_r} . \qquad [s^{-1}] \text{ (A6.4)}$$

If one wants to filter a signal to match a certain response time (or cut off frequency) (A6.3) and (A6.4) can be used to calculate the filter constant α_f. Then (A6.2) can be used to calculate a filtered signal, on condition that the signal is measured fast enough. So S_i may be assumed equal to the measured signal and s_i becomes the filtered signal. Furthermore the response time of the filtered signal should be an order of magnitude larger than the response time of the instrument.

Note that only very little information is needed to obtain the new value for the filtered signal; we use only the preceding and the current value of the measured signal. For other techniques, such as moving averages, it is always necessary to "remember" a series of measurements. The fact that little memory is needed and that very few calculations have to be carried out makes the application of (A6.2) a useful filtering technique, especially when large amounts of data have to be handled.

A disadvantage of filtering a signal is that information which is contained in the higher frequencies is lost. Therefore we also applied a technique for accelerating signals. Equation A6.2 is rewritten as:

$$S_i = \frac{s_i - a_f s_{i-1}}{1 - a_f} . \qquad \text{(A6.5)}$$

The filter constant a_f is again found from(A6.3). The real signal at any moment is calculated from the measured signal at that moment and the preceding measurement. In order to use (A6.5) the time interval between successive measurements should be sufficiently small, i.e. only a small fraction of the energy in the total spectrum should be contained in frequencies higher than the sample frequency. However if the time interval becomes to small, a_f becomes close to 1.0. In this case resolution problems will be magnified, as it is illustrated by the following example. When accelerating our wet bulb temperature signals, we used a sample interval of 0.08 s and an (estimated) cut off frequency of 0.4 s^{-1}, resulting in a filter constant of 0.82. The resolution of the registration was 2.5 mV, corresponding with 0.01 K. It can be seen from (A6.5) that under these circumstances the accelerated signal is only accurate to circa 0.05 K. Should we have used a sample interval of 0.04 s, a_f would become 0.90 and the accuracy of the accelerated signal circa 0.10 K.

An advantage of this way of acceleration is that computations are simple and that very little memory is required, which makes the method useful for handling large amounts of data. Acceleration could also be achieved be other means, for example Fourier techniques, but these would require a much larger amount of memory and more calculations.

Equation A6.5 was also used by Shaw and Tillman (1980). In the calculation of the filter constant they also included aliasing effects, which are entirely neglected in the preceding discussion. They found that the filter constant can be calculated from:

$$\alpha_f = 2 - COS - [\, COS^2 - 4\, COS + 3 \,]^{0.5} , \qquad [-] \text{ (A6.6)}$$

where

$$COS = \cos (2\, \pi\, \Delta t\, f_c) . \qquad [-] \text{ (A6.7)}$$

Although, at first sight, this looks very different from (A6.3), the results are virtually the same in the area of interest. For $0.02 < f_c * \Delta t < 0.08$ the difference for α_f as well as for $(1-\alpha_f)$ is less than 1 %. For $f_c * \Delta t$ less than 0.02, $(1-\alpha_f)$ becomes less than 0.1 and the method should not be used anyhow.

Shaw and Tillman have tested the described method of acceleration in fast response thermocouple psychrometry and compared the calculated specific humidity with Lyman-α measurements. The results were far better than when the wet bulb signal was not accelerated. Acceleration of the wet bulb signal also largely improved the calculated humidity spectrum.

For some runs at the 1983 Balgzand experiment we used accelerated wet bulb temperatures to calculate specific humidity and hence latent heat fluxes. When no acceleration was applied the latent heat fluxes were reduced by a factor 0.8. Filtering the other signals in stead of accelerating the wet bulb signal had almost the same effect (the absolute value of the sensible heat flux was slightly less). This gives some confidence in the acceleration technique. Compared to the latent heat fluxes obtained from the profiles however the fluxes were still a factor 2 too low. This is discussed in detail in section 4.1.4.

CURRICULUM VITAE

Johannes Hendricus van Boxel werd geboren op 23 december 1955 te Raamsdonk.

De lagere school doorliep hij in Raamsdonksveer en later in Etten-Leur. In 1974 behaalde hij zijn Atheneum B diploma aan het Thomas More College te Oudenbosch.

Daarna werd begonnen aan een studie Milieuhygiëne, specialisatie Luchthygiëne en -verontreiniging aan de Landbouw Hogeschool te Wageningen. Na de kandidaatsfase werden twee maal drie maanden stage besteed aan de modellering van de verspreiding van luchtverontreiniging. De doctoraalfase bestond verder uit 3 maanden Proceskunde, 6 maanden Meteorologie en 6 maanden Luchthygiëne en -verontreiniging. Het vak Proceskunde bestond uit een theoretische en praktische bestudering van de adsorptiekinetiek van coffeïne aan actieve kool. Bij het vak Meteorologie werden een aantal stabiliteitsparameters (parameters die de stabiliteit van de atmosfeer karakteriseren) theoretisch afgeleid en onderling vergeleken. Tijdens het vak Luchthygiëne en -verontreiniging werd een onderzoek gedaan naar de monstername efficientie van aerosolmeetapparatuur onder buitenlucht omstandigheden. In september 1981 werd het diploma behaald.

In datzelfde jaar nog werd begonnen aan een promotie onderzoek bij de vakgroep Meteorologie aan de Vrije Universiteit te Amsterdam. De resultaten van dat onderzoek zijn vastgelegd in dit proefschrift. Tijdens de periode dat hij bij de Vrije Universiteit werkzaam was, had hij als neventaak het opstarten en beheren van de PDP11 computer van het Instituut voor Aardwetenschappen aan deze universiteit.

Van januari tot en met oktober 1985 was hij tevens parttime werkzaam als programmeur op het Computer Centrum van het Rijks Instituut voor Volksgezondheid en Milieuhygiëne te Bilthoven.

Sinds november 1985 is hij als wetenschappelijk medewerker verbonden aan de Nederlandse organisatie voor Zuiver-Wetenschappelijk Onderzoek (ZWO) en gestationeerd bij de vakgroep Natuur- en Weerkunde van de Landbouw Hogeschool te Wageningen.